Development of extracellular polymeric substance-derived protective films against microbiologically influenced corrosion by *Desulfovibrio vulgaris*

A dissertation presented

by

Andrzej Ulrich Kuklinski

born in Rheinberg

to

The Faculty of Chemistry

in partial fulfilment of the requirements

for the degree of

Doctor of Natural Sciences (Dr. rer. nat.)

University Duisburg-Essen

Essen, Germany

2016

The dissertation presented was conducted in the Aquatic Biotechnology group of Prof. Dr. Wolfgang Sand at the Biofilm Centre of the Faculty of Chemistry of the University Duisburg-Essen from January 2008 to December 2013.

Date of the disputation: 2nd May, 2017

Supervisors:	Prof. Dr. Wolfgang Sand
	PD Dr.-Ing. Wolfram Fürbeth
Chairman:	Prof. Dr. Matthias Epple

ABSTRACT

It is widely accepted that microorganisms can play a pivotal role in corrosion by not only accelerating (microbiologically influenced corrosion, MIC) but also by inhibiting (microbiologically influenced corrosion inhibition, MICI) the (electro)chemical degradation processes. Both phenomena are caused by biofilms accommodating immobilised, often complex microbial consortia embedded in a matrix of extracellular polymeric substances (EPS). EPS are a heterogeneous mixture of (mainly) polysaccharides, proteins, lipids, and nucleic acids and greatly influence interfacial processes (and, hence, MIC and MICI). In this study, *Desulfovibrio vulgaris* was used as a model organism for examination of MIC of steel caused by sulphate-reducing bacteria (SRB).

A novel combination of scanning Kelvin probe force- and epifluorescence microscopy (SKPFM & EFM) was developed and evaluated to visualise localised effects of the bacterial cells on the surface potential of alloyed steel and pure iron in high resolution. EPS from cells grown in the presence of both working materials were extracted using DOWEX marathon C cation exchange resin. The strictly intracellular enzyme G6PDH was measured to ensure that extraction was not effected by cell lysis. Polysaccharides, proteins, uronic acids, humic acids, lipids, and nucleic acids from loosely and tightly bound EPS fractions as well as the TOC were quantified. Additionally, the polysaccharide and lipid moieties of the EPS were qualitatively analysed by gas chromatography. To mimic MICI, 25 differently functionalised cyclodextrins were used as EPS-analogue substances. Their protective effect was determined from MIC simulations with *Desulfovibrio vulgaris* under anaerobic conditions. Corrosion rates were determined gravimetrically after up to 21 d. The stability of the cyclodextrin films and their impact on biofilm formation was assessed by fluorescence microscopy.

Results from the SKPFM & EFM measurements showed that the surface potential of *Desulfovibrio vulgaris* cells was approximately 25 mV higher compared to the surrounding alloyed steel surface. After removal of the cells, the same spot showed a negative shift in surface potentials of approximately -25 mV compared to the surrounding surface. In agreement with observations reported in other studies which demonstrated changes in the same order of magnitude between austenitic and ferritic phases and at areas with defects of the

passivating oxide layer, these results provide strong evidence for a direct microbial influence on the passivating oxide layer of stainless steel.

For EPS analysis, 7- 15 % of the loosely bound and 39 – 64 % of the tightly bound fraction were identified by colorimetric methods. TOC measurements indicated that the remaining proportion is of inorganic nature. G6PDH activity was not detectable in any of the extracts. The total amount of polysaccharides, proteins, and lipids is greatly influenced by the working material present. However, a significant influence on the qualitative composition of polysaccharides and lipids could not be proven within this context. The strongest effect was observed for uronic acids with a significant increase to approximately 63 µg mg^{-1} EPS (compared to 19 µg mg^{-1} EPS in the controls without metallic substrata). Considering a 4-fold higher amount of Fe(III) ions in the EPS of cells grown in the presence of metallic substrata, a ratio of 2 moles glucuronic acids to 1 mole Fe(III) ions was calculated, indicating the formation of organometallic complexes and suggesting that uronic acids represent an important factor in MIC by SRB.

Out of the 25 differently functionalised varieties, (polymerised) carboxy(m)ethylated cyclodextrins showed the highest protective effect against MIC with 77 % lower corrosion rates after 21 d incubation. CLSM images show dense, up to 10 µm thick films clearly separating biofilms from the material surface. An influence on the biofilm formation itself was not found, suggesting that the cyclodextrin films work as a passive barrier against the microorganisms.

"Bazinga!"

Dr. Dr. Sheldon Lee Cooper

ACKNOWLEDGMENTS

First, I would like to thank Prof. Dr. Wolfgang Sand for giving me the chance to not only do my doctoral research in his Aquatic Biotechnology working group but also for enabling me to establish skills in managing interdisciplinary scientific projects and to present my results in various conferences around the world.

I would like to express my gratitude to my second assessor PD Dr.-Ing. Wolfram Fürbeth for accepting this task as well as for the opportunity to write my Master's thesis at the DECHEMA Research Institute, which was the starting point for several years of work in the field of microbiologically influenced corrosion of steel.

I would also like to thank Dr. Tilman Gehrke for his valuable help in the sugar and lipid separation from EPS, for discussing and proof-reading this work as well as for keeping the lab and instruments up and running.

I owe my thanks Mariël Grooters for her help introducing me to the lab and to the subtleties of EPS extraction. I also wish to thank Dr. Felipe Leon-Morales for countless discussions regarding the practical and scientific aspects of this work.

Furthermore, my thanks go to Christian Thyssen for additional proof-reading, Bianca Florian, Anne Heyer and Witold Michalowski for a great trip through Yucatan as well as Nanni Noël, Robert Barthen, Jens Kuhn, Igor Felschau, and all the other former members of the Aquatic Biotechnology group.

During my work, two Bachelor theses were successfully completed. I would like to thank Mark Pannekens for his hard work in developing a standard procedure for the polymerisation of cyclodextrins as well as Mara Werner for her work on their biodegradability. Additionally, I would like to thank Vanessa Roeben, who spend several late evenings on the derivatisation of EPS for the chromatographic identification of sugar monomers and lipids.

Many thanks to the Merck Chemicals GmbH who made it possible for me to finish this thesis despite starting a new and exciting job.

My special thanks go to my parents Monika and Michael as well as my sister Verena for their support during the whole time before, during and after doing this thesis.

Finally, my very special thanks go to Mareike.

Supported by:

on the basis of a decision
by the German Bundestag

This work was partially realised within the IGF projects 178 ZN, 263 ZN, and ZN04204-10 of the DECHEMA Research Institute. These projects were supported by the German Federal Ministry for Economic Affairs and Energy within the Programme for Funding Industrial Joint Research (IGF) based on a decision by the German Bundestag.

CONTENT

LIST OF FIGURES

LIST OF TABLES

GLOSSARY

A

AFM	atomic force microscopy
ara	arabinose

C

CD	cyclodextrin
CER	cation exchange resin
CLSM	confocal laser scanning microscopy
CPD	contact potential difference (between tip and surface in SKPFM)

D

DAPI	4'-6-diamidino-2-phenylindole
DEPC	diethylpyrocarbonate (used to inactivate RNase enzymes in water)
dH_2O	deionised water

E

EFM	epifluorescence microscopy
EPS	extracellular polymeric substances

F

fuc	fucose
FTIR	Fourier-transform infrared spectroscopy

G

g	gravitational force acceleration
gal	galactose
G6P	glucose-6-phosphate
G6PDH	glucose-6-phosphate dehydrogenase
GC	gas chromatography

I

IOB	iron-oxidising bacteria
IRB	iron-reducing bacteria

K

kDa	kilo Dalton
KDO	2-keto-3-deoxyoctonate
SKPFM	scanning Kelvin probe force microscopy

M

man	mannose
MIC	microbiologically influenced corrosion
MICI	microbiologically influenced corrosion inhibition
MilliQ™ water	ultrapure (bi-distilled) water
MOMO	Manganese-oxidising microorganism
MWCO	molecular weight cut-off

P

PBS	phosphate buffered saline

R

rha	rhamnose
rib	ribose

S

sor	sorbitol
SRB	sulphate-reducing bacteria
SRP	sulphate-reducing prokaryotes

T

TC	total carbon (inorganic + organic)
TCC	total cell count
TIC	total inorganic carbon
TOC	total organic carbon
Tris	tris(hydroxymethyl)-aminomethane

V

v/v	volume per volume

W

w/v	weight per volume

X

xyl	xylose

1 INTRODUCTION

1.1 Biofilms

Biofilms are immobilised, often complex microbial consortia embedded in a matrix of so-called extracellular polymeric substances (EPS). They evolve rapidly on virtually every biological or non-biological surface (Costerton, et al., 1995; Lappin-Scott & Costerton, 1995). The term surface thereby is not restricted to solid/aqueous interfaces but includes all two-phase water systems including such environments as the so-called neuston, the interfacial area between water and air (Cunliffe & Murrell, 2009; Wimpenny, 2000). Biofilms are not only abundant in natural but also industrial and medical environments (Costerton, et al., 1994; Costerton & Anwar, 1994; Khoury, et al., 1992). It is generally acknowledged that the clear majority of life on earth exists in form of biofilms. In fact, up to 99.9% of the microorganisms in aquatic habitats are assumed to live in biofilms. Therefore, the planktonic state of microbial life is probably only temporary to allow the distribution of cells and the colonisation of new surfaces (Donlan & Costerton, 2002). Due to their ubiquitous occurrence, biofilms can be assumed to be a universal microbial survival strategy (Flemming & Wingender, 2010; Beech & Cheung, 1995; Costerton, et al., 1995).

The formation of aquatic biofilms can be described as a consecutive process leading to a physically highly stable microbial consortium (Sauer, 2003; Stoodley, et al., 2002; Stoodley, et al., 1999; Costerton, et al., 1995). Initially, planktonic cells reversibly attach to surfaces, previously typically covered by an organic conditioning layer. It consists of substances such as proteins or carbohydrates from the aqueous phase, which spontaneously accumulate on the surface. These compounds mostly originate from the microorganisms themselves (actively secreted biosurfactants). The conditioning layer promotes attachment by facilitating hydrophobic interactions between the film itself and the microorganisms which helps to overcome repulsive effects of uncoated surfaces (Compère, et al., 2009; Neu, 1996). This early colonisation step is strongly dependent on the physical surface characteristics, i.e. its chemical composition and roughness. Generally, rough surfaces will be colonised more rapidly (Little, et al., 1992). In the next step, excretion of extracellular polymeric substances (EPS) by the microorganisms facilitates the irreversible attachment (3) to the surface. Then, microcolonies develop inside the EPS matrix by division of the immobilised cells. These two

steps mark the transition from the planktonic to the sessile state of microbiological life. Genetically, this transition is characterised by increased expression of specific genes involved in EPS production and secretion (Vera, et al., 2013; Sauer, 2003). In addition, a down-regulation of genes responsible for the expression of pili or flagella, and thus, a loss in motility can be observed. Other common characteristics of sessile (biofilm) cells compared to their planktonic counterparts are higher degradative capabilities, elevated levels of genetic exchange and increased secondary metabolite production (Sauer, 2003; O'Toole, et al., 2000). The microcolonies evolve further and planktonic cells of the same or other species may be incorporated, leading to the formation of a mature, continuous biofilm with a highly diverse microbial community (Costerton, et al., 1995; Costerton, et al., 1987; Marshall, 1980). Both the community as well as the three-dimensional structure of the biofilm are highly dependent on environmental factors such as the nutrient availability, the chemical composition of the substratum or physical factors such as temperature, pH or flow conditions. Under steady-flow conditions, for example, biofilms are formed from cell-clusters divided by interstitial voids and channels, a structure often referred to as the mushroom-model (Stoodley, et al., 1999; Costerton, et al., 1995). In contrast, floating biofilms evolving at water-air interfaces show much more complex structures due to absence of rapid fluid flow on their air-exposed surface (Branda, et al., 2005; Costerton, et al., 1995). Throughout their whole lifecycle, biofilms remain in a highly dynamic state. The microbial community as well as the 3-dimensional structure may alter at any time as a direct result of changing environmental conditions (Klause, et al., 2006; Sutherland, 2001). Additionally, specialised "swimmers" (subpopulations of motile bacteria) may create pores and tunnels within the biofilm that influence substance transport and diffusion rates and cause a constant change in the matrix structure (Houry, et al., 2012). In the final stage of the biofilm lifecycle, planktonic cells are released from the mature biofilm, either by active processes such as the production of polysaccharide lyases allowing the cells to leave the EPS matrix (Allison, et al., 1998) or because of external factors such as high shear forces, which may lead to the complete loss of larger biofilm parts. The released cells close the biofilm lifecycle by eventually colonising new surfaces and forming new biofilms (Sutherland, 2001).

The organisms of a biofilm are immobilised in a common, strongly hydrated slime matrix. The capsule is a result of the secretion of EPS and ensures the cohesion of the cellular biofilm components through its gel-like properties. As a diffusion barrier for dissolved gases

such as O_2, solid matter, and due to its water retaining property the matrix offers protection to the microorganisms against desiccation, raised salt and heavy metal loads, biocides and detergents. The formation of anoxic (i.e. oxygen-free and/or -limited) niches and concentration cells (e.g. for potential nutrients) allows the growth of an anaerobic flora also in oxygen-rich environments (Flemming & Wingender, 2010; Flemming, et al., 2007).

1.2 Extracellular polymeric substances

The EPS matrix constitutes the major part of most archaeal, bacterial, and eukaryotic biofilms and accounts for more than 90 % of their dry mass (Flemming & Wingender, 2010; Flemming & Wingender, 2002; Wingender, et al., 1999). EPS have both adhesive and cohesive properties by binding the biofilm to surfaces as well as forming a three-dimensional microenvironment. The latter facilitates the long-term immobilisation of cells and consequently promotes the formation of microconsortia (Flemming & Wingender, 2010; Laspidou & Rittman, 2002; Characklis & Wilderer, 1989; Geesey, 1982). Additionally, they determine the immediate environmental conditions for the organisms living in a biofilm by affecting factors such as porosity, density, water content, charge, sorption properties, hydrophobicity, and mechanical stability (Flemming, et al., 2007; Flemming & Wingender, 2002). Additionally, the EPS matrix provides a major water reservoir protecting the enclosed cells against desiccation; the fully hydrated EPS-matrix contains more than 97 % water (Flemming & Wingender, 2010; Sutherland, 2001). Moreover, EPS provide an external digestive system for the biofilm by retaining exoenzymes and particulate matter. Exoenzymes may break down and hydrolyse complex macromolecules, leading to a subsequent accumulation of low-molecular weight nutrients near the cells, which enhances the nutrient uptake and reduces diffusion-losses into the water phase (Laspidou & Rittman, 2002). Additionally, anionic compounds within the EPS-matrix can bind metal ions (Kumar, et al., 2007; Sand & Gehrke, 2006). The oxidation of e.g. Fe(II) and subsequent accumulation and/or precipitation of Fe(III) ions by exopolymers releases protons, which decrease the pH outside the cell and thus increase metabolic energy generation by enhancing the proton motive force (Beech & Sunner, 2004). Additionally, a reaction space for interfacial processes is provided. For example, acidophilic microorganisms dissolve metal sulphides by oxidising Fe(II) ions within the EPS matrix to Fe(III) ions, which attack the substratum and are reduced back to Fe(II) (Rohwerder, et al., 2003). EPS may also act as a reservoir for

excess energy by retaining e.g. excess carbon under unbalanced C/N ratios or facilitate redox reactions within the biofilm by acting as electron donor or acceptor. Finally, the EPS matrix has a direct impact on the genetic properties of the biofilm organisms by providing a gene pool where retained DNA facilitates horizontal gene transfer and improves cell-to-cell signalling (quorum sensing) by increased accumulation of the signalling molecules near the cells (Flemming & Wingender, 2002). In conclusion, the EPS matrix is largely responsible for the ecological advantage of biofilms over planktonic cells.

Chemical composition of EPS

Chemically, EPS are a complex biochemical mixture mainly consisting of polysaccharides, proteins, glycoproteins, glycolipids, and extracellular DNA (eDNA) as well as more complex compounds such as membrane vesicles (Flemming & Wingender, 2002; Schooling & Beveridge, 2006; Branda, et al., 2005; Beech & Cheung, 1995). Their composition is not only depending on the microbial consortium but also on different processes such as active secretion, shedding of cell surface material, cell lysis, and adsorption of organic and inorganic substances from the environment (Laspidou & Rittman, 2002). Additionally, environmental factors such as the substratum, surrounding medium, and its physical properties such as temperature or pH have a strong influence (Ozturk & Aslim, 2010; Harneit, et al., 2006; Branda, et al., 2005; Gehrke, et al., 1998; Becker, 1996; Zinkevich, et al., 1996; Beech, et al., 1991). Finally, not only the EPS composition of planktonic versus sessile cells differs considerably but also the EPS fraction tightly bound to the cell surface versus the loosely bound fraction, which is partially released into the surrounding medium (Wikieł, 2013; Kumar, et al., 2007; Comte, et al., 2006a; Branda, et al., 2005; Beech & Gaylarde, 1999).

Carbohydrate-rich polysaccharides often represent the largest fraction of EPS (Branda, et al., 2005; Beech & Cheung, 1995) and usually serve as constructive or sorptive components (Flemming, et al., 2007). They are crucial for the formation of mature biofilms. Mutants unable to produce polysaccharides were still able to form microcolonies on surfaces, but no continuous biofilms (Flemming & Wingender, 2010; Ryder, et al., 2007; Danese, et al., 2000; Watnik & Kolter, 1999). A wide variety of different homo- and heteropolysaccharides were identified in natural biofilms from aquatic and soil habitats. Homopolysaccharides range from simple structures with repeating units of glucose, galactose or rhamnose like in *Lactococcus lactis* NZ4010 (van Kranenburg, et al., 1997) up to complex, high-molecular

weight structures without any repeating units produced by *Lactobacillus reuteri* 180 (van Leeuwen, et al., 2008) and even cyclic glucans produced by e.g. *Rhizobium trifolii* TA-1 (Zevenhuizen, 1986). The most frequently mentioned and in-detail studied heteropolysaccharide is alginate, produced by mucoid *Pseudomonas aeruginosa* strains (Flemming, et al., 2007). Alike alginate, many heteropolysaccharides are polyanionic or -cationic (Flemming & Wingender, 2010). Strong and weak interactions between functional groups of the heteropolysaccharides not only strongly influence the structural integrity of the EPS matrix but may also provide strong binding to certain surfaces. For example, it may be speculated that carboxyl groups could influence attachment of EPS to corroding surfaces based on their iron-chelating properties. Uronic acids are largely responsible for the polyanionic nature of heteropolysaccharides and influence several processes between the EPS and the environment. They were found to be crucial for the metal sulphide dissolution by acidophilic microorganisms, as they were directly involved in the cycle of Fe(II)- and Fe(III) ions, which attack the mineral surface (Gehrke, et al., 2001; Gehrke, et al., 1998).

In some cases, the protein content can by far exceed the amount of polysaccharides in the EPS matrix. In fact, up to 75 % of the water-soluble EPS of *Pseudomonas putida* consists of proteins (Jahn, et al., 1999), which represent up to 96% of the total biofilm protein content. The protein fraction consists of extracellular enzymes including EPS-degrading- and redox-active enzymes (Flemming & Wingender, 2010). Other proteins serve for structural roles such as carbohydrate-binding lectins or complex amyloids (high-molecular-weight proteins of virtually unlimited length) which both promote adhesion to surfaces as well as the intrinsic stability of the EPS-matrix (Flemming & Wingender, 2010).

Lipids (amongst other substances like biosurfactants) are largely responsible for hydrophobic properties of the EPS matrix (Flemming & Wingender, 2010). They can be crucial for the attachment and adherence of biofilms to hydrophobic surfaces such as sulphur (Gehrke, et al., 1998). Protein and lipid conditioning films also influence bacterial attachment to hydrophobic surfaces such as contact lenses (Bruinsma, et al., 2001) as well as the hydrophobic properties of EPS in activated sludge flocs (Conrad, et al., 2003). The study of Gehrke, et al., (1998) provides some (of the very few) insights into the composition of the EPS lipid fractions, as lipids were mostly disregarded in EPS research.

The role of eDNA within the EPS matrix is still unclear. It was often seen as a remnant of lysed cells (Flemming, et al., 2007) but recent studies demonstrated that (potentially deliberately excreted) eDNA formed filamentous network-like structures, suggesting a structural role within a biofilm (Boeckelmann, et al., 2006). Observations on multispecies activated sludge flocs support this assumption, since significantly faster and stronger deflocculation occurred when eDNA was removed by DNAse compared to DNA-containing controls (Dominiak, et al., 2011). Another study by Vilain, et al., (2009) demonstrated that *Bacillus cereus* actively secreted DNA in early stages of biofilms and that this DNA was found both on material surfaces (indicating the formation of a conditioning film) as well as directly associated to the cell surface. Probably, nucleic acids are also involved in the attachment of cells to mineral surfaces (Omoike, et al., 2004). Boeckelmann, et al., (2006) observed both similarities as well as distinct differences between genomic and extracellular DNA. Other functions of eDNA such as electron transfer via the filaments or the promotion of cell-to-cell communication remain mostly speculative (Flemming, et al., 2007).

Although several studies investigated the chemical composition of EPS, their results should be scrutinised carefully. The EPS composition is strongly depending on both the method used to extract them from a biofilm as well as the methods used to identify and quantify the constituents (Lear, et al., 2010; Aguilera, et al., 2008; Comte, et al., 2006b; McSwain, et al., 2005). Additionally, the highly dynamic nature of EPS makes it nearly impossible to provide a complete biochemical profile of most EPS samples (Flemming, et al., 2007; Flemming & Wingender, 2002).

1.3 MIC - microbiologically influenced corrosion

Microbiologically influenced corrosion or biocorrosion describes the phenomenon of material damage directly or indirectly by microbial activity. The awareness for MIC has risen steadily during the last years and today it is believed that 10 - 20 % of all corrosion cases are related to microorganisms and their biofilms (Sand & Gehrke, 2003; Flemming, 1995). This ratio is even higher in the oil and gas industry, where up to 30 % of corrosion cases are directly related to microbial activity (Beech & Sunner, 2007).

It should be noted that the term MIC is not strictly limited to the corrosion of metals but is often also used to describe the detrimental influence of microorganisms on various materials. This negative influence ranges from the simple presence of biofilms leading to e.g. increased flow resistance in pipes, the degradation of plasticisers and subsequent embrittlement of plastics as well as corrosion of concrete in sewage pipes by sulphuric acid produced by sulphur-oxidising bacteria (Kuklinski & Sand, 2014; Thierry & Sand, 2011; Diercks, et al., 1991; Sand, 1987; Sand & Bock, 1984). However, these cases would go far beyond of the scope of this thesis and hence only the mechanisms involved in MIC of ferrous materials will be described further in detail.

1.3.1 MIC of metals under aerobic conditions

Under aerobic conditions, three groups of microorganisms are of special interest in MIC: Sulphur-oxidising bacteria (SOB), iron-oxidising bacteria (IOB) and Manganese-oxidising microorganisms (MOMO) (Kuklinski & Sand, 2014; Thierry & Sand, 2011).

Generally, all biofilms may lead to corrosion of metals by formation of aeration cells. Non-homogeneous biofilms will only partially cover a metal surface, creating cathodic oxygen-rich and anodic near-anoxic zones (by microbial respiration). This effect can be amplified by iron-oxidising bacteria which form so-called tubercles. The microbes oxidise Fe(II) ions to Fe(III) ions, which form dense, hard crusts of corrosion products around the cells, increasing the effect of differential aeration cells (Beech & Gaylarde, 1999). In contrast, sulphur-oxidising bacteria (e.g. *Acidithiobacillus ferrooxidans*) produce large amounts of sulphuric acid by oxidising compounds such as elemental sulphur, thiosulphate ($S_2O_3^{2-}$), trithionate ($S_3O_6^{2-}$), tetrathionate ($S_4O_6^{2-}$), and thiocyanate (SCN). Some species can withstand sulphuric acid concentrations of up to 12 % and pH values below 1. Consequently, strong acid-stress on the material may lead to pitting, crevice corrosion, or stress corrosion cracking (Thierry & Sand, 2011; Sand & Gehrke, 2003; Little, et al., 2000). On (highly) alloyed steels, manganese-oxidisers such as *Leptothrix discophora* may lead to an increase in the free corrosion potential (open circuit potential). This so-called ennoblement makes the material susceptible to severe chloride-induced pitting corrosion under otherwise non-critical conditions (Linhardt, 2006). The ennoblement is directly related to the metabolic oxidation of Mn(II)-ions from the aqueous phase to Mn(IV)-oxide, which then precipitates at the material surface. Usually, the passive nature of the material hinders the electron flow from

the metal towards oxygen in the aqueous phase and, hence, no corrosion occurs. Biomineralised Mn(IV)-precipitates act as a catalyst for the electron transport towards O_2, thus facilitating the break-down of the passive layer by chloride attack. Additionally, Mn(IV)-oxide itself may act as a direct oxidant (Kreikenbohm, et al., 2003).

1.3.2 MIC of metals under anaerobic conditions

In sterile anaerobic environments at near-neutral pH, the rates of proton reduction and, thus, iron dissolution are negligible, and iron-based materials are expected to last up to centuries (Enning, et al., 2012). However, there are several case studies demonstrating unexpectedly high corrosion rates, e.g. in buried pipes or marine structures, especially in the oil industry. Often, the corrosion rates are magnitudes higher than expected under these conditions: there are reports of extremely high pitting rates reducing the lifetime of oil subsea pipes to less than one year, where decades were originally predicted (Beech & Sunner, 2007). It is generally acknowledged that sulphate-reducing bacteria (SRB; more general sulphate-reducing prokaryotes, SRP) such as *Desulfovibrio vulgaris* are mainly responsible for these unexpected corrosion cases, particularly in environments with high sulphate content (Beech & Sunner, 2007; Hamilton, 1985; Lee, et al., 1995). Despite their importance for MIC and the vast amount of available literature dealing with SRP associated corrosion cases and phenomena, the underlying mechanisms are complex and still insufficiently understood (Beech & Sunner, 2007).

Already in 1934, von Wolzogen-Kühr and van der Vlugt recognised SRP as the corrosive agent when studying pitting corrosion on buried cast iron pipes in anoxic soil. They proposed a mechanism known as the cathodic-depolarisation-theory (CDT), in which the microorganisms use the iron itself as the only source of reducing equivalents for the sulphate reduction (Enning, et al., 2012; von Wolzogen-Kühr & van der Vlugt, 1934). However, the actual form of the reducing equivalents remained unclear. Due to the high affinity of SRP to hydrogen as growth substrate, molecular and even atomic (absorbed) hydrogen from the metal surface were considered as intermediate (Enning, et al., 2012; Coetser & Cloete, 2005; Booth & Tiller, 1960; von Wolzogen-Kühr, 1961; Bryant & Laishley, 1990). Figure 1 gives a schematic overview about the chemical processes involved in the CDT.

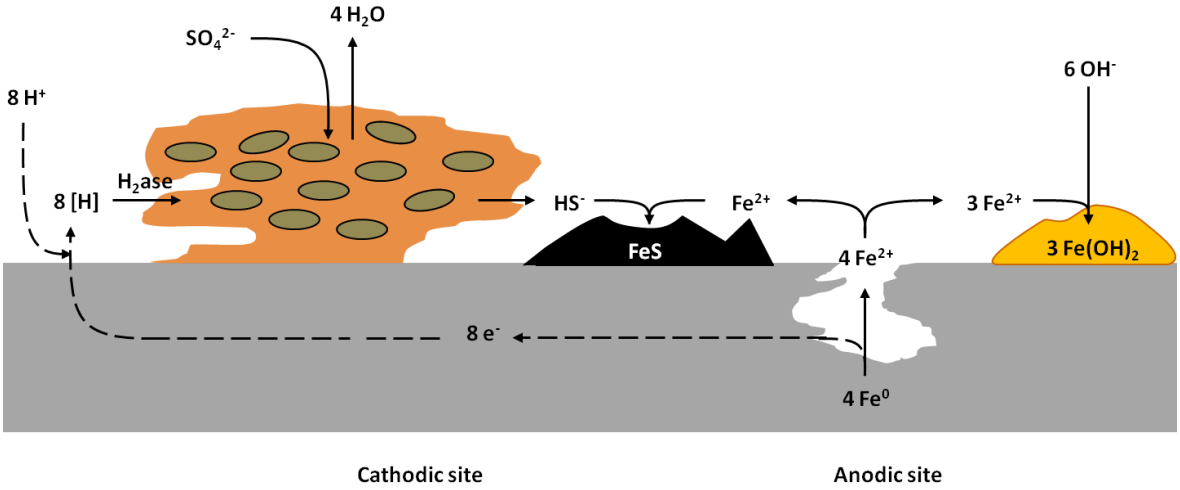

Figure 1 Schematic overview of the processes involved in MIC by SRP. Black lines indicate the reactions according to the cathodic-depolarisation-theory by von Wolzogen-Kühr, et al. (1934; scheme adapted from Dinh, 2003)

In brief, metal loses Fe(II) ions in aqueous solutions at the anodic site.

$$4\,Fe^0 \rightarrow 4\,Fe^{2+} + 8\,e^- \qquad (1)$$

The freed electrons react with protons from water dissociation to form hydrogen.

$$8\,H_2O \rightarrow 4\,H^+ + 8\,OH^- \qquad (2)$$

$$8\,H^+ + 8\,e^- \rightarrow 8\,H \qquad (3)$$

According to this model, SRP-hydrogenases scavenge the adsorbed hydrogen by catalysing its oxidation and the released electrons are used for sulphate-reduction.

$$SO_4{}^{2-} + 8\,H \rightarrow S^{2-} + 4\,H_2O \qquad (4)$$

Iron sulphide and iron hydroxide are formed as corrosion products, which precipitate.

$$Fe^{2+} + S^{2-} \rightarrow FeS\downarrow \qquad (5)$$

$$3\,Fe^{2+} + 6\,OH^- \rightarrow 3\,Fe(OH)_2\downarrow \qquad (6)$$

Iron sulphide acts as a galvanic couple together with metallic iron and increases the cathodic area. This results in a strong acceleration of the corrosion process by stimulating anodic processes. The overall net reaction can finally be summarised as

$$4\,Fe + SO_4{}^{2-} + 4\,H_2O \rightarrow 3\,Fe(OH)_2\downarrow + FeS + 2\,OH^-. \qquad (7)$$

The term "depolarisation" already indicates an undefined change in the electrochemical response of the system to the presence of the bacteria; the highly effective hydrogen scavenging of the SRP is thought to "pull" the primary oxidation (Enning, et al., 2012). In general,

the CDT represents an alternative to the classical hydrogen evolution by (electro)chemical desorption of adsorbed hydrogen. The chemical desorption is based on the combination reaction of 2 H_{ad} to H_2, whereas electrochemical desorption is caused by the reaction of H_{ad} with a hydrogen ion and an electron to H_2. In both cases, the desorption steps are rate-determining due to the increased activation energy needed compared to the discharge of hydrogen ions (Kuklinski & Sand, 2014).

However, the CDT is highly disputed and several authors are critical to the accelerated anaerobic corrosion due to H_2 utilisation (Venzlaff, et al., 2013; Enning, et al., 2012; Dinh, et al., 2004; Crolet, et al., 1993; Iverson, 1983; Schaschl, 1980; Costello, 1974; King, et al., 1973). Especially the role of hydrogenases still is subject to discussions due to contradictory results from several different studies.

Booth and Tiller (1960) demonstrated that hydrogenase-positive *Desulfovibrio desulfuricans* and hydrogenase-negative *Desulfovibrio orientis* both produced sulphide ions, followed by anodic polarisation due to the formation of a partially protective sulphide-layer. However, cathodic depolarisation was only observed in case of the hydrogenase-active *Desulfovibrio desulfuricans*. Case studies on oil pipeline corrosion revealed a direct correlation between hydrogenase activity and corrosion rates, even considering increased cell numbers of hydrogenase-negative SRP (Bryant, et al., 1991). Additionally, hydrogenase-positive SRP of the genus *Desulfovibrio* produced increased amounts of sulphide in anaerobic corrosion experiments compared to their hydrogenase-negative counterparts. The authors proposed that increased sulphide concentrations were caused by an increased metabolic activity of the hydrogenase-positive microbes due to their ability to use cathodically produced hydrogen in addition to lactate as electron donor for the sulphate-reduction (Cord-Ruwisch & Widdel, 1986).

To the contrary, several (kinetic) studies demonstrated that H_2 scavenging did not accelerate iron (aut)oxidation, i.e. did not "pull" this reaction as proposed before. Spruit and Wanklyn (1951) observed that in autotrophic growth of *Desulfovibrio desulfuricans* the ratio of corroded iron to reduced sulphate was much greater (up to 48) than the theoretical limiting value of 4 predicted by the cathodic depolarisation theory (von Wolzogen-Kühr & van der Vlugt, 1934). This indicates that not all the liberated hydrogen is used for sulphate reduction and, based on their observations, the authors proposed a loss by evolution of

hydrogen gas (Spruit & Wanklyn, 1951). In a more recent study, Mori, et al., (2010) investigated the general influence of hydrogen-consuming microorganisms such as acetogens, sulphate-reducing bacteria, and methanogens. All organisms consumed hydrogen chemically generated by iron granules that were provided as sole electron donor, but did not significantly induce corrosion on the granules. Venzlaff, et al., (2013) questioned the role of hydrogenases from a thermodynamical point of view: The redox potential of the electron donor (eq. 1) is more negative than that of the electron acceptor (eq. 2) and the reaction of oxidation of iron by H^+ may happen spontaneously. To stop this spontaneous reaction, a hydrogen film would have to build up on the surface with a local fugacity of $p_{H_2} > 10^{11.3}\ Pa$ which is extremely unrealistic considering the extremely fast diffusion of H_2 (which is used by the bacteria). A direct influence of SRP on corrosion seems only possible from a electrokinetic point of view via the reduction of H^+ to H_2. However, at neutral pH, H_2 formation on iron is slow due to limited proton availability and combination reactions forming H_2.

Several alternative mechanisms have been proposed to overcome the questionable role of hydrogenases (table 1). In all these models, SRP stimulate corrosion indirectly by chemical reaction of their metabolites such as H_2S (by precipitation as FeS), elemental sulphur or corrosive iron phosphates (Venzlaff, et al., 2013; Iverson, 1983; King, et al., 1973), with except of the electrical MIC (EMIC) theory (Venzlaff, et al., 2013; Enning, et al., 2012; Dinh, et al., 2004).

Table 1 Alternative mechanisms to the cathodic depolarisation theory (modified from Thierry & Sand, 2011)

Name referred to in literature	Main mechanisms	Role of hydrogenases for corrosion	References
Depolarisation by H_2S	Cathodic reduction of microbiologically produced hydrogen sulphide	Secondary; Production of H_2S	Hardy, 1983; Costello, 1974; Booth, et al., 1968
Depolarisation by $FeSO_4$	Formation of an iron/iron sulphide galvanic cell, iron sulphide acting as the site for cathodic reduction of molecular hydrogen	Secondary; Regeneration of $FeSO_4$	King, et al., 1973
Elemental sulphur	Formation of a concentration cell with elemental sulphur acting as the reactant	Secondary; Production of S^0	Schaschl, 1980
Iverson's mechanism	Production of a volatile and corrosive iron phosphate metabolite	Not defined	Iverson, 1983
Local acidification of anodes	Localised acidification of anodes due to the formation of iron sulphide corrosion products	None	Crolet, et al., 1993
Electrical microbiologically influenced corrosion (EMIC)	Direct electron transfer from material surface to cells	May facilitate electron flow from Fe to the sulphate reduction enzymes via Fe → cytochrome → H_2ase(1) → H_2 → H_2ase(2) → electron transport system → sulphate reduction enzymes; may also have no influence on corrosion and function only in growth with external hydrogen	Venzlaff, et al., 2013; Enning, et al., 2012; Dinh, et al., 2004

Electrical microbiologically influenced corrosion (EMIC)

The EMIC theory is based on observations made with SRB strains isolated from marine soil by growing on iron as sole electron-donor and CO_2 or CO_2 plus acetate as carbon source (Dinh, et al., 2004). Two strains, IS4 and IS5, belonging to the genus *Desulfobacterium* and *Desulfovibrio*, respectively, showed higher rates of sulphate-reduction than possible by mere H_2-scavenging. They severely corroded the metallic substratum, reaching corrosion rates of up to 0.7 mmpy, whereas the H_2-scavenging controls were not corrosive under the same conditions (Enning, et al., 2012; Dinh, et al., 2004). Because of the speed of sulphate reduction, these organisms must obtain reducing equivalents more efficiently, bypassing H_2 as a transporter. Additionally, H_2 accumulated in cultures of strain IS4 with iron, and thus cannot be the rate-limiting intermediate. The authors proposed that efficient use of metallic iron for sulphate reduction would only be possible by direct electron uptake via cell-surface-associated redox-active components (Dinh, et al., 2004). In case of *Desulfovibrio vulgaris*, cytochromes have been suggested to participate in iron corrosion by allowing an electron flow from the metal (via cytochrome and periplasmic hydrogenase 1 to H_2 to a second hydrogenase) into the electron transport system and finally to the sulphate reduction enzymes (Laishley & Bryant, 2003). The accumulation of H_2, however, does not necessarily indicate that H_2 is a direct biochemical intermediate connecting two hydrogenases but may as well be formed via a branch because of an imbalance between electron donation by fresh iron and electron consumption by sulphate reduction. From further studies, Enning, et al., (2012) proposed a scheme of the stoichiometry of direct (lithotrophic) corrosion (figure 2).

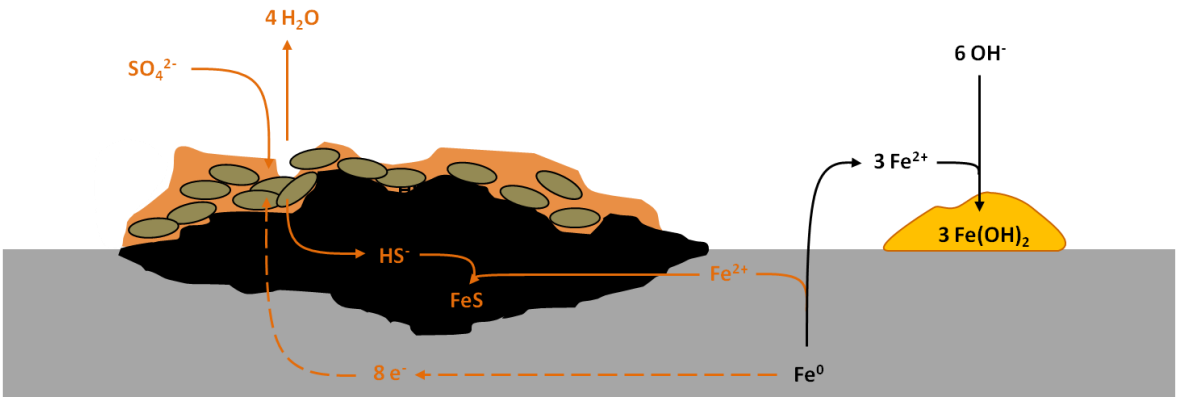

Figure 2 Proposed mechanism of direct electron transfer from metal to SRP. Orange lines indicate electron flow and chemical processes according to the electrical microbiologically influenced corrosion (EMIC; Enning, et al., 2012)

In contrast to the CDT, the increase in the cathodic area due to FeS deposits does not lead to any catalytic enhancement of the abiotic cathodic proton reduction. Instead, FeS acts as a semiconductor mediating the electron flow from the metal to the cells (Venzlaff, et al., 2013).

From the different theories regarding MIC by SRP it becomes obvious that the exact corrosion mechanism is still unclear. Furthermore, the possible role of EPS in biocorrosion is not taken into consideration in all these models. And yet, Beech, et al., (1998) found evidence for the direct involvement of a high molecular weight, thermostable protein in pitting corrosion of mild steel by *Desulfovibrio indonesiensis*. Generally, negatively charged EPS constituents are likely to be involved in electrostatic interactions with multivalent cations such as Ca(II), Cu(II), or Fe(II)/Fe(III) (Beech & Sunner, 2007). Based on this ability, Beech and Sunner (2004) proposed a model of iron corrosion involving EPS similar to that of metal sulphide dissolution by acidophilic bacteria such as *Acidithiobacillus ferrooxidans* (Rohwerder, et al., 2003; Sand, et al., 1995): EPS-bound Fe(III) ions are reduced to Fe(II) ions through direct electron transfer from the base metal. (Re)oxidation of Fe(II) ions results in electron transfer to the final electron acceptor, probably through a series of redox reactions (Beech & Sunner, 2007; Beech & Sunner, 2004). However, the influence of organic and inorganic EPS constituents in direct proximity to the surface on the corrosion process has yet to be determined (Beech & Sunner, 2007).

In conclusion, anaerobic microbial corrosion by SRP is a complex field depending on various factors such as chemical effects of the metabolites as well as physical microbe-metal interactions. Although direct electron uptake may present a central mechanism (Venzlaff, et al., 2013), it should be noted that its role for MIC by *Desulfovibrio vulgaris* (the model organism used in this work) remains purely speculative.

1.4 MICI - microbiologically influenced corrosion inhibition

The microbiological influence on materials is not always detrimental. Contrary to their role in MIC, microorganisms can exhibit protective effects to materials - a phenomenon known as microbiologically influenced corrosion inhibition (MICI) (Videla & Herrera, 2009; Little & Ray, 2002). Like MIC, MICI in its widest sense can be used to describe corrosion mitigating effects on various materials, including concrete, plastics or metals. However, in literature

MICI is primarily used in conjunction with the protection of metallic materials such as iron, steel, copper or aluminium against corrosion of both environmental or microbiological origin (Kuklinski & Sand, 2014; Thierry & Sand, 2011; Nagiub & Mansfeld, 2001).

Also, MICI is usually caused by biofilms rather than by planktonic microorganisms. Thanks to the complexity of biofilms, the mechanisms involved in MICI are also far more complex than these in classical corrosion protection e.g. by corrosion inhibitors, where usually only a single electrochemical mechanism causes the protective effect. The dynamic nature of biofilms additionally hampers the identification of single electrochemical mechanisms (Kuklinski & Sand, 2014). Furthermore, several metabolically diverse species from different habitats seem to have protective effects. Interestingly, some microorganisms can, depending on material and environment, be both protective and detrimental (San, et al., 2014; Juzeliunas, et al., 2007; Mansfeld, 2007). Currently, it is often not possible to deduce the relevant electrochemical mechanisms for MICI for a certain species. Therefore, the categorisation of the protective mechanisms in groups of common characteristics seems to be the most reasonable approach to understand MICI (Kuklinski & Sand, 2014).

Different classifications have been proposed in literature. Zuo (2007) proposed the discrimination of mechanisms along three different groups: (I) the removal of corrosive agents, (II) the inhibition of cell adhesion or biofilm growth of detrimental organisms, and (III) the formation of protective layers. Another classification along only two major groups was proposed by Videla and Herrera (2009) who differentiate between the (I) neutralisation of corrosive agents and (II) the formation of protective films. Several of the mechanisms discussed in literature could be assigned to both groups, demonstrating the issues with such an artificial division. But taking the need for a direct contact between cells and material surface into consideration helps classifying the mechanisms.

For the first group, an intimate contact between the cells and the surface is not strictly necessary. For example, strong oxygen consumption in the surrounding medium might already slightly decrease the corrosion rates of metal (Dubiel, et al., 2002). However, a direct contact will strongly increase the protective effect. In contrast, the formation of protective films inevitably needs direct contact to establish sufficiently dense films. The same is true for the need of respiring bacteria. All mechanisms mentioned in the first group need actively respiring bacteria to maintain the protective effect. If the active cell metabolism

stops, e.g. the oxygen concentration (and consequently the corrosion rate) might increase again. For the second group, also non-respiring cells might be sufficient to maintain a protective effect after the initial formation of the films or barriers. However, also in this case actively respiring microorganisms will increase the protective effect considerably (Kuklinski & Sand, 2014).

Table 2 provides a brief overview about the seven mechanisms most frequently mentioned in literature, the group they have been assigned to in this thesis as well as the respective bacterial species involved.

Table 2 Mechanisms in MICI and involved microorganisms (modified from Kuklinski & Sand, 2014)

Group	Mechanism	Microorganisms	References
Neutralisation of corrosive agents	Oxygen consumption	*Escherichia coli* DH5α, *Pseudomonas fragi*, *Pseudomonas* sp. S9, *Serratia marcescens, Shewanella oneidensis**	Pedersen, et al., 2009; Dubiel, et al., 2002; Jayaraman, et al., 1997b
	Competition for electron donors	*Arthrobacter sp., Bacillus polymyxa, Micrococcus sp., Pseudomonas sp., Vibrio sp.*	Roberts, 1947; Potekhina, et al., 1999
	Secretion of corrosion inhibitors	*Bacillus licheniformis**, *Bacillus subtilis*[#], *Paracoccus denitrificans*	Örnek, et al., 2002; Örnek, et al., 2001; Hansen, et al., 1996
Formation of protective films	Diffusion barriers	*Aeromonas salmonicida*, *Clavibacter michiganensis, Pseudomonas aeruginosa*	San, et al., 2014; San, et al., 2012; Werner, et al., 1998
	Passivating (oxide) films	*Pseudomonas cichorii, Pseudomonas putida, Ralstonia eutropha, Rhodococcus* sp. strain C125	Chongdar, et al., 2005; Da Silva, et al., 2004; Volkland, et al., 2000a; Volkland, et al., 2000b
	Induction of surface composition changes	*Bacillus mycoides*, *Lactobacillus helveticus, Pseudomonas fluorescens*	Juzeliunas, et al., 2007; Meylheuc, et al., 2006
	Prevention of microbial adhesion and/or biofilm formation	*Aneurinibacillus migulanus*[†], *Bacillus brevis*[†], *Bacillus parabrevis*[†], *Bacillus subtilis*[†]*, *Paenibacillus polymyxa*[†], *Staphylococcus sciuri*[†], *Desulfovibrio alaskensis*[‡], *Desulfovibrio vulgaris*[‡], *Lactobacillus acidophilus*[‡], *Lactobacillus casei*[‡], *Lactobacillus fermentum*[‡], *Pseudomonas aeruginosa, Pseudomonas NCIMB 2021*[‡]	de Araujo, et al., 2011; Gana, et al., 2011; Zeraik, et al., 2010; Stadler, et al., 2010; Morikawa, 2006; de Paiva, 2004; Zuo, et al., 2004; Leriche, et al., 2000; Gubner, et al., 2000; Jayaraman, et al., 1999b; Jayaraman, et al., 1999a; Velraeds, et al., 1996; Neu, 1992

**genetically modified*

[†]excretion of antimicrobials (growth inhibition), [‡]adhesion-inhibition of detrimental microorganisms

Oxygen consumption

Pure biofilms of *Pseudomonas fragi* and *Escherichia coli* DH5α reduced the corrosion of SAE 1018 steel in batch cultures up to 10-fold compared to sterile controls. The corrosion rates were comparable to the respective anaerobic sterile medium (Jayaraman, et al., 1997b; Jayaraman, et al., 1997a). Electrochemical measurements further demonstrated that in continuous flow reactors, biofilms of both organisms could reduce the corrosion rates 10-fold compared to an aerobic sterile medium over a period of 14 days. Further experiments with inactivated biofilms (by glutaraldehyde or kanamycin treatment) clearly showed that the biofilms did not act as a passive barrier but actively respiring cells were necessary to achieve the protective effect. Control experiments with anaerobic sterile media indicated oxygen consumption to be the main protective mechanism under these conditions. In case of *Pseudomonas fragi*, other studies showed an up to 20-fold decrease in corrosion rates on mild steel under continuous flow. It was demonstrated that the strong corrosion-reducing effect of this organisms could not be explained by oxygen consumption only. However, the exact mechanism remained unknown (Ismail, et al., 2002). Oxygen-depletion was also identified as the cause for corrosion-reduction by *Shewanella oneidensis* (Dubiel, et al., 2002). The bacterium reduces Fe(III) to Fe(II), which protects the steel surface by scavenging free oxygen. Additionally, by using mutants unable to form biofilms, the authors demonstrated that both planktonic cells and biofilms reduced corrosion rates, but the reduction was significantly reduced for the planktonic cells. Another member of the *Pseudomonadaceae*, *Pseudomonas* sp. S9, as well as the marine *Serratia marcescens* EF190 also reduced corrosion of SIS 1146 steel. Interestingly, in absence of nutrients both organisms did no longer show protective effects but enhanced deterioration of the material, with a stronger corrosion observed for *Serratia marcescens* (Pedersen & Hermansson, 2009).

Competition for electron donors

Fe(III)-reducing bacteria such as *Arthrobacter* sp., *Bacillus polymyxa* and *Micrococcus* sp. have been shown to be able to strongly reduce corrosion of metals by MIC. Anaerobic industrial or natural environments are frequently colonised by sulphate-reducers, denitrifiers, Fe(III)- and Mn(IV)-reducers, methanogens or sulphidogens. Fe(III)-reducers have an increased affinity for relevant substrates such as hydrogen and acetate, and thus directly

compete with other organisms depending on these substrates (such as aforementioned SRP, methano- and sulphidogenic bacteria). Eventually, this may lead to a strong decrease of these potentially detrimental organisms in the environment (Potekhina, et al., 1999). In natural deposits, Lovley and Phillips (1987) observed that in presence of Fe(III)-reducing bacteria the residual levels of molecular hydrogen and acetate are significantly lower than in deposits where only methanogenic or sulphidogenic bacteria were present. By artificially introducing Fe(III) into such deposits, the activity of both methanogenic and sulphidogenic organisms was reduced by 95 %. As stated before, under aerobic conditions Fe(III)-reduction additionally leads to a decline in oxygen concentration, further increasing the protective effect of e.g. *Shewanella oneidensis* (Dubiel, et al., 2002). Under anaerobic conditions, Fe(III)-reducing bacteria from the genera *Pseudomonas*, *Micrococcus*, *Arthrobacter* and *Vibrio* can remove up to 90 % of corrosion products already formed on the metal surfaces. When introduced into technical systems containing SRP and other corrosive microorganisms, these organisms did not only remove the corrosion products but also protected the metal surface against further corrosion. It is assumed that the protective effect is not only based on the destruction of ecological niches for detrimental organisms but also on the ability of the microorganisms to transfer electrons and protons to and from the metal surface by establishing a galvanic couple. This may lead to the formation of a passivating layer of absorbed hydrogen (H_{ad}) on the surface (Potekhina, et al., 1999). The exact mechanism of electron transfer between cells and surface is still unknown, but recent studies with *Shewanella oneidensis* MR-1 and *Shewanella* sp. MR-4 on poised electrodes suggest that riboflavins might act as soluble redox shuttles (Marsili, et al., 2008; von Canstein, et al., 2008). Additionally, type IV pili and outer membrane cytochromes may be involved (Richter, et al., 2009).

Secretion of corrosion inhibitors

Polyglutamate- or polyaspartate-producing mutants of *Bacillus licheniformis* and *Bacillus subtilis* have been found to stronger protect aluminium 2024 against pitting in artificial seawater compared to their wild types. Electrochemical measurements indicated a passivating effect of these biopolymers (Örnek, et al., 2001). Possibly, the protective effect of both intermediates is caused by carboxylic aluminium-chelating groups. It can be speculated that the lower protective efficacy of polyaspartate versus polyglutamate may be related to its

structural nature and/or the concentration of the respective anionic peptide in solution (Kuklinski & Sand, 2014). The same experiments indicated that also the wild types might produce another substance able to stop pitting, because the protective effect could not be related solely to the formation of anaerobic conditions at the aluminium surface by microbial oxygen consumption (Örnek, et al., 2001). This observation helped to explain the protective effect of the same bacteria on brass in non-marine media. Also in this case the protective effect was stronger than explained by oxygen consumption alone, so it was speculated that an unknown corrosion inhibitor played a significant role. However, in this case the polyglutamate- or polyaspartate-producing mutants did not further increase the protective effect (Örnek, et al., 2002). Another substance class of interest are the so-called siderophores, iron-chelating oligopeptides. They are produced by virtually all organisms at neutral pH. The protective effect of siderophores on pitting of aluminium has been demonstrated by Hansen and McCafferty (1996). The catechol-containing siderophore parabactin, produced by *Paracoccus denitrificans* (Peterson & Neilands, 1979), showed an inhibitive effect on the critical pitting potential of aluminium. Additionally, it increased the polarisation resistance of the material with time. Siderophores also exhibit protective effects on stainless steel under marine conditions by enhancing the passivity of the material. Eashwar and co-authors (1995b; 1995a) proposed that this enhancement is caused by decreasing the passivation current i_p. They also predicted that maximum siderophore production and ennoblement occur at pH 8. Although this theory has not been thoroughly tested, it explained observations that ennoblement (increased corrosion potentials E_{corr}) has been maintained over long periods without any signs of localised corrosion. Additionally, the suppression of siderophore production by addition of respiratory inhibitors supposedly led to a strong reduction of E_{corr} (Little, et al., 2008).

Diffusion barriers

Biofilms may act as passive diffusion barriers against various corrosive agents such as chloride ions and acidic compounds. In contrast to oxygen consumption where active cell respiration is inevitable, protection based on diffusion barriers may already be exerted by dead cells or EPS-footprints (Kuklinski & Sand, 2014). Werner, et al., (1998) observed an unexpected protective effect of usually detrimental SRP against chloride-induced pitting

corrosion of stainless steel 304. The authors found that the pitting potential was significantly lower than expected from the level of corrosive H_2S produced by the microorganisms. Additionally, the metastable pitting rate was significantly decreased compared to abiotic controls. The protective effect of the SRP is probably related to less diffusion of the aggressive chloride ions to the metal surface suggesting the biofilm matrix acts as a passive barrier (Kuklinski & Sand, 2014). This theory was recently supported by San, et al., (2014) who demonstrated that biofilms of *Pseudomonas aeruginosa* protect NiZn alloys against corrosion in chloride-containing media. EDS data from this study shows lower concentrations of chloride on the surfaces covered with biofilms compared to abiotic controls. However, the protective effect might additionally be related to oxygen consumption by the biofilms. Similar results were found for *Aeromonas salmonicida* and *Clavibacter michiganensis* on NiCo alloys (San, et al., 2012). Additionally, microorganisms may protect metals against hydrogen embrittlement in sour acidic environments. These environments are particularly aggressive due to sulphide poisoning of the hydrogen recombination reaction at the surface which causes the presence of high amounts of hydrogen directly at the metal surface. These processes may be altered in the presence of an organic film like the EPS matrix. Additionally, the adsorption of hydrogen by the metal surface may be reduced (Videla & Herrera, 2009). However, to date this protective effect remains speculative.

Passivating oxide films

The microbially influenced formation of oxide films has first been reported by Volkland, et al., (2000b; 2000a). They demonstrated that in phosphate-buffered solutions with ≥ 20 mM phosphate, biofilms of *Rhodococcus* sp. strain C125 and *Pseudomonas putida* m2 induced the formation of passivating vivianite ($Fe_3(PO_4)_2$ x 8 H_2O) films and reconditioned already existing vivianite coatings. The reaction of the iron oxide layer on the corroding steel surface with phosphate forming these films is most likely related to the bacterial oxygen consumption directly at the metal surface. In absence of active cells or at low cell density no formation of the vivianite layers was observed, indicating that microbial oxygen consumption directly at the surface was causal. This assumption is supported by the fact that other aerobic microorganisms such as *Pseudomonas aeruginosa* PO1, *Pseudomonas putida* WCS358, *Pseudomonas fluorescens* p62 and *Escherichia coli* ML30 showed a similar vivianite-inducing effect, but to a much lesser extent. Additionally, due to the observation that

re-phosphating took only place when trace elements were omitted from the medium, the authors speculated that siderophores might be involved in this process (Volkland, et al., 2001a). Another mechanism was proposed by Da Silva and co-authors (2004) indicating that hydrogenases from *Ralstonia eutropha* could induce the production of vivianite even when separating the microorganism from the electrode surface by dialysis membranes. Regarding MIC, vivianite-coated mild steel coupons were protected against corrosion by SRP for more than two weeks. A film thickness of 2-3 µm was sufficient to achieve this protective effect (Volkland, et al., 2001b). The production of phosphate-oxide films has also been observed for *Pseudomonas cichorii* (Chongdar, et al., 2005). The phosphate film contained high amount of bacterial EPS, indicating the formation of iron-EPS complexes. However, it is not clear whether the EPS contributed to the protective effect of the phosphate film.

Induction of changes of chemical surface properties

It has been demonstrated that biosurfactants can cause surface composition changes on alloyed steel as well as to influence the formation of oxide films on aluminium in atmosphere. Biosurfactants are surface-active compounds produced by a wide variety of microorganisms. Low-molecular-weight surfactants can reduce surface tensions while high-molecular-weight compounds bind tightly to surfaces (Ron & Rosenberg, 2001). Chemical structure and surface affinity of the surfactants depend on several factors such as the excreting microorganism, nutrients, and temperature (Kuklinski & Sand, 2014). Consequently, an enormous amount of different biosurfactants serving different roles exist, which are e.g. antibacterial, increase the bioavailability of hydrophobic substrates or regulate the surface-covering by microorganisms (Ron & Rosenberg, 2001). Biosurfactants produced by *Lactobacillus helveticus* 1181 and *Pseudomonas fluorescens* 495 were shown to reduce the pitting susceptibility of stainless steel (Meylheuc, et al., 2006). These surfactants formed dense organic films on the surface and caused a segregation of chromium towards the metal surface, which strongly increased its resistance. Additionally, the surfactants modified the acid-base characteristics of the surface and reduced the formation of biofilms by *Listeria monocytogenes*. For aluminium, Juzeliunas, et al., (2007) demonstrated that biofilms of *Bacillus mycoides* significantly reduced corrosion over a period of up to 12 months when the working material was exposed to the atmosphere. Electroimpedance spectra (EIS) showed the formation of a two-layer structure with an inner oxide film and an outer

biofilm. Compared to sterile (corroded) controls, the oxide layer in presence of microorganisms was about 3-fold thinner but, at the same time, its resistance was roughly 3-fold increased (8.2 kΩcm^2 vs. 31.3 kΩcm^2), indicating a structural change in the oxide layer. The authors concluded that the protective effect of the biofilm was related to the increased charge transfer resistance of the altered oxide film. However, no further data regarding the structure of the oxide films is available. Hence, this structural change still needs to be confirmed.

Prevention of microbial adhesion and biofilm formation

Several biofilm-forming microorganisms show a reducing impact on the formation of corroding layers on steel and, thus, a MIC-mitigating effect. Usually, the mechanism is based on secretion of antimicrobial substances. Gramicidin S producing biofilms of *Bacillus brevis* reduced the formation of detrimental biofilms of sulphate-reducing *Desulfovibrio vulgaris* and thus corrosion of mild steel in static batch cultures (Jayaraman, et al., 1999a). Genetically engineered 2 day old biofilms of *Bacillus subtilis* producing the antimicrobials indolicidin and bactenicin reduced corrosion of mild steel 6 to 12-fold in continuous reactors over a period of up to 300 h while the population of *Desulfovibrio vulgaris* was 36-fold reduced (Jayaraman, et al., 1999b). Zuo and Wood (2004) also used gramicidin-S-producing *Bacillus brevis* to protect mild steel against MIC by both the sulphate-reducing *Desulfosporosinus orientis* and Fe-reducing *Leptothrix discophora*. When biofilms of *Bacillus brevis* were grown on mild steel coupons, the corrosion rates were (based on EIS data) approximately 20-fold lower compared to biofilms of *Paenibacillus polymyxa* used as not gramicidin producing controls (corrosion rates of 25 and 111 mmpy, respectively). In terms of weight-loss, a 4-fold reduction was achieved. After 13 days of incubation, SEM images showed that the steel surface beneath the protective biofilm remained largely unharmed, with polishing grooves still being intact and without visible formation of corrosion products (Zuo & Wood, 2004). The same authors used gramicidin S producing strains of *Aneurinibacillus migulanus* ATCC 9999 (previously *Bacillus migulanus* 9999), *Bacillus brevis* Nagano, and *Bacillus brevis* 18-3, gramicidin and tyrocidine-producing *Bacillus parabrevis* ATCC 10068 (previously *Bacillus brevis* 10068), polymyxin-producing *Pseudomonas polymyxa* ATCC 10401 (previously *Bacillus polymyxa* 10401), as well as the subtilin-producing *Bacillus subtilis* ATCC 6633 to assess their potential to decrease corrosion of mild steel in process

water from the three-mile-island nuclear power plant. Additionally, an artificial antimicrobial consortium producing gramicidin, gatavalin, polymyxin, subtilin, and tyrocidine consisting of *Bacillus brevis* 18–3, *Bacillus brevis* Nagano, *Bacillus subtilis* ATCC 6633, *Pseudomonas polymyxa* ATCC 21830 (previously *Bacillus polymyxa* 21830), *Bacillus parabrevis* 10068, *Bacillus circulans* ATCC 31228, and *Acidianus migulanus* ATCC 9999 was applied as a protective biofilm on mild steel against sulphate-reducing *Desulfovibrio orientis* and *Desulfovibrio vulgaris*. Electrochemical impedance data clearly showed the inhibition of the SRB by biofilms producing gramicidin S. By washing out planktonic cells from the batch cultures it was demonstrated that the antimicrobial effect was caused by the biofilms rather than planktonic cells. Metal coupons covered with gramicidin S producing biofilms showed no signs of corrosion (i.e. iron sulphide film formation) after exposure to *Desulfovibrio orientis* (in Baars' medium) or *Desulfovibrio vulgaris* (in process water) during the whole test period of 6 or 12 days, respectively. To test whether a protective consortium could be applied to protect steel against MIC by simple inoculation and without the need to pre-grow biofilms, a mixture of the protective consortium was added to continuous flow reactors together with process water containing *Desulfovibrio vulgaris*. Biofilms of the antimicrobial consortium delayed the growth of *Desulfovibrio vulgaris*, protected mild steel (for one more day compared to non-antimicrobial controls), and decreased the corrosion rate 2- to 10-fold (50 - 90 %) for up to 8 days (based on impedance data). However, after 12 days no significant difference in mass loss between protective and non-protective biofilms (corrosion rates of 77 mmpy vs. 85 mmpy) was observed. The authors concluded that the protective effect was based on the spatial separation of detrimental SRB from the surface as well as a general reduction in their cell numbers. Additionally, oxygen consumption by the protective biofilms reduced the corrosion rates further. The latter was also observed for non-protective control biofilms not producing any antimicrobial substances, but corrosion reduction was much higher in presence of the protective biofilms (Zuo, et al., 2004). Gana, et al., (2011) demonstrated the antagonistic effect of *Bacillus* sp. strain B21 on a consortium of SRP isolated from the In-Amenas oilfield in the southern Algerian Sahara. When compared with a chemical biocide commonly used in the oil industry (THPS, tetrakishydroxymethylphosphonium sulphate), the antimicrobial effect of strain B21 co-cultured with the SRP consortium was significantly increased.

1.4.1 Biogenic inhibitors

Due to the European Biocidal Product Directive, several effective agents against MIC such as tributyltin compounds have already been banned or will be forbidden soon (Regulation 528/2012; European Parliament and Council, 2012). Considering this ban, studies about eco-friendly biogenic alternatives gained interest and several new studies were conducted. Substances ranging from the sulphur-containing amino acid methionine (Oguzie, et al., 2007) over plant extracts (Oguzie, et al., 2010; Oguzie, 2008; Oguzie, 2007) and crude mixtures of extracts from green algae or cashew nuts (Loto, et al., 2011; Loto, 2005; Tadros, 2005) to saccharides (Müller, 2002; Beccaria & Mor, 1978) were investigated. These substances showed protective effects on various materials in different environments, but most of the studies were of pure empirical nature lacking any systematic approach.

Based on the assumption that most of the protective effects of biofilms can be attributed to their EPS, Stadler, et al., (2008) studied cell-free EPS extracts from 14 different microorganisms as biogenic alternatives to the approaches. The study included 3 different SRP of the genus *Desulfovibrio*, 5 different *Pseudomonadaceae*, 2 different *Lactobacilli*, *Rhodococcus opacus*, *Citrobacter freundii*, *Enterobacter aerogenes*, and *Arthrobacter* sp. All these organisms had been described as protective in several studies regarding MIC or the prevention of bacterial attachment. The authors identified several EPS as promising for further research, including those from *Desulfovibrio alaskensis* and *Desulfovibrio vulgaris*. In another study, Stadler, et al., (2010) further investigated the influence of EPS from the latter organism on biofilm formation of SRP of the same genus and found a strongly decreased attachment of this detrimental organisms in short-term experiments. However, the strong heterogeneity of the crude EPS extracts causes inhomogeneous film formation on the surfaces, strongly influencing an electrochemical assessment of their protective properties. Dong, et al., (2011) added EPS from thermophilic SRP to the bulk solution and protecting the underlying steel supposedly by hindering the oxygen reduction. The effect was strongly dependent on the concentration of the crude EPS extract and excessive amounts became detrimental instead, possibly by chelating Fe(II) ions from the cathodic sites and thus shifting the equilibrium to further metal dissolution.

In addition to their protective potential against "classical" electrochemical corrosion, EPS and EPS-analogue substances can reduce the initial attachment and thus biofilm formation

of detrimental organisms, rendering them particularly interesting for MIC issues. The ability of biosurfactants (a part of the EPS-matrix) to label surfaces as covered and thus prevent adhesion was described by Neu (1996; 1992) as "microbial footprints". Amongst the organisms leaving such footprints are *Acinetobacter calcoaceticus*, *Streptococcus cricetus* and *Streptococcus mitis*. For the latter two, the adhesion-reducing effect on other and organisms of the same species has been demonstrated (Neu, 1996; Cowan & Busscher, 1993; Pratt-Terpstra, et al., 1989). Biosurfactants from two different *Lactobacillus isolates* (*Lactobacillus fermentum* B54 and *Lactobacillus acidophilus* RC14) reduced the initial adhesion (up to 4 h after inoculation) of *Enterococcus faecalis* to glass in flow-cell experiments by up to 77 % compared to untreated surfaces (Velraeds, et al., 1996). From FTIR spectra comparing anti-adhesive biosurfactants with these from *Lactobacillus casei* subsp. *rhamnosus* 36 (which showed no reducing effect) the authors concluded that a protein-like substance was responsible for this effect (Velraeds, et al., 1996). This assumption is supported by another study investigating the effect of EPS on attachment of *Burkholderia cepacia* and *Pseudomonas aeruginosa*. Hwang, et al., (2012) attributed the adhesion-reducing effect of proteins to increased steric repulsion in high-ionic strength conditions and developed a mathematical model for bacterial adhesion behaviour considering their observations. Leriche and Carpentier (2000) observed that biofilms of *Staphylococcus sciuri* significantly reduced attachment of *Listeria monocytogenes* to stainless steel surfaces. The authors found a direct correlation between EPS content and adhesion-reduction indicating that the anti-adhesive effect was caused by EPS rather than cell-to-cell interactions. However, no experiments using pure (cell-free) EPS were performed to further support this assumption. A more systematic approach to the anti-adhesive properties of EPS was done by Gubner and Beech (2000). The authors investigated three different types of EPS, (I) "planktonic" EPS released into the medium, (II) "capsular" EPS from planktonic cells, and (III) EPS from biofilm cells grown on stainless steel (all produced by continuous cultures of *Pseudomonas* NCIMB 2021) on their anti-adhesive effect using two different stainless steels (AISI 304 and 316, respectively). All three types of EPS reduced the attachment of the same species considerably, however to a varying degree that also depended on the steel grade. No correlation between hydrophobicity or roughness to the reducing effect was found. At a concentration of 0.5 mg mL^{-1}, capsular EPS from planktonic cells showed the lowest number of microorganisms attached to the working materials. EPS from biofilm cells, in contrast,

slightly increased microbial attachment. Based on FTIR analyses the authors concluded that the anti-adhesive effect is depending on the different chemical composition of the EPS extracts. Capsular EPS from planktonic cells were proven to be the most effective extracts showing significantly lower amounts of uronic acid residues as well as a considerably different protein structure compared to the other ones. More recently, de Paiva (2004) demonstrated that coatings with EPS extracts from sulphate-reducing *Desulfovibrio alaskensis* reduced the attachment of the potentially detrimental *Desulfovibrio indonesiensis* to stainless steel. However, the same EPS facilitated the attachment of *Desulfovibrio alaskensis* itself. These findings might be caused by the "microbial footprints".

Due to the hardly predictable and complex chemical nature of EPS, chemically pure, EPS-analogue substances seem to be a more reasonable approach for a technical application (Kuklinski & Sand, 2014). Surfactin, an anionic lipopeptide from *Bacillus subtilis* as well as the rhamnolipid (a glycolipid) from *Pseudomonas aeruginosa* reduced the attachment of *Staphylococcus aureus*, *Listeria monocytogenes*, and *Micrococcus luteus* to polystyrene conditioned with these substances. Surfactin caused a strong decrease by 30 - 70 % in attachment of all three organisms, whereas the rhamnolipid mainly reduced attachment of *Listeria monocytogenes* and *Staphylococcus aureus* (by approximately 20 %), while slightly increasing the adhesion of *Micrococcus luteus*. The anti-adhesive behaviour of both biosurfactants was related to altered hydrophobicity of the polystyrene due to the surfactants (de Araujo, et al., 2011; Zeraik & Nitschke, 2010). Another interesting substance group are the glucans. Roux, et al., (2010) successfully used α(1,3)(1,6)-D-glucan enzymatically produced by *Lactobacillus reuteri* (van Leeuwen, et al., 2008) against corrosion of steel rebars in concrete. Electrochemical measurements revealed that the protective effect of the glucan is based on a modification of the cathodic corrosion reaction, indicating a direct reaction of glucan with the steel surface. Later, Scheerder, et al., (2012) used the same glucan as anti-corrosive additives for coatings. However, the authors modified the glucan by oxidation and acetylation to reduce water sensitivity. Results showed good protection of the glucan-admixed coating in outdoor experiments under marine conditions. The authors proposed a working mechanism by which the carboxylic acid groups of the modified glucan form a complex with both Fe(II) and Fe(III) ions from the anodic corrosion reaction and build an insoluble protective barrier on the steel surface (Scheerder, et al., 2012). Similar observations were made by Finkenstadt, et al., (2011), who investigated the protective

mechanism of glucans produced by *Leuconostoc mesenteroides*. Alpha(1,6)-linked D-glucose with 3 % branching through α(1,3)-linkages and alternan, build from alternating units of α(1,3)- and α(1,6)-linked D-glucopyranosyl with 11 % branching were tested for their ability to protect low carbon steel SAE 1010 against corrosion in 5 % NaCl solution. The authors found that the adherence of glucan-films to steel surfaces is facilitated by interactions between metal ions and functional groups within the different glucans. The authors stated that the removal of the emerging Fe(III) ions from the anode would considerably accelerate the conversion of Fe(0) to Fe(II) by acting as a strong oxidant. The reduction of both electron acceptors available at the interface partially inhibits this anodic reaction. Additionally, formation of a passivating Fe(II) oxide film on the steel surface was observed when the α(1,3)- and α(1,6)-linked D-glucopyranosyl-alternan was applied, further reducing the corrosion rate (Finkenstadt, et al., 2011).

1.4.2 Non-biogenic inhibitors

Summarising the results described above (especially for glucans as EPS model substances), the protective effects of EPS are probably mainly based on certain functional groups such as carboxylic acids inside the EPS-matrix (Scheerder, et al., 2012; Finkenstadt, et al., 2011). Thus, commercially available and easily modifiable substances represent a promising approach to mimic the protective effects of EPS, while overcoming the challenges of the latter such as their highly complex and often heterogeneous structure. One promising class of substances for environmentally friendly corrosion protection are cyclodextrins.

Comparable to glucans, cyclodextrins are oligomers build from α-D-glucose units but with a cyclic rather than a linear structure. They were first isolated end of the 19th century as products of the microbial degradation of starch (Villiers, 1891; cited from Saenger, 1980). The three main types of cyclodextrins are α-, β-, and γ-cyclodextrins with 6, 7, or 8 glucose units, respectively (figure 3). Cyclodextrins with more than 8 glucose units are highly soluble and difficult to isolate (Connors, 1997). Based on this basic structure, various modifications with a different number, type, and position of functional groups can be synthesised (Khan, et al., 1998).

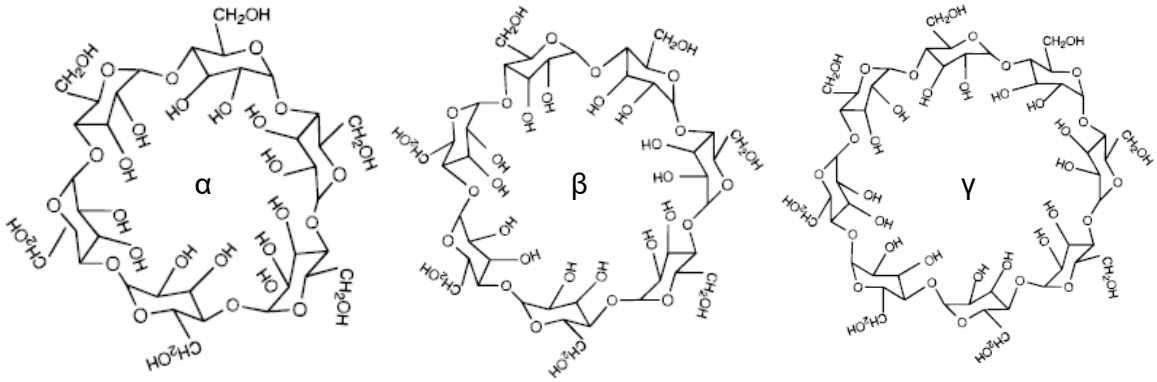

Figure 3 General structure of cyclodextrins (Connors, 1997). Typical cyclodextrins are α-cyclodextrins are consisting of 6 α-1,4-glycosidically bound glucose subunits, β-cyclodextrins of 7, and γ-cyclodextrins of 8 subunits. Cyclodextrins with more than 8 subunits are difficult to isolate and not commonly found in technical applications.

Cyclodextrins are produced enzymatically from starch by cyclodextrin glucanotransferases of various bacteria such as *Bacillus macerans*, various other *Bacilli*, *Micrococci* and organisms of the genus *Klebsiella* (Loftsson & Duchene, 2007). Structurally, the glucose monomers are linked by α-1,4-glycosidic bonds, forming a ring-like structure with primary and secondary hydroxy-groups at the edges, CH-groups at the C-3 and C-5 carbon atoms and glycosidic oxygen at the inner ring. The outer ring is polar due to the hydroxy-groups while the inner ring is relatively non-polar.

The high chemical versatility of cyclodextrins led to their use in various studies, ranging from catalytical effects (Ishiwata & Kamiya, 1999) to antigen-like bindings (Szejtli, 1988). Moreover, randomly methylated cyclodextrins have been studied regarding their suitability for bioremediation of contaminated soils (Molnar, et al., 2005; 2002). Commercially, cyclodextrins are used in various applications such as taste stabilisers, to increase solubility or stability of various chemical compounds and in pharmaceutical applications (Loftsson & Duchene, 2007; Hedges, 1998; Szejtli, 1988).

Cyclodextrins have already been used in corrosion protection by incorporating organic corrosion inhibitors into the cavity. This allowed a controlled and steady release of the inhibitors from e.g. protective sol-gel coatings (Zheng & Li, 2010; Khramov, et al., 2005; Zheludkevich, et al., 2005; Khramov, et al., 2004). Moreover, it added self-healing properties to these coatings, by specifically releasing inhibitors when the coating was damaged (He & Shi, 2009; Zheludkevich, et al., 2007). Another interesting feature of the cyclodextrins (especially regarding the prevention of MIC) is their stability against (biological) degradation after modification. Studies regarding the stability in soil (Fenyvesi, et al., 2005) and

under aerobic composting (Verstichel, et al., 2004) showed that all natural, non-modified cyclodextrins are rapidly degraded. In contrast, randomly methylated β-cyclodextrins (RAMEB) were virtually non-degradable over a period of up to 49 days. Both studies showed that in soil more than 40 % of the initial cyclodextrin concentration can still be found after 2 years.

1.5 Novel tools to study the influence of microorganisms on materials

In the last decade, it has become apparent that atomic force microscopy (AFM) might be useful to visualise and quantify the localised effect of microorganisms on corrosion-sensitive working materials. It allows high-resolution visualisation of both surface features of the substratum as well as of single-cells or clusters. Basically, AFM is an indirect non-optical microscopic technique based on measuring the deformation of springs (cantilevers) by scanning tunnelling microscopy (Binnig, et al., 1986). Later, the method was refined by replacing the tunnelling microscope by a simpler detection method where a weak laser beam is focused on the cantilever and reflected onto a photo sensor (Meyer & Amer, 1988). The movement of this laser is used to determine the deformation of the cantilever, and the deflection of the cantilever tip is directly proportional to the tip-sample interaction force, given by the equation

$$F = -k \times x \qquad (8)$$

where F is the deflection force and k equals the spring constant of the cantilever which represents the cantilever deflection in distance units.

Due to the indirect measuring principle, the resolution of AFM is only limited by the thickness of the cantilever tip and even atomic resolution can be achieved when working in ultrahigh vacuum (Glessibl, 2005; Binnig, et al., 1987). The resolution power is significantly reduced when scanning in ambient air or liquids, but still sub-nanometre (molecular) resolution can be achieved (Weisenhorn, et al., 1990a). For the visualisation of surfaces in ambient air or water two basic modes exist. In contact mode, a defined and constant physical contact is maintained between the cantilever tip and the surface while it is moved across the surface line by line. In this mode, the spring constant of the cantilever is a critical component (Binnig, et al., 1986). The high lateral force of too stiff cantilevers may damage soft surfaces such as biological samples and produce scanning artefacts. Too soft cantilevers, in

contrast, are extremely sensitive against vibrations (noise) from the environment, resulting in poor vertical and lateral resolution, especially on rough surfaces (e.g. metal sulphides). Frequency-modulated AFM (also called intermittent contact or tapping mode AFM) helps to overcome these limitations while additionally increasing the resolution compared to contact AFM. In this mode, the cantilever oscillates at a fixed amplitude over the material surface and the frequency is used as feedback signal (Glessibl, 2005) which additionally strongly reduces the lateral force on the specimen. However, too high forces may damage the cantilever tip itself or the samples e.g. by penetrating their surface. Besides the pure visualisation of a surface, intermittent contact mode can deliver additional information about the specimen such as its hardness or chemical composition by observing the phase shift of the cantilever oscillation caused by electrochemical forces between tip and surface (Magonov & Elings, 1997).

The non-specific tip-sample interaction forces render AFM applicable to a wide range of samples. Shortly after its introduction, AFM was mainly used to visualise crystalline surfaces such as graphite and silicon (Marti, et al., 1988) or NaCl-crystals (Meyer & Amer, 1990), organic monolayers such as polymerised n-(2-aminoethyl)-10,12-tricosadiynamide (Marti, et al., 1988) or even polymeric liquid films (Mate, et al., 1989). However, already in 1988, possible applications of AFM for biological samples were discussed (Hansma, et al., 1988). In the same year, Gould, et al., (1988) investigated amino acid crystals of DL-leucine, revealed individual methyl groups at the ends of the amino acids and thus demonstrated the potential usefulness of AFM for biological samples. In rapid succession, AFM was used to visualise a variety of biological specimens such as single-stranded DNA and antigen-antibody reactions (Weisenhorn, et al., 1990b), immobilised proteins (Weisenhorn, et al., 1990a) or membrane proteins such as bacteriorhodopsin (Butt, et al., 1990a) and also whole cells of *Halobacterium halobium* (Butt, et al., 1990b). Since then, AFM has frequently been used in studies with single cells and/or biofilms (Wright, et al., 2010; Ivnitskya, et al., 2007; Nunez, et al., 2005; Auerbach, et al., 2000; Surman, et al., 1996). AFM has proven to be a valuable tool especially in investigations about processes strongly depending on interfacial reactions between microbes and surfaces such as bioleaching (Noel, et al., 2010; Harneit, et al., 2006; Kinzler, et al., 2003; Gehrke, et al., 1998) and biocorrosion (Xu, et al., 2002; Telegdi, et al., 1998; Beech, 1996; Steele, et al., 1994; Bremer, et al., 1992). However, especially when investigating biological samples, the high versatility due to the non-specific

tip-sample interaction also limits the capacity of AFM to discriminate between different surface features such as microbes and particles, unless their exact shape is known (Mangold, et al., 2008a).

This limitation can be overcome by combining AFM with epifluorescence microscopy (EFM). In contrast to AFM, the resolution of EFM is usually limited by Abbe's diffraction limit to half the wavelength of the light used (see also Mangold, et al., 2008a; Stelzer, 2002). Novel methods employing super-resolution lenses (Zhang & Liu, 2008) or special photo switchable fluorophores combined with stochastic image reconstruction (Rust, et al., 2006) lowered the resolution limit to down to 20 nm, but are still far from the sub-nanometre resolution of AFM. Generally, all classical fluorescence-based methods used in microbiology can be combined with AFM, if they do not alter the structure of the specimen. This includes methods such as lectin-staining for the visualisation of EPS or fluorescence in situ hybridisation (FISH) to identify single species in mixed consortia (Florian, et al., 2010). Usually, the combination of AFM and EFM is achieved by mounting the AFM head on inverted microscopes (Kolodny, et al., 2001; Horton, et al., 2000; Lieberman, et al., 1996; Henderson & Sakaguchi, 1993). However, this strongly limits the versatility of this combination to biological samples on translucent surfaces such as glass or mica. Recently, a combination of AFM and EFM allowing the investigation of the same location by both techniques using independent instruments was introduced at demand of Prof. Wolfgang Sand's Aquatic Biotechnology working group and developed together with JPK Instruments in Berlin (Mangold, et al., 2008a; Barner, 2007). It has since been used in various studies focusing on leaching bacteria on metal sulphide surfaces (Florian, et al., 2010; Noel, et al., 2010; Florian, et al., 2009; Sand, et al., 2009; Mangold, et al., 2008b; Mangold, et al., 2008a).

Beyond the combination of AFM with EFM, other extensions to the AFM-technique such as flow cells (Africa, et al., 2010; Coles, et al., 1997), chemical mapping using specifically functionalised cantilevers (Frisbie, et al., 1994) or electrochemical set-ups (Hirasawa, et al., 1997) demonstrate its high versatility. Regarding electrochemical interfacial processes, Scanning Kelvin probe force Microscopy (SKPFM) is of special interest. SKPFM was developed in 1991 by Nonnenmacher, et al., (1991b; 1991a) to allow high-resolution visualisation of the contact potential difference (CPD) between AFM tip and surface as well as simultaneous imaging of the topography. The technique is based on the classical vibrating-

plate Kelvin method (Nonnenmacher, et al., 1991b; Zisman, 1932; Kelvin, 1898) which is usually unable to record topography during the scan and also, compared to AFM-based SKPFM, features inferior resolution of ≥ 1 µm, although some instruments reach ≥ 0.1 µm (Rohwerder & Turcu, 2007; Yee, et al., 1991).

SKPFM imaging involves scanning the surface line by line in intermittent contact mode to first determine the topography. After each line, the conductive cantilever is lifted to a fixed distance from the surface (typically < 100 nm) and the same line is scanned again to determine the CPD between tip and surface. During this second line scan, the dither piezo driving the physical oscillation of the cantilever is turned off and a voltage V_{tip} is applied to the cantilever, consisting of a direct current (dc) component and an alternating current (ac) component with the frequency ω (9).

$$V_{tip} = V_{DC} + V_{AC}\sin(\omega t) \qquad (9)$$

The different charges of the tip and the surface result in a capacitive force F_{cap} (10).

$$F_{cap} = 0.5\left(V_{tip} - \theta(x)\right)^2\left(\frac{dC}{dz}\right) \qquad (10)$$

The capacitive force is determined by the applied tip voltage V_{tip}, the surface potential $\theta(x)$ and the tip-surface capacitance $C(z)$. The cantilever oscillation is driven by the first harmonic force (11).

$$F_{cap\,\omega} = \left(\frac{dC}{dz}\right)[(V_{dc} - \theta(x))V_{AC}\sin(\omega t)] \qquad (11)$$

For each point x of the line, the feedback loop changes $V_{dc}(x)$ to null the force component (and, hence, stop the cantilever oscillation). $V_{dc}(x)$ equals the surface potential $\theta(x)$ (Kratochvílová, et al., 2009; Rohwerder & Turcu, 2007).

Technically, a laser is focused to the cantilever and reflected by it onto a 4-quadrant photo detector. The laser position is fed into both a topography and CPD feedback loop. During the topography scan, the topography feedback is used to control the z-piezo to maintain a constant cantilever oscillation which is driven by the dither piezo. During the potential mapping, the CPD feedback changes the DC component of the applied tip-voltage until the cantilever oscillation stops (i.e. the dc voltage equals the CPD). Figure 4 shows a schematic representation of the JPK™ SKPFM set-up used in this thesis.

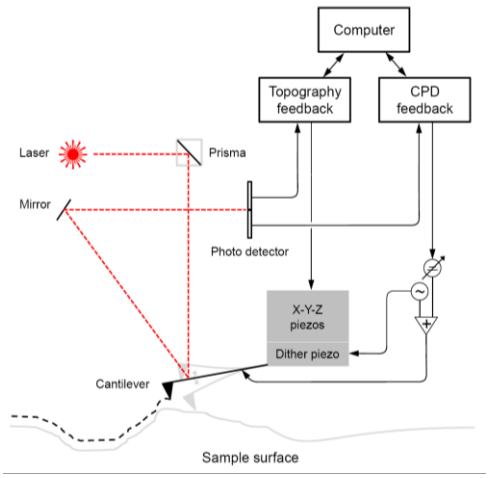

Figure 4 Schematic representation of the JPK™ SKPFM set-up. The laser is focused onto the cantilever by a prism, reflected by it to a mirror and finally onto a 4-quadrant photo detector. The position of the laser on the photo detector is converted into an electrical signal, which is fed into the computer via the topography feedback. The latter controls the position of the X-Y-Z-piezos to maintain a constant electrical signal (so-called deflection voltage). The necessary Z-movement of the piezo to maintain this deflection voltage is recorded and used to construct the height profile of each x-y-coordinate. For the mapping of surface potentials, a second CPD feedback loop is used, which controls DC component and records the value necessary to stop the cantilever oscillation.

1.6 Aims of this study

Corrosion of iron and steel represents a serious economical, technological and potentially ecological challenge. Nowadays, it is widely accepted that microorganisms can play a pivotal role in corrosion by not only accelerating (MIC) but also inhibiting (MICI) the involved processes (Zarasvand & Rai, 2014; Videla & Herrera, 2009; Mansfeld, 2007; Sand, 1997). Both phenomena are (in)directly related to biofilms and their surrounding EPS, in fact, most protective effects can probably be ascribed to the EPS rather than the living biofilm itself (Stadler, et al., 2008). However, to date, little is known about the influence of the underlying substratum (such as steel or pure iron) on the EPS composition as well as the localised electrochemical effects of the microorganisms on the material surface.

To better understand MIC and to be able to develop novel, environmentally-friendly countermeasures, this study was divided into three main aims:

- Establishing a novel combination of Scanning Kelvin probe force- and epifluorescence microscopy for opaque samples to visualise and quantify the localised electrochemical effect of SRP on alloyed steel, mild steel and pure iron.
- Identifying the possible influence of metal substrates on the composition of both the loosely bound and tightly bound EPS fractions of *Desulfovibrio vulgaris* as a model organism for microbiologically influenced corrosion by SRB.
- Developing and evaluating an EPS-derived, cyclodextrin-based approach to reduce or prevent MIC by SRB.

2 MATERIALS

2.1 Chemicals

All substances were of analytical grade unless stated otherwise.

Table 3 List of chemicals

Substance	Formula	Manufacturer
1,10-Phenantrolinium chloride	$C_{12}H_8N_2$ x HCl x H_2O	Merck
2-Keto-3-deoxyoctonate ammonium salt	$C_8H_{17}NO_8$	Sigma
4',6-Diamidine-2-phenylindole (DAPI)	$C_{16}H_{15}N_5$	Sigma
4-Amino benzoic acid	$C_7H_7NO_2$	Merck
Acetic acid anhydride	$C_4H_6O_3$	Sigma
Acetic acid, glacial	$C_2H_4O_2$	Sigma
Acetone (technical grade, >99 %)	C_3H_6O	
Acetyl chloride	C_2H_3ClO	Merck
Ammonium acetate	$C_2H_7NO_2$	Sigma
Ammonium chloride	NH_4Cl	Roth
β-Nicotinamide dinucleotide phosphate (β-NADP)		Sigma
β-Hydroxydiphenyl	$C_{12}H_{10}O$	Sigma
Biotine	$C_{10}H_{16}N_2O_3S$	Roth
Boric acid	H_3BO_3	Sigma
Calcium chloride dihydrate	$CaCl_2$ x 2 H_2O	Roth
Calcium-D-pantothenate	$C_9H_{17}NO_5$	Fluka
Chloroform	$CHCl_3$	Roth
Cobalamine	$C_{62}H_{88}CoN_{13}O_{14}P$	Sigma
Cobalt(II) chloride hexahydrate	$CoCl_2$ x 6 H_2O	Sigma
Concanavalin A, fluoresceineisothiocyanate-conjugated (ConA-FITC)		Sigma
Concanavalin A, tetramethylrhodamineisothiocyanate-conjugated (ConA-TRITC)		Sigma
Copper sulphate, anhydrous	$CuSO_4$	Fluka
Copper(II) chloride dihydrate	$CuCl_2$ x 2 H_2O	Sigma
Cyanocobalamine	$C_{62}H_{88}CoN_{13}O_{14}P$	Sigma
D-Glucuronic acid sodium salt monohydrate	$C_6H_9NaO_7$ x H_2O	Sigma
Dichloromethan	CH_2Cl_2	Merck
Dimethyl sulphoxide (DMSO)	C_2H_6OS	Merck
Dipotassium hydrogen phosphate, anhydrous	K_2HPO_4	Merck

Table 3 Continued

Substance	Formula	Manufacturer
Disodium carbonate	Na_2CO_3	Sigma
Disodium sulphate, anhydrous	Na_2SO_4	Roth
Ethanol (≥ 96 %), technical grade	C_2H_6O	
Folic acid	$C_{19}H_{19}N_7O_6$	Fluka
Folin-Ciocalteus phenol reagent		Merck
Glucose	$C_6H_{12}O_6$	Sigma
Glucose-6-phosphate (G6P)	$C_6H_{13}O_9P$	Sigma
Glucose-6-phosphate dehydrogenase (G6PDH) from *Leuconostoc mesenteroides*		Sigma
Glutardialdehyde (25 %)	$C_5H_8O_2$	Merck
Humic acid		Sigma
Hydrochloric acid	HCl	Roth
Hydroxylamine	NH_2OH	Roth
Iron(II) sulphate heptahydrate	$FeSO_4$ x 7 H_2O	Roth
Iron(III) chloride tetrahydrate	$FeCl_3$ x 4 H_2O	Roth
L-Ascorbic acid	$C_6H_8O_6$	Sigma
Liponic acid	$C_8H_{14}O_2S_2$	Fluka
Magnesium chloride	$MgCl_2$	Sigma
Magnesium sulphate heptahydrate	$MgSO_4$ x 7 H_2O	RTY Ltd.
Manganese chloride tetrahydrate	$MnCl_2$ x 4 H_2O	Fluka
Methanol	CH_4O	Roth
n-Hexane	C_6H_{14}	Roth
Nickel chloride hexahydrate	$NiCl_2$ x 6 H_2O	Fluka
Nicotinic acid	$C_6H_5NO_2$	Fluka
n-methylimidazole	$C_4H_6N_2$	Sigma
p-Aminobenzoic acid	CH_2Cl_2	Sigma
Periodic acid (99 %)	H_5IO_6	Sigma
Phenol	C_6H_6O	Merck
Phosphoric acid (15 %)	H_3PO_4	Roth
PicoGreen© reagent		Invitrogen
Potassium hydrogen phtalate	$C_{12}H_{25}KO_4S$	Sigma
Potassium hydroxide	KOH	Sigma
Pyridoxine-HCl	$C_8H_{11}NO_3$	Fluka
Riboflavine	$C_{17}H_{20}N_4O_6$	Sigma
Sodium arsenate	$NaAsO_7$	Sigma
Sodium borohydride	$NaBH_4$	Sigma

Table 3 Continued

Substance	Formula	Manufacturer
Sodium carbonate	Na_2CO_3	Sigma
Sodium chloride	NaCl	Sigma
Sodium DL-lactate (60 %)	$NaC_3H_5O_3$	Merck
Sodium dodecyl sulphate (SDS)	$C_{12}H_{25}NaO_4S$	Sigma
Sodium hydrogen carbonate	$NaHCO_3$	Sigma
Sodium hydrogen phthalate	$C_8H_5KO_4$	Sigma
Sodium hydroxide	NaOH	Sigma
Sodium molybdate dihydrate	Na_2MoO_4 x 2 H_2O	Merck
Sodium tartrate, anhydrous	$C_4H_4O_6Na_2$	Sigma
Sodium tetraborate	$Na_2B_4O_7$	Sigma
Sulphuric acid	H_2SO_4	Roth
Syto9™		Molecular Probes
Thiamine-HCl x $2H_2O$	$C_{12}H_{18}N_4OSCl_2$	Sigma
Thiobarbituric acid	$C_4H_4N_2O_2S$	Sigma
Trifluoroacetic acid	$C_2HF_3O_2$	Sigma
Tris(hydroxymethyl)-aminomethane (Tris)	$C_4H_{11}NO_3$	Roth
Trisodium citrate dihydrate	$C_6H_5O_7$ x 3 Na x 2 H_2O	Roth
Tween20 (polysorbat 20)	$C_{58}H_{114}O_{26}$	Sigma
Tween80 (polysorbat 80)	$C_{64}H_{124}O_{26}$	Sigma
Vanillin	$C_8H_8O_3$	Sigma
Zinc(II) chloride	$ZnCl_2$	Merck

Table 4 Fatty acid methyl ester (FAME) standard kits for gas chromatography

Substance	Product no.	Manufacturer
Fatty Acid Methyl Esters, Saturated Straight Chain	ME7-1KT	Supelco
Fatty Acid Methyl Esters, Saturated Straight Chain	ME19-1KT	Supelco
Fatty Acid Methyl Esters, Unsaturated Kit	ME14-1KT	Supelco

2.2 Cultivation media

Desulfovibrio vulgaris was grown in modified Postgate medium C (von Rège, 1999). The pH of solution A (table 5) was adjusted to 8.5 using 5 M KOH and the solution was autoclaved at 121 °C, 1.5 bar for 20 minutes. Solution B (table 6) was added by filtering through sterile 0.22 µm filters and the final pH was adjusted to 7.5 using sterile 1 M KOH or 1 M H_2SO_4.

Table 5 Solution A for Postgate medium C

Substance	Chemical formula	Amount
Ammonium chloride	NH_4Cl	1.0 g
Calcium chloride dihydrate	$CaCl_2 \times 2\ H_2O$	0.04 g
Di-potassium hydrogen phosphate, anhydrous	K_2HPO_4	0.5 g
Magnesium sulphate heptahydrate	$MgSO_4 \times 7\ H_2O$	0.06 g
Sodium-DL-lactate (60 %)	$NaC_3H_5O_3$	4.2 mL
Sodium sulphate, anhydrous	Na_2SO_4	4.5 g
Yeast extract		1.0 g
Deionised water		980 mL

Table 6 Solution B for Postgate medium C

Substance	Chemical formula	Amount
Ascorbic acid	NH_4Cl	1.0 g
Iron sulphate heptahydrate	$FeSO_4 \times 7\ H_2O$	0.004 g
Trisodium citrate dihydrate	$Na_3C_6H_5O_7 \times 2\ H_2O$	0.5 g
Deionised water		20 mL

For all other experiments, a yeast-free variant of the modified Postgate medium C was developed to reduce accumulation of organic substances to the metal surfaces. Basically, yeast was replaced by defined trace element (from DSMZ medium 320, table 9) and vitamin solutions (from DSMZ medium 141, table 10). After preparing solutions A (table 7) and B (table 8), the final medium was prepared as described before.

Table 7 Solution A for Postgate medium C without yeast

Substance	Chemical formula	Amount
Ammonium chloride	NH_4Cl	1.0 g
Calcium chloride dihydrate	CaCl2 x 2 H2O	0.04 g
Di-potassium hydrogen phosphate, anhydrous	K_2HPO_4	0.5 g
Magnesium sulphate heptahydrate	$MgSO_4 \times 7$ H2O	0.06 g
Sodium-DL-lactate (60 %)	$NaC_3H_5O_3$	4.2 mL
Sodium sulphate, anhydrous	Na_2SO_4	4.5 g
Deionised water		980 mL

Table 8 Solution B for Postgate medium C without yeast

Substance	Chemical formula	Amount
Ascorbic acid	NH_4Cl	1.0 g
Iron sulphate heptahydrate	$FeSO_4 \times 7\ H_2O$	0.004 g
Trisodium citrate dihydrate	$Na_3C_6H_5O_7 \times 2\ H_2O$	0.5 g
Vitamin solution (table 9)		10 mL
Trace element solution (table 10)		1 mL
Deionised water		9 mL

Table 9 Vitamin solution for Postgate medium C without yeast

Substance	Chemical formula	Amount
Biotin	$C_{10}H_{16}N_2O_3S$	2.0 mg
Cobalamine	$C_{62}H_{88}CoN_{13}O_{14}P$	0.1 mg
Calcium-D-pantothenate	$C_9H_{17}NO_5$	5.0 mg
Folic acid	$C_{19}H_{19}N_7O_6$	2.0 mg
Nicotinic acid	$C_6H_5NO_2$	5.0 mg
p-Aminobenzoic acid	CH_2Cl_2	5.0 mg
Pyridoxine-HCl	$C_8H_{11}NO_3$	10.0 mg
Riboflavin	$C_{17}H_{20}N_4O_6$	5.0 mg
Thiamine-HCl x $2H_2O$	$C_{12}H_{18}N_4OSCl_2$	5.0 mg
Deionised water		1000 mL

Table 10 Trace element solution SL-10 for Postgate medium C without yeast

Substance	Chemical formula	Amount
Boric acid	H_3BO_3	0.006 g
Cobalt chloride hexahydrate	$CoCl_2 \times 6H_2O$	0.19 g
Copper chloride dehydrate	$CuCl_2 \times 2\ H_2O$	0.002 g
Hydrochloric acid 25%, 7.7M)	HCl	10 mL
Iron chloride tetrahydrate	$FeCl_2 \times 4\ H_2O$	1.5 g
Manganese chloride tetrahydrate	$MnCl_2 \times 4\ H_2O$	0.1 g
Nickel chloride hexahydrate	$NiCl_2 \times 6\ H_2O$	0.024 g
Sodium molybdate dihydrate	$Na_2MoO_4 \times 2\ H_2O$	0.036 g
Zinc chloride	$ZnCl_2$	0.07 g
Deionised water		990 mL

First, $FeCl_2$ was is dissolved in HCl, then diluted in water. Afterwards the other salts are added and finally dH_2O is added to a final volume of 1000 mL.

2.3 Functionalised cyclodextrins

All functionalised cyclodextrins were obtained from CycloLab Cyclodextrin Research & Development Laboratory, Ltd., Hungary. Table 15 gives an overview about all variants.

Table 11 List of functionalised cyclodextrins

Cyclodextrin	DS[t]	Abbreviation
6-mono-O-((1-4)-a-D-glucuronyl-(1-4)-a-D-glucosyl) β-cyclodextrin		A
6-N-monofluorescein(5/6)thioureido-carboxymethylated β-cyclodextrin Na-salt	3.5	FITC-CMBCD
Carboxyethylated α-cyclodextrin	3	CEACD
Carboxyethylated β-cyclodextrin Na-salt	3	CEBCD
Carboxyethylated γ-cyclodextrin Na-salt		CEGCD
Carboxylated poly(1->4)-β-D-glycosyl-(1->4)-β-glucose		B
Carboxymethylated hydroxypropyl β-cyclodextrin Na-salt		CMHPBCD
Carboxymethylated α-cyclodextrin	3	CMACD
Carboxymethylated β-cyclodextrin	2.8	CMBCD 2.8
Carboxymethylated β-cyclodextrin Na-salt	3	CMBCD
Carboxymethylated γ-cyclodextrin	4	CMGCD
Diethylamino ethylated poly(1->4)-β-D-glucosyl-(1->4)-β-D-glucose		C
Highly oxidized β-cyclodextrin Fe(III)-salt		D
Highly oxidized β-cyclodextrin Na-salt		E
Oxidized β-cyclodextrin Fe(III)-salt		G
Oxidized β-cyclodextrin Na-salt		F
Poly(1->4)-D-galacturonyl(1->4)-D-galacturonyl-(1->2)-L-rhamnose) Fe(II/III)-salt		H
Poly((1->4)-β-L-guluronyl(1->4)-α-D-mannuronic acid) Na-salt		I
Poly((1->4)-D-galacturonyl(1->4)-D-galacturonyl-(1->2)-L-rhamnose)		N
Poly(1->6)-D-glucosyl-(1->6)-α-D-glucose		K
Soluble carboxymethylated β-cyclodextrin polymer		CMBCDPSI
Soluble quaternary-amino-β-cyclodextrin polymer		QABCDP
Sulphated poly(1->3)-β-D-(2-N-acetylamido)-galacturonyl-(1->4)-β-D-glucuronic acid) Na salt		L
Sulphated poly(1->6)-D-glucosyl-(1->6)-α-D-Glucose) Na-salt		M
Sulphated β-cyclodextrin Na-salt	12	O
Sulphobutylether-β-cyclodextrin Na-salt	4	P
Sulphobutylether-β-cyclodextrin Na-salt	6.2 ± 0.2	Q
Sulphopropylated β-cyclodextrin Na-salt		SPBCD

[t] *average degree of substitution per cyclodextrin molecule*

2.4 Metal specimens

Three different working materials were used in this thesis: pure iron, non-alloyed ("carbon") and alloyed steel. Table 12 gives an overview about the sources of the materials and their respective quality classes; table 13 shows the typical composition of the materials.

Table 12 Designation and sources of the metal specimens

Material	Material No.[†]	Quality	Source
Pure iron	ARMCO[‡]	Grade 2 Surface black/dark	REMAG, Mannheim
Non-alloyed steel	1.0037	R.ST.37-2; ST.37-2 Surface black/dark	Albin Stapf GmbH & Co. KG, Frankfurt/Main
Alloyed steel	1.4301	X5CrNi18-10 (V2A) 3c Surface bare metal	MVG Metallverkaufs-GmbH & Co. KG, Frankfurt/Main

[†]*Material numbers according to DIN 17007 (2003)*
[‡]*Trade name for technically pure iron ≥ 99.8 %*

Table 13 Typical chemical composition

Material No.	Max. constituents except Fe (%)							
	C	Si	Mn	Cr	Ni	Mo	P	S
ARMCO[†]	0.01	-	0.1	-	-	-	0.01	0.008
1.0037[‡]	0.2	0.31	1.4	0.5	0.12	0.03	-	-
1.4301[‡]	0.07	1	2	18	9	-	-	-

[†]*www.aksteel.de*
[‡]*According to manufacturer/distributor*

2.5 Equipment and software

Table 14 Instruments

Instrument	Model / Specification	Manufacturer
Anaerobic glove box	R772	DW Scientific
Analytical scales	Acculab m-prove AY612 Acculab ATILON ATL-124-I	Sartorius
Atomic force microscope	BioMAT workstation with NanoWizard II AFM head and JPK Kelvin probe module	JPK Instruments
Bottle top filter	PSF, autoclavable	Nalgene
Centrifuge (1.5 mL reaction tubes)	18/14, fixed rotor	VWR
Centrifuge (50 / 20 mL vessels)	Heraeus Multifuge 1-SR, rotor 75002006	Heraeus
Centrifuge (500 mL vessels)	Sorvall RC6+, rotor F10S-6x500Y	Thermo
Clean bench	Herasafe KS15	Thermo
Conductivity meter		WTW
Confocal laser scanning microscope	Axiovert A100M equipped with AxioCam MRm, air objective LD-Achroplan 40x/0,6cor and oil-immersion objective Plan-Neofluar 100x/1,3 Oil; fluorescence excitation by argon laser at a wavelength of 488 nm (filter: Ch3: BP 505-550)	Zeiss
Dry cabinet	B5060	Heraeus
Epifluorescence microscope	AxioImager.A1m equipped with AxioCam MRm, 100x oil immersion objective EC Plan-Neofluar 100x/ 1,30 Oil and filter sets 49 (DAPI, ex. G 365 nm, beam splitter FT 395 nm, em. BP 445/50 nm), 10 (FITC/Syto9, ex. BP 450-490 nm, beam splitter FT 510 nm, em. BP 515-565 nm), and XX (TRITC, ex. BP 450-490 nm, beam splitter FT 510 nm, em. BP 515-565 nm); fluorescence excitation by mercury vapour lamp HBO 100	Zeiss
Gas Chromatograph	Fractovap 4160, LT programmer 400, amplifier EL580, detector: FID	Carlo Erba
Haemocytometer	Custom, depth = 0.02 mm	Assistent
Hybridisation oven	Shake'n'Stack	Hybaid
Incubators	B6200 ST5050	Heraeus
Lyophilisator	Alpha 2-4	Christ
Microplate reader	Infinite Pro M200	Tecan Instruments
pH meter		WTW
Phase contrast microscopy	DMLS, objective C-Plan 40x/0.6T PH2	Leica Zeiss

Table 14 Continued

Instrument	Model / Specification	Manufacturer
Polishing machine	LaboPol-1	Struers
Spectrophotometer	Cary 50	Varian
Stirring plate	RCT REO	Ikamag
TOC analyser	TOC-VCPH	Shimadzu
Ultrasonic bath	Sonorex Digitec DT510H	Bandelin
Ultrasound processor	UP200s	Dr. Hielscher
Vacuum centrifuge	RVC 2-25	Christ
Water bath	1003	Gesellschaft für Labortechnik mbH

Table 15 Consumables

Type	Model / Specification	Manufacturer
Anaerobiosis system	Anaerocult A	Merck
Cation exchange resin CER)	DOWEX marathon C™ sodium form	Sigma
Centrifuge tubes (50 mL)	Corning	Roth
Dialysis tubing	Zellutrans T1, MWCO 3.5 kDa	Roth
Dialysis tubing	SpectraPor 3, MWCO 3.5 kDa	SpectraPor
Diamond lubricant	Oil-based for water-free preparations	ATM
Diamond suspension	Oil-based polycrystalline; particle size 1 and 6 µm, respectively	ATM
Grinding paper	Silicium carbide HV 30 – 800; P180, P500, P800 and P1200	Struers
Microplates (96-well)	Microplate 96/F-PP, flat bottom, PP	Eppendorf
	BRANDplate pureGrade S, flat bottom, PS	Brand
Polishing cloth for diamond polishing	MD-Floc; medium-haired artificial silk for 6 µm particle size MD-Nap; short-haired artificial silk for ≤ 1 µm particle size	Struers
Reaction tubes (1.5 mL)	1.5 mL and 2 mL	Sarstedt
Rollrand	22x45 mm	Oehmen
Sterile filters for bottle filters	Cellulose-acetate, 0.2 µm, d=47 mm	Roth
Sterile syringe filters	0.22 µm	Roth

Table 16 Software for data processing

Software	Version	Manufacturer
AxioVision	4.8	Zeiss
Clarity Lite	5.0	DataApex
ImageJ	1.4x	W. Rasband, National Institutes of Health, USA
Office	2007	Microsoft
OriginPro 2015	b9.2.214	Origin Labs
SPM Control	3.3	JPK
SPM Data Processing	4.2	JPK
ZEN 2012 (Black Edition)	8.1	Zeiss

3 METHODS

3.1 Growth and maintenance of *Desulfovibrio vulgaris* stock and working cultures

Desulfovibrio vulgaris was selected as a model organism to simulate MIC by SRB. It was obtained from the German Collection of Microorganisms and Cell Cultures (DSMZ, no. 644). Stock cultures were prepared in 100 ml serum bottles filled with 80 ml medium. The bottles were tightly closed with butyl rubber stoppers and aluminium crimp caps under sterile conditions. Each bottle was flushed with N_2 through sterile olives filled with cotton wool for at least 15 minutes to establish the anaerobiosis. After inoculation, the bottles were incubated for 3 days at 37 °C. Afterwards, stocks were stored at 4 °C for not more than 6 months. At least three parallels have been prepared; stocks used to inoculate working cultures have not been used to inoculate fresh stocks to prevent accidental contamination.

Working cultures were prepared from these stocks in 100 ml Schott bottles. The bottles were also sealed with butyl rubber gaskets and closed using screw caps with hole. The working cultures were inoculated using a 2 % inoculum from the stocks. Establishing of anaerobiosis and incubation was done as described before. The working cultures were stored at 4 °C for not more than six weeks.

3.2 Preparation of metal coupons

All metal samples were provided as 1 mm thick sheets. The sheets were cut into coupons of either 30 x 20 x 1 mm or 20 x 15 x 1 mm by the workshop of the DECHEMA Research Institute (Frankfurt/Main, Germany). For the EPS extraction experiments, metal coupons of 200 x 25 x 1 mm were used and a 4-mm hole was drilled near the top for fixation in the culture vessels.

3.2.1 Surface preparation

Two different grades of surface finishing were used: wet-ground or mirror-polished. All coupons were manually wet-ground on a polishing machine using silicon carbide (SiC) paper (P180). The coupons were rinsed with water, cleaned with ethanol (70 %) and de-

greased with acetone in an ultrasonic bath for five minutes. Remaining acetone was evaporated using a hair dryer. The samples were stored protected from dust in a desiccator until use.

For mirror-finish, coupons prepared as described above were successively further ground with P500, P800 and P1200 SiC-paper. Between each grinding step, the coupons were thoroughly washed with dH_2O to remove particles from the grinding process. After the final grinding with P1200, the coupons were cleaned and degreased as described above. Then, the surface was polished with 6 µm polycrystalline, oil-based diamond suspension using medium-haired artificial silk polishing cloth, the remaining diamond suspension was removed with ethanol (96 %) and the coupons were again cleaned by ultrasonication in acetone. Next, the surface was polished using 1 µm diamond suspension on short-haired artificial silk polishing cloth. Finally, the coupons were thoroughly cleaned and degreased (as described before) and stored in a desiccator until use.

3.2.2 Sterilisation

All metal specimens were heat-sterilised by dry heat at 130 °C for 7 h in suitable glass vessels covered with aluminium foil. To prevent the condensation of water from the ambient air water on the metal surfaces during cooling down, the glass vessels were placed into a second glass vessel filled with Silica gel to absorb humidity.

3.3 Determination of total cell number

Total cell numbers were determined using a modified Thoma counting chamber with a chamber depth of 0.2 mm. Cells were counted at 400-fold magnification under phase contrast. At least 5 individual squares with a total cell number between 100 and 300 cells were counted; samples were diluted using sterile dH_2O if necessary. The total cell number (TCC) was calculated according to

$$TCC = \frac{n}{A\ x\ D\ x\ F} \times 1000$$

TCC = Total cell count [mL^{-1}]
n = Average cell number per small square
A = Area of a small square (0.0625 mm^2)
D = Depth of the chamber (0.2 mm)
F = Dilution factor

3.4 Investigations on the contact potential difference (CPD) of biofilms and material surfaces by combined SKPFM & EFM

3.4.1 Production of *Desulfovibrio vulgaris* biofilms on material surfaces

Mirror-polished coupons (20 x 15 x 1 mm, chapter 3.2) of alloyed steel, carbon steel as well as pure iron were put into 10-mL sterile lever lid vessels sealed with aluminium foil and transferred into a glove box. Cells from a well-grown *Desulfovibrio vulgaris* stock culture were harvested and the cell number was adjusted to 5 x 10^8 mL^{-1} by resuspension in the respective amount of fresh, oxygen-stripped, and yeast-free Postgate medium C. 10 mL of the *Desulfovibrio vulgaris* medium were then added to the vessels containing the metal coupons and incubated inside the glove box at 30 °C for 30 min up to 3 days. Afterwards, the coupons were removed, thoroughly rinsed with oxygen-free, sterile MilliQ™ water and immediately stained according to chapter 3.6.3 and visualised.

3.4.2 Removal of attached biofilms from material surfaces

To visualise the electrochemical influence of attached cells of *Desulfovibrio vulgaris* on the underlying metal surface, a combination of ultrasound and detergent with minimal influence on the material itself was developed. Therefore, the efficiency of the three detergents Tween 20 (Chen & Stewart, 2000), Tween 80 (Parkar, et al., 2003), and SDS (Whittaker, et al., 1984) for the removal of *Desulfovibrio vulgaris* biofilms on alloyed steel as well as their possible effect on the metal surface (and its surface potential) was investigated.

The Tween detergent solutions (1 % v/v) and SDS detergent solutions (0.1, 0.5, and 1 % w/v, respectively) in sterile dH_2O were flushed with nitrogen under strong agitation for at least 1 h prior to use to strip oxygen from the solutions.

Alloyed steel coupons (30 x 15 x 10 mm, P180) were incubated with *Desulfovibrio vulgaris* for 24 h as described in chapter 3.6.2. After incubation, the coupons were removed, mounted to glass objective slides, thoroughly rinsed with sterile dH_2O to remove all loosely attached cells, and the biofilms were fluorescently stained as described before. The biofilms were visualised by EFM and the surface coverage was calculated on a percentage basis from at least 10 individual visual fields. Afterwards, the glass slides with the metal coupons

were transferred to 50 mL centrifuge tubes wrapped with aluminium foil to prevent photobleaching of the nucleic acid stain. The tubes were transferred to a glove box and 35 mL of the respective, oxygen-free detergent solution were added. The caps of the tubes were tightly closed and additionally sealed with laboratory film to maintain anaerobic conditions during the following ultrasound treatment. The tubes were removed from the glove box and transferred to an ultrasonic bath (30 min at room temperature). Afterwards, the tubes were transferred back into the glove box. The glass slides with mounted coupons were carefully removed, thoroughly rinsed with 2 x 5 mL oxygen-free dH_2O and dried under a nitrogen stream. The residual biofilm was again visualised by EFM and the remaining biofilm-covered surface was calculated.

Additionally, samples of both alloyed and non-alloyed steel were analysed by SKPFM to assess the possible influence of the removal procedure on the metal itself, i.e. the surface potential and topography, to ensure that no cell residues remained at the surface and that the removal procedure did not alter the surface.

3.4.3 Visualisation of biofilms and CPD mapping

The surface potential (more specifically the contact potential difference, CPD) between cells, material and the AFM tip was visualised using the BioMAT Workstation equipped with a Kelvin force module allowing quasi-simultaneous acquisition of both topography and CPD to evaluate the influence of CPD and attachment and vice versa. The topography was recorded in intermittent contact mode at a line rate of 0.3 Hz and the maximum vibration amplitude of 8 V; the CPD in hover mode with a 50-nm air gap at 2.5 V vibration amplitude. These values were obtained from a test series on an alloyed steel coupon with a gold-grit sputtered onto it. They delivered the highest potential contrast with a minimum of topographical artefacts and are one of the results of this thesis.

Up to three different spots of each sample were visualised before and after ultrasound treatment. The spots were selected using the JPK alignment cross marker by first removing the sample from the shuttle stage, focusing a defined crossing on the marker (figure 5) and re-mounting the sample. The spatial deviation of the different sample spots was negligible with approximately less than ± 5 µm.

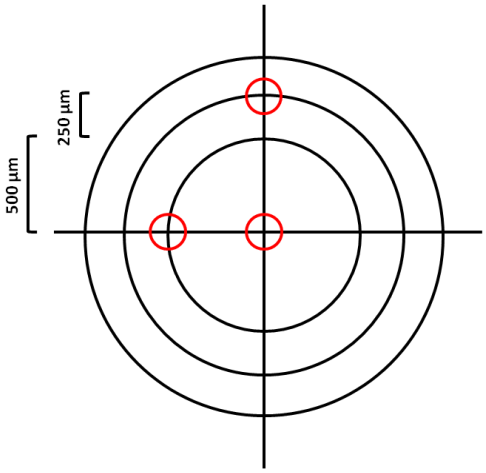

Figure 5 Reproducible selection of scanning areas. To scan different areas before and after ultrasound treatment, the AFM was first aligned to a certain intersection (indicated by the red circles) on a JPK instruments™ cross marker slide. Then, the sample was mounted and the respective sample area was visualised. Afterwards, another intersection was selected on the cross-marker and another sample area was visualised. The same procedure was repeated after treatment of the sample.

3.4.4 Determination of CPD between cell and surface

The difference in CPD between cells and surface was calculated using the PeakAnalyzer tool of OriginPro 2015. The average CPD of the material surface was defined as the baseline. Its anchor points were calculated from the 2nd derivation of the filtered moving average. The baseline (i.e. average material CPD) was created by connecting 8 anchor points using a constant fit (figure 6, red line).

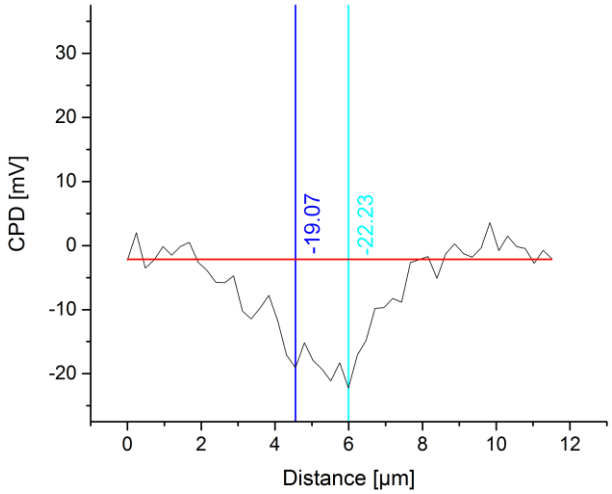

Figure 6 Estimation of CPD variations between cells and surface. (–) Baseline, (–) first and (–) second maximum. The contact potential difference between surface (baseline) and cells (maxima) was calculated by averaging the maxima and subtracting the baseline (in this example -19.97 and -22.23 mV).

The CPD of the cells was calculated from the difference of 2 maxima along the position of the cell and the baseline (maxima indicated by the blue lines in figure 6).

3.5 Investigations on the influence of metal substrata on the biochemical composition of EPS from *Desulfovibrio vulgaris*

3.5.1 Extraction of extracellular polymeric substances

Desulfovibrio vulgaris was grown in 5 L bottles filled with 5 L of modified Postgate medium C without yeast for 4 d at 37 °C under constant bubbling with N_2. A 100-mL inoculum from a well-grown pre-culture with a total cell number of approximately 5 x 10^8 mL^{-1} was used. To prevent accumulation of emerging H_2S inside the incubation chamber, a sulphide trap containing 20 % $ZnCl_2$ was connected to each bottle. The cells were grown either in absence of metal (control) or in presence of pure iron or alloyed steel. For the latter two, 20 wet-ground (P180) metal strips of each 200 x 25 x 1 mm were placed in the culture bottles, providing a total surface area of approximately 2000 cm^2. Figure 7 shows a photograph of the experimental set-up.

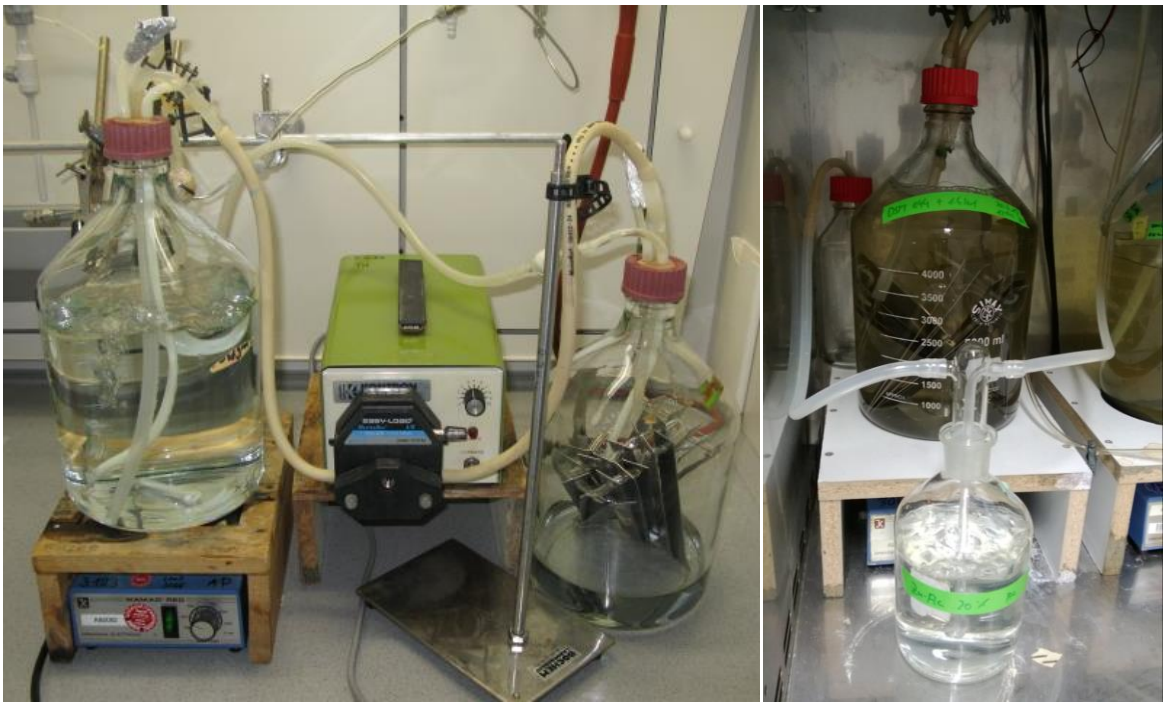

Figure 7 Experimental set-up for growth of *Desulfovibrio vulgaris* in presence of steel. (Left) Transfer of culture medium onto ARMCO metal strips under anaerobic conditions. (Right) Incubation under constant N_2 bubbling with connected H_2S trap and overflow bottle.

To prevent formation of rust on the pure iron coupons before start of the experiment, the medium had to be extensively flushed with N_2 before the metal coupons were submerged. The metal coupons were first put into an empty 5 L bottle and sterilised as described before. A second 5 L bottle with the culture medium was prepared and sterilised. The bottles

were connected using sterile tubing which allowed transfer of the medium from one bottle to the other and N_2 flushing at the same time. Both bottles were now flushed with N_2 through sterile cotton wool filled olives for at least 60 min. Finally, the medium from the second bottle was pumped into the bottle containing the metal samples using a peristaltic pump while still maintaining constant N_2 flushing.

General extraction procedure

After the cultures entered the early stationary phase (cell number 5 x 10^8 mL^{-1}, typically after 96 h incubation), both loosely bound EPS from the medium as well as tightly bound EPS from the cells were extracted, whereby the differentiation of these two fractions is based entirely on their extractability. Loosely bound EPS were extracted from the medium by simple pelletation of the cells. Tightly bound fractions had to be extracted using physical extraction with a cation exchange resin. The extraction method is based on the methods described elsewhere (Aguilera, et al., 2008; Wingender, et al., 2001). Figure 8 shows an overview about the whole extraction process.

Extraction of loosely bound EPS fractions

Cells were harvested from the culture by pelletation. Therefore, a total volume of 4.8 L culture was distributed into 400 mL centrifugation vessels and centrifuged at 11,000 *g* for 20 min at 4 °C. The supernatant containing EPS was collected (fraction I) and immediately frozen at -20 °C or sterile filtered as described below. The cell pellet was resuspended in 200 mL PBS extraction buffer (0.6 g L^{-1} KCl, 4.21 g L^{-1} NaCl, 4.42 g L^{-1} NaH_2PO_4 and 2.62 g L^{-1} Na_3PO_4 in dH_2O, pH 7.5, conductivity adjusted to 10 mS m^{-1} by diluting with dH_2O to match the conductivity of the growth medium), pelleted again as described before and the supernatant containing residual amounts of EPS was carefully removed, collected (fraction II), sterile filtered and frozen.

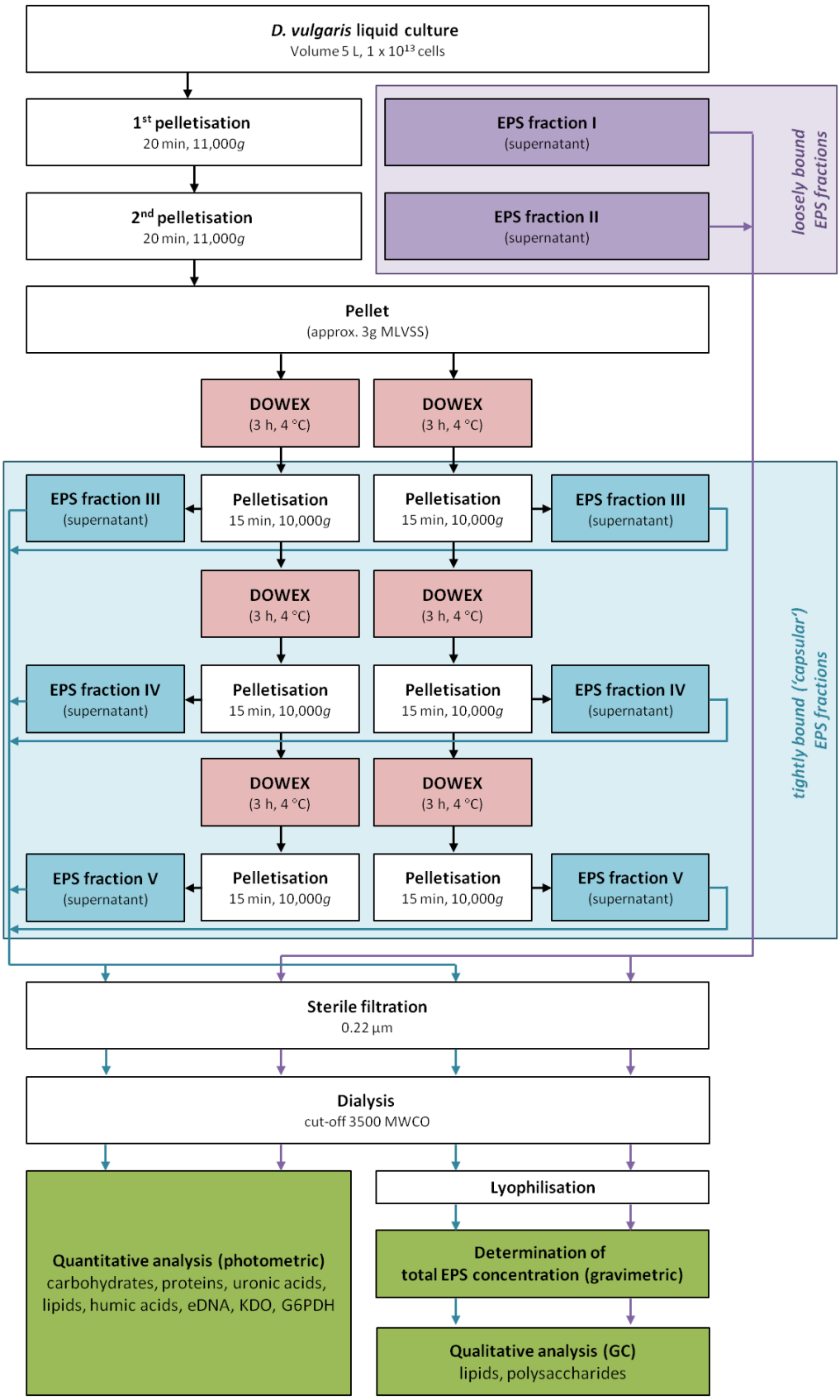

Figure 8 Scheme of the EPS extraction protocol. Loosely bound fractions (I) + (II) are taken from the supernatant medium after pelletisation of the cells. Tightly bound EPS fractions (III) to (IV) are extracted using DOWEX marathon C cation exchange resin. After extraction, the cells are pelleted and the supernatant containing EPS is collected.

Extraction of tightly bound EPS fractions

The weight of the residual cell pellet was determined (typically about 3 g) and the pellet was resuspended in 82 mL of the PBS extraction buffer. The cell suspension was divided into two parts of 41 mL each. From each suspension, 1 mL sample was collected to determine the total cell count. The residual suspension was transferred into 250 mL bottles filled with 20 g cation exchange resin (Dowex® Marathon™ C sodium form). The resin was prior activated by stirring in PBS extraction buffer for 1 h at room temperature in the dark; the buffer was removed using coffee filters and the resin could dry for 5 minutes before transfer to the 250 mL bottles. The tightly bound EPS was extracted for 3 h at 4 °C and 300 rpm in the dark. Then, the supernatant was decanted into 50 mL centrifugation vessels. Remaining cells and exchange resin were removed by centrifugation at 10,000 *g* for 15 min at 4 °C and the supernatant containing the EPS was transferred into fresh 50 mL centrifuge vessels, frozen at -20 °C or immediately sterile filtered as described below. The pellet was resuspended in 40 mL extraction buffer and transferred back into the 250 mL bottles. The extraction procedure was repeated 3 times (EPS fractions III – V), with the duration of the last extraction reduced to 2 h. All handling was performed under sterile conditions either using a sterile workbench or next to the Bunsen burner flame and all equipment was sterilised by autoclaving before use.

Purification of EPS extracts

The EPS extracts were sterile filtered using 0.22 µm cellulose-acetate filters and bottle top filters. Frozen supernatants were thawed at 4 °C beforehand.

The sterile supernatants were transferred into 3500 MWCO cellulose dialysis tubing. The dry tubing was delivered conserved in glycerol and needed to be thoroughly washed under running dH_2O before. It was then stored in 50 % ethanol at 4 °C until use (according to the manufacturer's recommendations). The supernatants were dialysed over night against running dH_2O followed by 2 times against at least the 10-fold volume of MilliQ™ water. Finally, the supernatants were carefully removed from the dialysis tubing, transferred into 50 mL centrifugation vessels and frozen until further analysis.

For each extraction, several negative controls had to be performed. For the loosely bound fraction I, modified Postgate medium C without lactate, sodium sulphate and iron sulphate

was used; for fraction II the extraction buffer was used. Both solutions were autoclaved, dialysed as described before and analysed. For the tightly bound fractions III - V, sterile extraction buffer was subjected to the same Dowex® extraction procedure as the EPS samples.

3.5.2 Quantitative biochemical analysis of EPS extracts

Total EPS dry weight

Defined volumes (typically 20 – 30 mL) dialysed supernatants or negative controls were transferred into sterile 50 mL centrifuge tubes, which were carefully dried and weighed (accuracy 0.1 mg) before. Caps were loosely attached and the samples were frozen at -20 °C. The caps were removed and the tubes were closed with laboratory film (Pechiney Plastic Packaging, US). The film was multiperforated and the samples were lyophilised on 30 °C pre-warmed plates at 1.0 mbar until only powder remained. Then, samples were final dried at 0.01 mbar for at least another 24 hours. The samples were removed and the tubes were weighed again to determine the weight difference before and after lyophilisation. From this difference, the amount of precipitate (containing EPS and unspecific residuals from the medium) per mL of supernatant was calculated. For calculating the EPS amount in the supernatant, the concentration of precipitate from the respective negative controls was subtracted. The lyophilised samples were stored in a desiccator and later used for qualitative analysis of the polysaccharide and lipid fractions.

Polysaccharides

Total carbohydrate content of the EPS extracts was determined by a modified phenol-sulphuric acid assay (DuBois, et al., 1956). 0.2 mL sample were transferred into a 1.5 mL reaction tube, 0.2 mL phenol solution (5 % w/v in dH_2O) were added and the sample was mixed immediately. 1 mL H_2SO_4 conc. was added, the sample was mixed again and allowed to cool down at room temperature for at least 10 min. Afterwards, 250 µL of each sample were transferred into the designated well of a microplate. The absorbance at 485 nm (carbohydrates and humic acids) and 570 nm (humic acids) was measured using a multimode microplate reader and the specific adsorption for carbohydrates was calculated. For each determination, a 6-point calibration (0 – 100 µg mL^{-1}) was performed using glucose and humic

substances, respectively, as standard. The carbohydrate content of each sample or standard was determined in duplicate or triplicate.

Proteins and humic acids

The concentration of proteins and humic acids was determined using a modified Lowry assay (Frølund, et al., 1996). As a result of this thesis, the method was adapted to microplates to allow higher sample throughput while reducing the amount of sample necessary. The Lowry reagent for protein determination was prepared by combining 100 parts sodium carbonate solution (5.72 g L^{-1} NaOH and 27.0243 g L^{-1} Na_2CO_3 in dH_2O) with 1 part sodium tartrate solution (24.062 g L^{-1} $C_4H_4O_6Na_2$ in dH_2O) and 1 part copper sulphate solution (9.098 g L^{-1} $CuSO_4$ in dH_2O). For the humic acids determination, copper sulphate solution was replaced by the same amount of dH_2O. For the microplate assay, 175 µL of the respective reagent were added to 125 µL sample and the solution was mixed carefully by repeated aspirating and dispensing. After 20 min at room temperature, 25 µL FCP reagent (2.5 mL Folin-Ciocalteus phenol reagent in 3 mL dH_2O) were added and the solution was carefully mixed again. After another 30 min at room temperature, the absorbance at 625 nm of each sample was determined using a multimode microplate reader (as described before). The absorbance for proteins and humic acids was corrected as described elsewhere (Frølund, et al., 1996). For each microplate, independent 6-point calibrations (0 – 150 µg mL^{-1}) for both proteins (using BSA as standard) and humic acids were performed without absorbance correction.

Uronic acids

The uronic acid content was determined according to the method described by Blumenkrantz & Asboe-Hansen (1973). 1.2 mL reagent I (2.51 g L^{-1} $Na_2B_4O_7$ in H_2SO_4 conc., stirred for 24 h) were added to 200 µL frozen sample in reagent tubes and incubated for 5 min at 100 °C in a water bath. Afterwards, the samples were cooled down to room temperature on ice. Then, 20 µL dH_2O (sample blank) or reagent II (30 mg β-hydroxydiphenyl in 20 mL NaOH) were added and after additional 5 min 250 µL of each sample were transferred to microplates and the adsorption at 520 nm was measured. For each determination, a 7-point calibration (0 – 100 µg mL^{-1}) was performed using glucuronic acid as standard. For

each sample, the adsorption was corrected by subtracting the respective sample blind. The uronic acid content of each sample or standard was determined at least in duplicate.

Lipids

Lipids were isolated from the EPS supernatants by extraction with chloroform:methanol (2:1 v/v) in a biphasic system (Folch, et al., 1957) and colorimetrically quantified using a modified sulpho-phospho-vanillin assay for microplates (Cheng, et al., 2011). The EPS extracts were 25-fold pre-concentrated by lyophilisation and 1.5 parts chloroform:methanol solution was added. The solution was thoroughly mixed for 10 minutes and NaCl (200 g L^{-1} in dH_2O) was added to a final concentration of 0.73 % (w/v) in the aqueous phase to facilitate the transfer of residual lipids from the aqueous to the organic phase. The sample was mixed again and the phases were separated by centrifugation at 5000 *g* for 5 min. The organic phase was collected and analysed immediately. For the colorimetric quantification of the lipids, 50 µL of the concentrated lipid extract were transferred into the designated well of a polypropylene microplate. The solvent was evaporated at 85 °C and 100 µL H_2SO_4 conc. were added. After 30 min incubation at 85 °C, the microplate was quickly cooled down to room temperature at -20 °C in a freezer (approximately 2 min) and the background absorbance at 540 nm was determined for each well using a multimode microplate reader (as described before). Then, 50 µL phospho-vanillin reagent (0.2 mg mL^{-1} vanillin in 15 % H_3PO_4) were added to each well. After 10 min incubation at room temperature the absorbance was determined again. For each microplate, a calibration series from 0 – 10 µg lipids was performed. 10 mg olive oil were dissolved in 1000 µL chloroform:methanol solution and 0 – 10 µL of the standard were pipetted into designated wells. The lipid content of each sample or standard was determined in duplicate or triplicate.

Nucleic acids

The concentration of DNA in the EPS extracts was determined using the Quant-It™ PicoGreen® dsDNA Kit (Invitrogen, US). The method was adapted to micro titre plates to allow higher sample throughput and to reduce the amount of sample necessary. All solutions were prepared according to the manufacturer's instructions. 1x TE buffer was prepared by diluting the supplied 20x TE buffer concentrate (200 mM Tris-HCl, 20 mM EDTA, pH 7.5; Invitrogen/Molecular Probes) 20-fold in DEPC-treated sterile dH_2O. The PicoGreen®

reagent was prepared by diluting the supplied PicoGreen® reagent concentrate 200-fold in 1x TE buffer. 100 µL sample were transferred into the designated well of a 96-well microplate. After all samples were transferred, 100 µL PicoGreen® reagent were added to each well and the sample was mixed carefully by repeated aspirating and dispensing with a micropipette. After 5 min incubation in the dark, the sample fluorescence (excitation at 480 nm, fluorescence detection at 520 nm) was measured using a multimode microplate reader. The microplate reader was set to orbitally shake the plate for 5 s with 1.5 mm amplitude before the measurement. For each microplate, a high-range 5-point standard curve (0 – 1 µg mL^{-1}) was prepared and recorded according to the manufacturer's manual. The DNA content of each sample or standard was determined in duplicate or triplicate.

Total iron, Fe(II)-, and Fe(III) ions

The iron content of EPS extracts was determined using the phenantrolinium assay according to DIN EN ISO 14719:2011. The method was adapted for high sample throughput using 96-well 2-mL microplates. Up to 920 µL sample were transferred into the designated well of the microplate and 40 µL ammonium acetate solution (400 g ammonium acetate dissolved in 500 mL glacial acetic acid and filled up to 1000 mL with dH_2O) as well as 40 µL phenantrolinium solution (5 g L^{-1} 1,10-phenantrolinium chloride in dH_2O) were added. Deionised water was added to a total volume of 1000 µL and the samples were mixed thoroughly by repeated aspiring and dispensing. 300 µL of each sample were then transferred to another 96-well microplate (330 µL chamber volume) and the Fe(II) concentration was determined by measuring the adsorption at 492 nm after 15 min incubation using a multimode microplate reader. Then, 10 µL hydroxylamine solution (200 g L^{-1} β-hydroxylamine in deionised water) were added to each sample and after another 15-min incubation in the dark the total iron concentration was determined by measuring the absorbance again. The Fe(III) concentration was determined by subtracting the Fe(II) amount from the amount of total iron. For each microplate, a 5-point calibration (0 – 12 µg mL^{-1}) from a freshly prepared iron standard (0.8 g L^{-1} in dH_2O) was performed. The iron content of each sample or standard was determined in duplicate or triplicate.

2-keto-3-deoxyoctonate

EPS extracts were analysed for KDO, the strictly intracellular essential oligosaccharide of the lipopolysaccharide of Gram-negative cell walls according to the method described elsewhere (Karkhanis, et al., 1978). In brief, 500 µL EPS-extract, standard or blank were filled into 2-mL safelock reaction tubes, 500 µL 0.2 M H_2SO_4 were added, the solution was mixed thoroughly and the tubes were incubated in a water bath at 100 °C for 30 min. 250 µL the solution were transferred into fresh 1.5 mL reagent tubes, 125 µL 0.04 M periodic acid (7.68 g L^{-1} HIO_4 in 0.125 N H_2SO_4) were added, the solution was again mixed thoroughly and incubated at room temperature for 20 min. Then, 125 µL sodium arsenate (2.6 % w/v $NaAsO_2$ in 0.5 M HCl) were added and the sample was mixed again. After the brownish colouration disappeared, the sample was mixed with 250 µL TBA (0.6 % w/v in dH_2O) and incubated at 100 °C for another 15 min in a water bath and, while still hot, 500 µL DMSO were added. After cooling down to room temperature, the sample was transferred to a 1 mL photometer cuvette and the adsorption at 548 nm was measured against a blank using a single beam spectrophotometer. For each determination, a 6-point calibration (0 – 10 µg mL^{-1}) using KDO as standard (10.17 mg KDO ammonium salt in 100 mL dH_2O) was performed. The KDO content of each sample or standard was determined in duplicate or triplicate.

Enzymatic activity of glucose-6-phosphate dehydrogenase

Supernatants containing EPS were analysed for the presence of activity of the strictly intracellular enzyme glucose-6-phosphate dehydrogenase (G6PDH) by the method of Ng and Dawes (1973) using the miniaturised microplate assay described elsewhere (Michalowski, 2012). The remaining cell pellets of *Desulfovibrio vulgaris* after EPS extraction were permeabilised by ultrasound (on ice to keep temperatures below 40 °C). The cell extracts were used to confirm the presence of G6PDH inside the cells. To confirm functionality of the assay, positive controls using 0.1 µg mL^{-1} standards from *Leuconostoc mesenteroides* (Sigma) were performed. Cell extracts without addition of glucose-6-phosphate (G6P) as substrate served as negative controls to exclude unspecific influence of matrix residuals on the assay. Per sample (well) 290 µL substrate solution were prepared by mixing 100 µL Tris/HCl buffer (120 mM, 1.45 g Tris in dH_2O, pH adjusted to 8.6 with 1 M HCl) with 75 µL

G6P solution (20 mM, 0.045 g G6P in 8 mL dH_2O), 50 µL β-NADP solution (10 mM, 0.045 g β-NADP in 6 mL dH_2O), 18 µL $MgCl_2$ solution (250 mM, 5.08 g $MgCl_2$ x H_2O in 100 mL dH_2O) and 47 µL dH_2O. 200 µL of each dH_2O (blank), negative and positive controls as well as the samples were transferred into the designated wells of a 96-well microplate. After all samples were transferred to the plate, the samples were immediately processed or 20-fold concentrated by vacuum centrifugation at 30 °C until dryness and following addition of 10 µL dH_2O to each well. 290 µL substrate solution (without G6P for negative controls) preheated to 37 °C were added to each well and the solutions were mixed thoroughly by repeated aspirating and dispensing. The absorbance at 340 nm of each well was measured at intervals of 1 min over a period of 3 h using a multimode microplate reader. To ensure proper mixing of the solutions, the plate reader was set to 5 s orbital shaking with 1.5 mm amplitude prior to each measurement cycle. All samples and controls were measured at least in duplicates.

Total organic carbon

Total organic carbon content of the EPS extracts was determined instrumentally by the combustion catalytic oxidation/NDIR method using a Shimadzu TOC-V_{CPH} total carbon analyser. The TOC of each sample was determined indirectly by independently measuring total carbon (TC) and total inorganic carbon (TIC). All samples were measured against MilliQ™ water as a blank. All EPS extracts were diluted up to 10-fold with MilliQ™ water prior to the measurement. 5-point calibrations from 0 to 20 mg L^{-1} were performed for TC and TIC from 1000 mg L^{-1} standards (TC: 2.125 g L^{-1} potassium hydrogen phthalate in MilliQ water, TIC: 3.5 g L^{-1} $NaHCO_3$ and 4.41 g L^{-1} Na_2CO_3 in MilliQ water).

3.5.3 Identification of lipid and polysaccharide monomers from EPS fractions

The gas chromatographic separation and identification of lipid and sugar monomers from EPS extracts was performed as described elsewhere (Gehrke, et al., 2001). Both were analysed directly from combined lyophilisates of the first and second supernatant of both the loosely bound and tightly bound EPS fractions, respectively (see chapter 3.5.1). Figure 9 shows a schematic overview of the different derivatisation procedures involved.

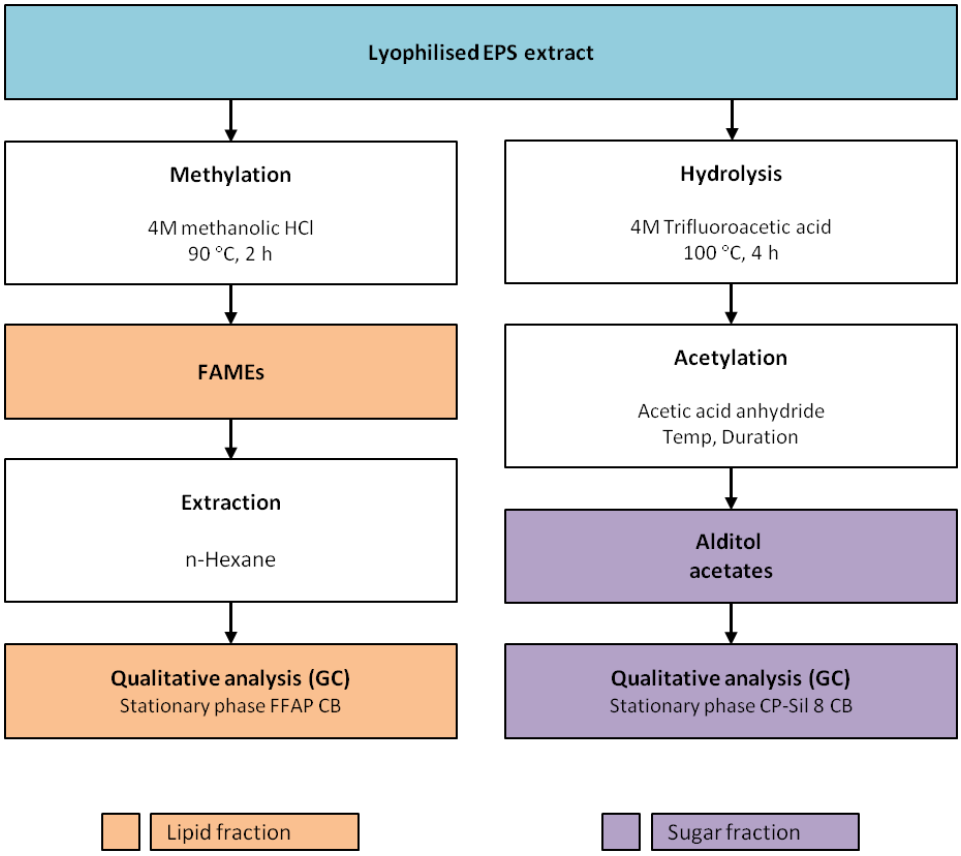

Figure 9 Schematic overview of the derivatisation procedure for the qualitative analysis of lipid and polysaccharide fractions from lyophilised EPS extracts

In brief, lipids were converted to fatty acid methyl esters (FAMEs) prior to the chromatographic separation. Therefore, approximately 15 mg lyophilised EPS extract (plus 1 µmol undecanoic acid C11:0 as internal standard) were methylated with 200 µL 4 M methanolic HCl (freshly prepared from calculated amounts of methanol and acetyl chloride) at 90 °C for 2 h. After cooling down, 500 µL MilliQ™ water were added and the FAMEs were extracted with 3x 500 µL n-Hexane (phase separation by centrifugation at 700 *g* for 3 min). The organic extracts were combined, washed acid-free with 2x 500 µL MilliQ™ water, dried with $CaCl_2$ and concentrated by partial evaporation under a nitrogen stream.

The chromatographic separation of lipids was performed using a FFAP CB stationary phase (internal diameter of the column 0.32 mm, thickness of the stationary phase 0.3 µm, length 25 m) and helium as mobile phase (2 mL min^{-1}). Injection volume was 1 - 2 µL (split 1:25) at 200 °C injector temperature. A linear temperature gradient from 115 °C (2 min) to 240 °C (60 min) at a rate of 4 °C min^{-1} was run. Detection was done by a flame ionisation detector (FID) using hydrogen (30 mL min^{-1}) and artificial air (300 mL min^{-1}) as fuel gases at a detector temperature of 275 °C. A 5-point calibration was performed from a 20 µM multi-standard

stock prepared from individual standards C6:0 to C28:0 (table 4). Undecanoic acid (C11:0) was used as internal standard to calculate peak area correction factors for the quantification and peaks were annotated based on the calculated retention index (Julin, et al., 1983) of each compound (table 17).

Table 17 Composition of fatty acid multi-standard with corresponding retention times and - indices

Compound	Abbreviation	Ret. time (min)	Ret. index[†]
Caproic acid	C6:0	1.6	600
Caprylic acid	C8:0	2.5	800
Nonanoic acid	C9:0	3.4	900
Capric acid	C10:0	4.8	1000
Undecanoic acid (internal standard)	C11:0	6.6	1100
Lauric acid	C12:0	8.9	1200
Myristic acid	C14:0	14.3	1400
Myristoleic acid	C14:1	15.4	1440
Palmitic acid	C16:0	19.8	1600
Palmitoleic Acid	C16:1	20.7	1633
Stearic acid	C18:0	25.2	1800
Elaidic acid	C18:1	25.8	1824
Linoleic acid	C18:2	27.1	1876
Nonadecanoic acid	C19:0	27.7	1900
Linolenic acid	C18:3	28.6	1936
Arachidic acid	C20:0	30.2	2000
Eicosenaoic acid	C20:1	30.7	2021
Heneicosanoic acid	C21:0	32.6	2100
Behenic acid	C22:0	35.0	2200
Erucic acid	C22:1	35.6	2221
Tricosanoic acid	C23:0	37.9	2300
Lignoceric acid	C24:0	41.3	2400
Pentacosanoic acid	C25:0	45.6	2500
Hexacosanoic acid	C26:0	51.0	2600
Heptacosanoic acid	C27:0	58.0	2700
Octacosanoic acid	C28:0	66.8	2800

[†]*estimated from retention time and number of carbon atoms (Julin, et al., 1983)*

For the separation and identification of neutral sugar monomers and amines, approximately 15 mg lyophilised EPS extract (plus 5 µmol Erythritol as internal standard) were hydrolysed in 4 M trifluoroacetic acid (100 °C, 4 h). After evaporation of the acid and repeated

washing with MilliQ™ water on a rotary evaporator (6 – 10x), the dry sample was finally resuspended in 100 µL MilliQ™ water.

For the derivatisation to alditol acetates, 100 µL 1 N NH_3 and 100 µL $NaBH_4$ (200 mg mL^{-1} in DMSO) were added. The sample was reduced for 90 min at 40 °C in a water bath and 100 µL concentrated acetic acid were added dropwise to remove excess borohydride. 200 µL N-methylimidazole and 2 mL acetic acid anhydride were added and the sugars were acetylated for 1 h at 40 °C in a water bath. Afterwards, the sugar derivatives were extracted in a biphasic system by adding 4 mL MilliQ™ water and 1 mL $CHCl_2$. After phase separation (centrifugation at 1000 *g* for 5 min), the organic phase containing the alditol acetates was dried over $CaCl_2$.

The chromatographic separation was performed using a CP-Sil 8 CB stationary phase (internal diameter of the column 0.32 mm, thickness of the stationary phase 0.25 µm, length 30 m) and helium as mobile phase at a flow rate of 2 mL min^{-1}. 1 µL of the $CHCl_2$ extract were injected (split 1:10) at 200 °C injector temperature. A linear temperature gradient from 150 °C (10 min) to 200 °C (10 min) at a rate of 4 °C min^{-1} was used and the fractions were detected as described before. A 5-point calibration was prepared from a 20 µM multistandard consisting of rhamnose, fucose, ribose, arabinose, mannose, glucose and galactose and peaks were annotated based on their relative retention times compared to the internal standard. The amount of alditol acetates was calculated considering a peak area correction factor based on the response of the internal standard.

3.6 Investigations on the influence of cyclodextrins on MIC of steel

3.6.1 Cyclodextrin film of steel surfaces

The cyclodextrin coating procedure is based on the method described elsewhere (Pannekens, 2012). Additional polymerisation was used to increase both the homogeneity of the cyclodextrin films as well as their stability against dissolution into the surrounding medium.

Under sterile conditions, stainless steel coupons (prepared according to chapter 2.4) were transferred into 30 mL screw cap bottles. The cyclodextrin solution was prepared by dissolving 150 mg cyclodextrin in 50 mL centrifuge tubes filled with 15 mL oxygen-free sterile

dH_2O (final concentration 10 mg mL^{-1}) and 60 µL of a fluorescently labelled carboxymethyl-β-cyclodextrin (FITC-CMBCD) solution (10 mg mL^{-1}) were added. Afterwards, all materials were transferred into an anaerobic glove box and 15 mL cyclodextrin solution were added to each coupon. Controls were performed using 15 mL oxygen-free dH_2O. Then, the screw cap bottles were tightly closed and incubated inside the glove box for 2 h. Finally, the cyclodextrin solution was carefully removed using a pipette and the coupons were dried for at least 2 days under anoxic conditions (in the dark to prevent photobleaching of the fluorescently labelled cyclodextrin).

To increase film stability, the cyclodextrin films were polymerised using a 10-fold excess of glutardialdehyde in hydrochloric dH_2O under sterile conditions at a pH of 2 (e.g. Badruddoza, et al., 2013). In brief, steel coupons were transferred into 25 mL glass beakers. A dip-coating solution was prepared by filling 19916 µL sterile dH_2O (adjusted to pH 2 using 1 M hydrochloric acid solution) into 50 mL centrifuge tube and adding 84 µL glutardialdehyde (25 %) followed by 80 µL fluorescently labelled FITC-CMBCD solution (10 mg mL^{-1}). The solution was mixed thoroughly and immediately used to dip-coat the coupon in the beaker (conditions as described before).

3.6.2 Simulation of MIC

Precisely weighed non-alloyed steel coupons (30 x 20 x 1 mm, prepared as described before) were put into sterile 30 mL screw cap bottles in a tilted position (figure 10).

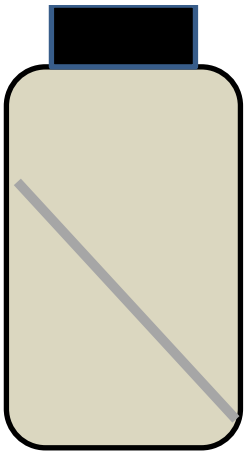

Figure 10 Set-up for MIC simulations. (Grey) metal coupon, (brown) growth medium containing *Desulfovibrio vulgaris*.

Under anoxic conditions (10 % H_2, 10 % CO_2, 80 % N_2), 24 mL yeast-free Postgate C medium were added and 1 mL of a well-grown *Desulfovibrio vulgaris* stock culture (approximately 5 x 10^8 cells mL^{-1}) were added. The screw cap bottles were tightly closed, transferred into

an anaerobic container (to ensure anaerobiosis during incubation) and incubated at 37 °C for 7 days up to 3 weeks. Afterwards, the coupons were removed and thoroughly cleaned in EDTA solution (30 g L^{-1} in dH_2O) in an ultrasonic bath for 5 min to remove remaining corrosion products, transferred into a glove box and carefully rinsed with oxygen-free dH_2O. The coupons were dried at least 2 days inside the glovebox and weighed again. The corrosion rates were determined gravimetrically by measuring the weight loss and calculated according to:

$$R_{corr} = 87.6 \times {}^{W}/_{D \times A \times T} \qquad \text{(Rajendran, et al., 2013)}$$

R_{corr} = corrosion rate [mmpy]
W = weight loss [mg]
D = metal density [g cm^{-3}]
A = sample area [cm^2]
T = time of exposure of the metal sample [h]

The relative corrosion reduction was calculated based on the corrosion rates of uncoated reference coupons for each simulation run:

$$Corrosion\ reduction\ [\%] = 1 - {}^{R_{corr}(sample)}\Big/_{R_{corr}(reference)} \times 100$$

$R_{corr}(sample)$ = corrosion rate [mmpy] of the coated sample
$R_{corr}(reference)$ = corrosion rate [mmpy] of the uncoated reference

Additional sterile controls were performed to not only check sterility but also to check the absence of corrosion. In case of cyclodextrin-coated coupons, additional controls using only glutardialdehyde/CMBCD-FITC cyclodextrin were prepared to compensate for their potential influence on corrosion rates and to exclude possible impact of glutardialdehyde on growth of *Desulfovibrio vulgaris*.

3.6.3 Fluorescence-staining of biofilms

Biofilms on mirror-polished coupons were stained by applying 250 µL of a Syto9 solution (3 µM, 5 min) or DAPI solution (0.01 % DAPI in 4 % formaldehyde, 10 min). Afterwards, EPS were stained by applying 250 µL of a tetramethylrhodamine isothiocyanate- or fluorescein isothiocyanate conjugated Concanavalin A (ConA-TRITC and –FITC, respectively) lectin solution, respectively, for another 10 min and thoroughly rinsed with sterile MilliQ™ water. All handling was performed under anoxic conditions to prevent formation of rust on pure iron and carbon steel coupons. Afterwards, the samples were dried under a nitrogen

stream and either stored in a desiccator (for visualisation of cyclodextrin films or biofilm by EFM or CLSM) or immediately visualised by SKPFM (chapter 3.4.3).

3.6.4 Estimation of the surface area covered by biofilms

From each coupon, 10 - 100 individual visual fields were visualised by EFM. The relative biofilm surface coverage was estimated from the total DAPI- or Syto9-fluoresceing area from saved images of each visual field using a custom-made automatic script for ImageJ (appendix 7.1).

3.6.5 Visualisation of cyclodextrin films

Topographic AFM images did not provide any additional information about the surface character of the cyclodextrin films before or after the corrosion experiments because it was not possible to distinguish between the films and the bare material itself, only if the typical grooves of the wet-ground steel surface were fully covered (data not shown). After MIC experiments, single cells from the biofilms covering the cyclodextrin films were clearly identifiable but it was not possible to elucidate whether microbial cells migrated into the cyclodextrin film or if the cyclodextrin film beneath the cells was still intact. Additionally, no difference between the surfaces of non-polymerised and polymerised cyclodextrin films was visible (data not shown). Hence, the cyclodextrin films were visualised either by epifluorescence microscopy (EFM) or confocal laser scanning microscopy (CLSM). In contrast to EFM, CLSM allows to obtain high-resolution images with optical sectioning, i.e. by focusing different depths of a specimen without superimposition of the information, 3d images of the specimen can be created. The instrumental set-up for both instruments is described in table 14. For EFM, optimal exposure was used. In CLSM, the samples were visualised using a pinhole of 1000 and a detector gain of 834.

4 RESULTS

4.1 Development of a fully defined growth medium for MIC simulations with *Desulfovibrio vulgaris*

To exclude any influence of yeast on the corrosion processes, a fully defined medium based on an already modified Postgate medium C (von Rège, 1999) was developed. Yeast was replaced by trace element and vitamin solutions according to DSMZ media 320 and 141, respectively. To test the suitability of the medium for *Desulfovibrio vulgaris*, growth curves using both media were determined over a total time of 14 d (figure 11).

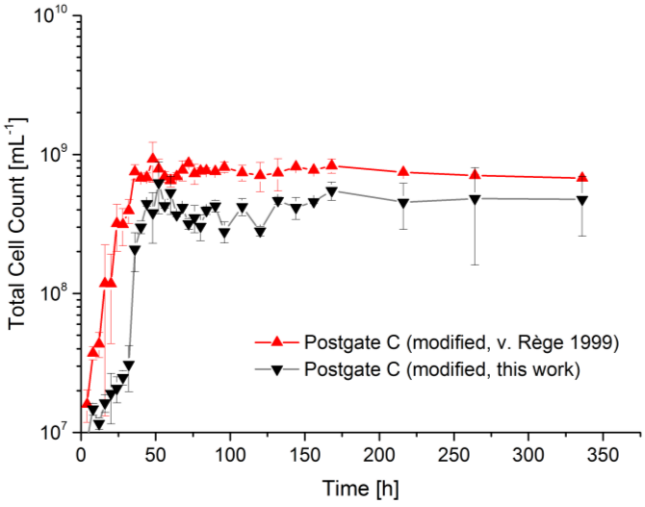

Figure 11 Growth of *Desulfovibrio vulgaris* in Postgate medium C (modified, von Rège, 1999) vs. yeast-free Postgate medium C (this work). 3 independent biological replicates for each medium were grown under anaerobic conditions at 37 °C for a total of 14 d. Total cell count was determined using modified Thoma chambers (depth = 0.02 mm).

Initially, the fully determined medium shows a slightly longer lag phase compared to the original medium. The cell number in the stationary phase (between 108 and 336 h) were comparable ($7.5 \times 10^8 \pm 8.4 \times 10^7$ vs. $4.4 \times 10^8 \pm 1.2 \times 10^8$ cells mL^{-1} for the original and fully defined medium, respectively). No difference in EPS production was found (data not shown) indicating that the yeast-free modification of the Postgate medium did not have any negative effect on growth and metabolism of the cells.

4.2 Analysis of the contact potential difference (CPD) of biofilms and material surfaces by combined SKPFM & EFM

A novel combination of SKPFM & EFM was used to visualise and analyse the influence of *Desulfovibrio vulgaris* on the contact potential difference (CPD, often referred to as surface potential) of pure iron, carbon steel, and alloyed CrNi steel.

4.2.1 Definition of standard scanning parameters for SKPFM

First, standard parameters for the visualisation of the CPD had to be defined. For this, a steel coupon with a gold grit sputtered onto the surface was kindly provided by Francesco Depentori of the DECHEMA Research Institute. Parameters such as the tip velocity, the height of the air gap between tip and surface, and the vibration amplitude of the cantilever during the potential mapping strongly influence the contrast in potential images (figure 12).

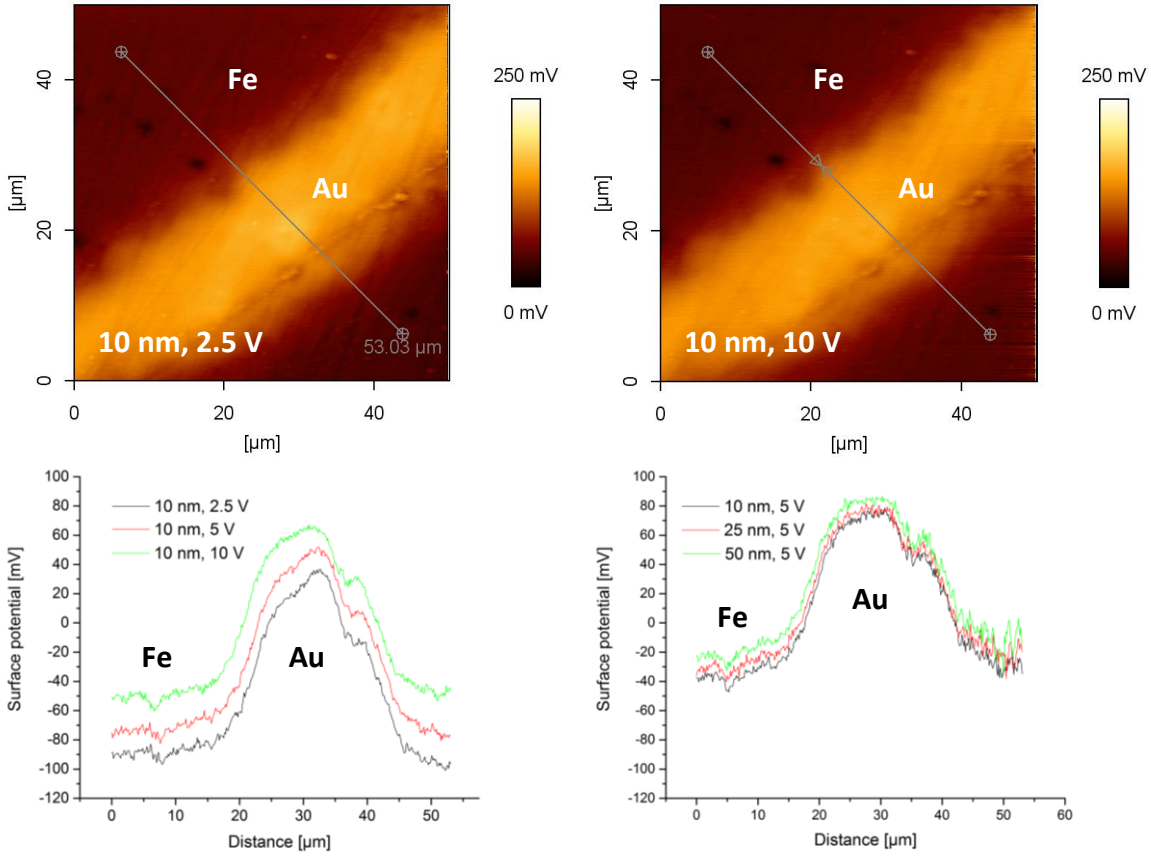

Figure 12 Influence of SKPFM scanning parameters on CPD contrast. (Top) CPD mapping, (left) air gap 10 nm, amplitude 2,5V, (right) air gap 10 nm, amplitude 10 V. (Bottom) surface potential line scans along the grey lines indicated in top images; (left) fixed air gap 10 nm, amplitude 2.5, 5, and 10 V; (right) fixed amplitude of 5 V, air gap 10, 25, and 50 nm. Brighter parts (higher surface potentials) show a section of the gold grit (Au), darker parts represent metal surface (Fe). CPD mapping was done using an ElectriTap 300 cantilever in SKPFM hover mode at a line rate of 0.5 Hz (tip velocity 50 µm s^{-1}); air gap and vibration amplitude see above.

The optimal vibration amplitude of the cantilever was determined by keeping a constant air gap of 10 nm. A vibration amplitude of 5 V produced the highest contrast. However, at values between 2.5 to 10 V the difference in contrast was negligible (figure 12, top). Line profiles along the same coordinates of the mapping images recorded at 3 different amplitude values were effectively identical (figure 12, bottom left).

Afterwards, the air gap was optimised by increasing the air gap from 10 to 25, and finally to 50 nm. Again, no significant difference in contrast was observed, but larger air-gaps showed a tendency to increase the background noise of potential images (see line scans in figure 12, bottom right). On bacterial samples, however, the best results were obtained with lower amplitudes of 2.5 V at 50 nm air gap, as smaller air gaps and especially higher amplitudes produced strong artefacts. The most significant influence on scanning quality of biological samples was caused by the tip velocity; slow line rates significantly increased image quality and reduced artefacts (data not shown).

Based on these results, the following standard parameters for biological samples were specified: tip velocity of ≤ 0.3 Hz (equivalent tip velocity of 3 µm s^{-1} for a typical image size of 5 x 5 µm), air gap of 50 nm, 2.5 V vibration amplitude.

4.2.2 Definition of the test conditions

Influence of sterile media on the CPD of pure iron, carbon and alloyed steel surfaces

Coupons of pure iron, carbon and alloyed steel were incubated for 7 d under anoxic conditions in yeast-free Postgate medium C at 30 ± 2 °C. Afterwards, the samples were immediately dried under a nitrogen stream for at least 30 min and visualised by SKPFM.

Before incubation, all coupons showed a similar surface with clearly visible grooves from the polishing process (see figure 13, top). The potential profiles of all materials before incubation were identical (data not shown) and comparable to alloyed steel after incubation. Both carbon steel and pure iron show the formation of grain boundary like structures after incubation. The potential profiles appear to have a higher background noise compared to the results before incubation (see figure 13, middle and bottom, respectively).

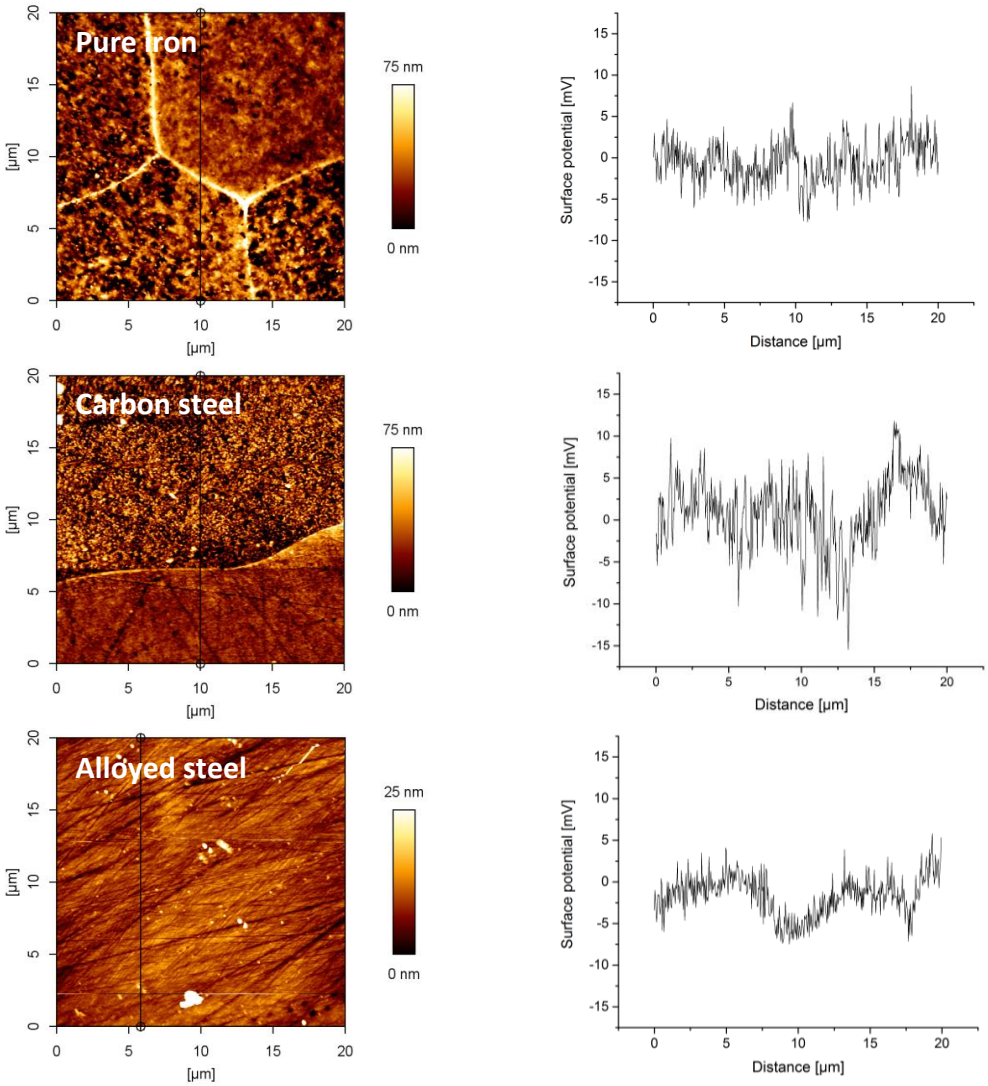

Figure 13 Topography and CPD line profiles of pure iron, carbon-, and alloyed steel after 7 d in sterile medium. (From top to bottom) Alloyed steel, pure iron, and carbon steel; (left) topography, (right) cross-sectional CPD profiles along the black lines indicated in the topography images. Wet ground (SiC P180) and diamond polished coupons (20 x 15 x 1 mm) were rinsed with deionised water, cleaned with ethanol (70 %), degreased with acetone and sterilised for 8h at 130 °C under N_2. The coupons were incubated in sterile yeast-free Postgate medium C under anoxic conditions (80 % N_2, 10 % H_2, 10% CO_2) at a temperature of 30 ± 2 °C for 7 d. Afterwards, the coupons were thoroughly rinsed with N_2-flushed sterile dH_2O, immediately dried under a nitrogen stream, glued to objective slides and visualised by SKPFM. Images show the lock-in amplitude, recorded at an amplitude of 8 V. The cross-sectional CPD profiles were calculated from CPD mapping images recorded in SKPFM hover mode using an ElectriTap 300 cantilever with a 50-nm air gap at a vibration amplitude of 2.5 V and a line rate of 0.3 Hz (tip velocity 12 µm s^{-1}).

However, the absolute min/max variation was not significantly increased and hence no influence on the CPD by sterile medium could be observed.

Removal of attached biofilms without influencing the CPD profiling

To allow measuring the CPD below cells, a suitable method for cell removal had to be developed. This method should not influence surface potentials or the material itself while

reliably removing all biological material. For that, ultrasound treatment with 5 different detergents (each 1 % w/v Tween 20 and Tween 80, SDS at a concentration of 1, 0.5, and 0.1 % w/v as well as dH_2O as control) was performed. To prevent oxygen-corrosion of the non-alloyed materials, the whole treatment was performed under anoxic conditions. No significant difference was observed between Tween 20 (38 ± 23 % less surface area covered by biofilm), Tween 80 (40 ± 21 %), 0.1 % SDS (19 ± 38 %) and the control (29 ± 12 %). The highest efficacy was observed for SDS at a concentration of 0.5 and 1 % (99.8 ± 0.2 % and 99.5 ± 0.3 % biofilm removal, respectively, figure 14).

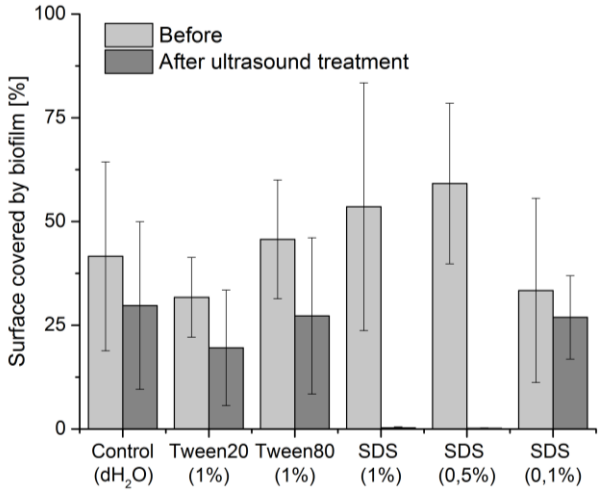

Figure 14 Efficacy of detergents in removing biofilms for combined SKPFM & EFM investigations. Biofilms were grown on alloyed steel coupons (30 x 15 x 10 mm, P180) for 24 h (initial cell number 1 x 10^8 mL^{-1}) at 37 °C under anaerobic conditions. After incubation, the coupons were glued to objective slides, biofilms were stained by Syto9 (3 µM, 10 min) and visualised by EFM. Afterwards, the glass slides with coupons were put into 50 mL vessels and 35 mL of the respective detergent solution were added. The samples were then treated for 30 min in an ultrasonic bath in the dark. Afterwards, the coupons were rinsed thoroughly with 2 x 5 mL deionised water, dried under a N_2 stream and residual biofilms were again visualised by EFM. For each coupon, at least 10 individual visual fields automatically analysed (cf. appendix, chapter 7.1).

Figure 15 shows exemplary fluorescence images of the material surface before and after ultrasound treatment. The fluorescence images before ultrasound treatment clearly show a continuous biofilm of *Desulfovibrio vulgaris* (green). In contrast, no biofilm is visible after treatment in SDS 0.5 % but some fluorescing particles were still visible.

Subsequent AFM images of the SDS treated surfaces showed no apparent residual cells or cell debris, but confirmed the presence of particles of unknown composition and origin (data not shown). Based on these results, ultrasound treatment in 0.5 % SDS was selected for further experiments to remove attached cells.

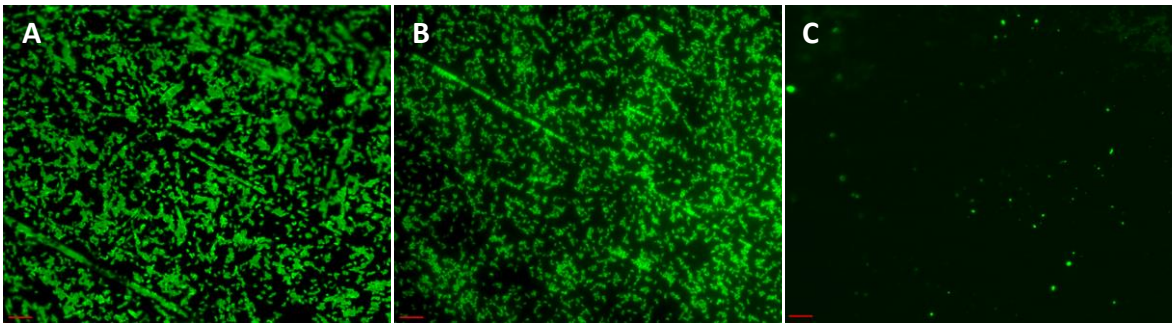

Figure 15 Visualisation of *Desulfovibrio vulgaris* biofilms on alloyed steel surfaces before and after ultrasound treatment. (A) Biofilm before ultrasound treatment, (B) biofilm after ultrasound treatment with dH_2O (control), (C) material surface after treatment with SDS 0.5 % w/v. Biofilms were grown on alloyed steel coupons (30 x 15 x 10 mm, P180) for 24 h (initial cell number 1 x 10^8 mL^{-1}) at 37 °C under anaerobic conditions. After incubation, the coupons were glued to objective slides, biofilms were stained by Syto9 (3 µM, 10 min) and visualised by EFM. Afterwards, the glass slides with coupons were put into 50 mL centrifuge vessels and 35 mL of the respective detergent solution were added. The samples were then treated for 30 min in an ultrasonic bath in the dark. Afterwards, the coupons were rinsed thoroughly with 2 x 5 mL deionised water, dried under a N_2 stream and residual biofilms were again visualised by EFM. For each coupon, at least 10 individual visual fields automatically analysed (cf. appendix, chapter 7.1).

Morphological changes of *Desulfovibrio vulgaris* cells and development of CPD after emersion

During this study, it became apparent that potential mappings of different microbial cells may show a broad distribution of surface potentials (i.e. CPD) of single cells (data not shown). To identify the reason for the seemingly random results, morphological changes of the cells as wells as the constancy of CPD measurements after emersion of the samples were investigated. Figure 16 shows topographical images of a single *Desulfovibrio vulgaris* cell during the first 48 h after emersion. Morphologically, no difference in cell shape can be observed during the first 6 h. After 12 h and above, however, the cell appears flatter and wider, with a more bulbous shape.

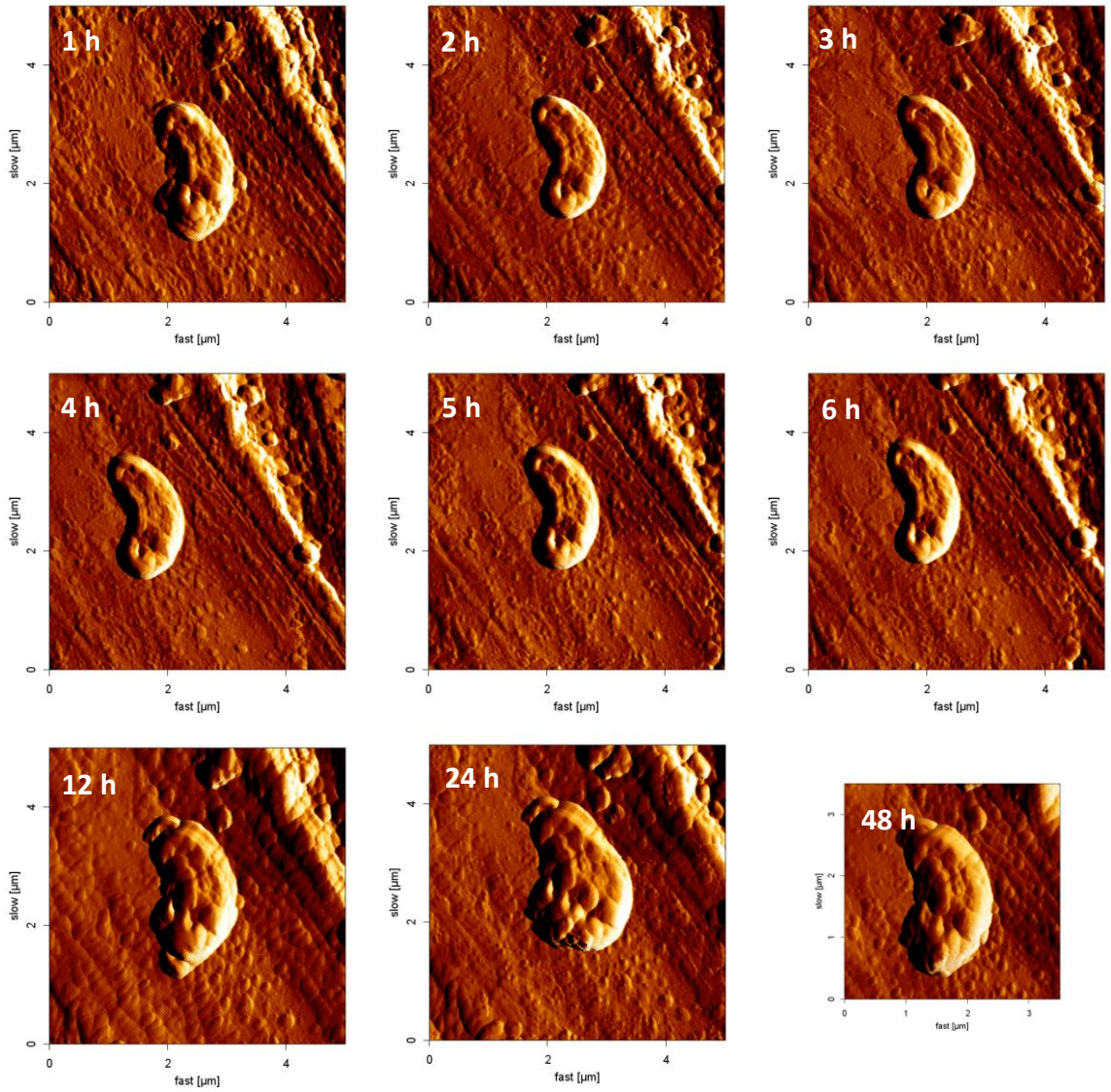

Figure 16 Topographic time series of *Desulfovibrio vulgaris* attached to mild steel. Labels indicate the time after emersion. A wet ground (SiC P180) carbon steel coupon (20 x 15 x 1 mm) was rinsed with dH_2O, cleaned with ethanol (70 %), de-greased with acetone and sterilised for 8h at 130 °C under N_2. The coupon was incubated with *Desulfovibrio vulgaris* (initial cell number 5 x 10^8 ml^{-1}) in yeast-free Postgate medium C under anoxic conditions (80 % N_2, 10 % H_2, 10 % CO_2) at 30 ± 2 °C for 30 min. Afterwards, the coupon was thoroughly rinsed with N_2-flushed sterile dH_2O, immediately dried under a N_2 stream, fixed to an objective slide and visualised by SKPFM. Images show lock-in amplitude, recorded using an ElectriTap 300 cantilever at an amplitude of 8 V at a line rate of 0.5 Hz (tip velocity 2.5 µm s^{-1}).

Additionally, cross-sectional CPD profiles along the cells 1 and 12 h after the end of sample incubation were evaluated and compared. After 1 h, a distinct difference in CPD between approximately 10 and 30 mV between the cell and material surface was visible (figure 16, top right). After 12 h, this difference was slightly lower with values reaching approximately 20 mV (figure 16, bottom right).

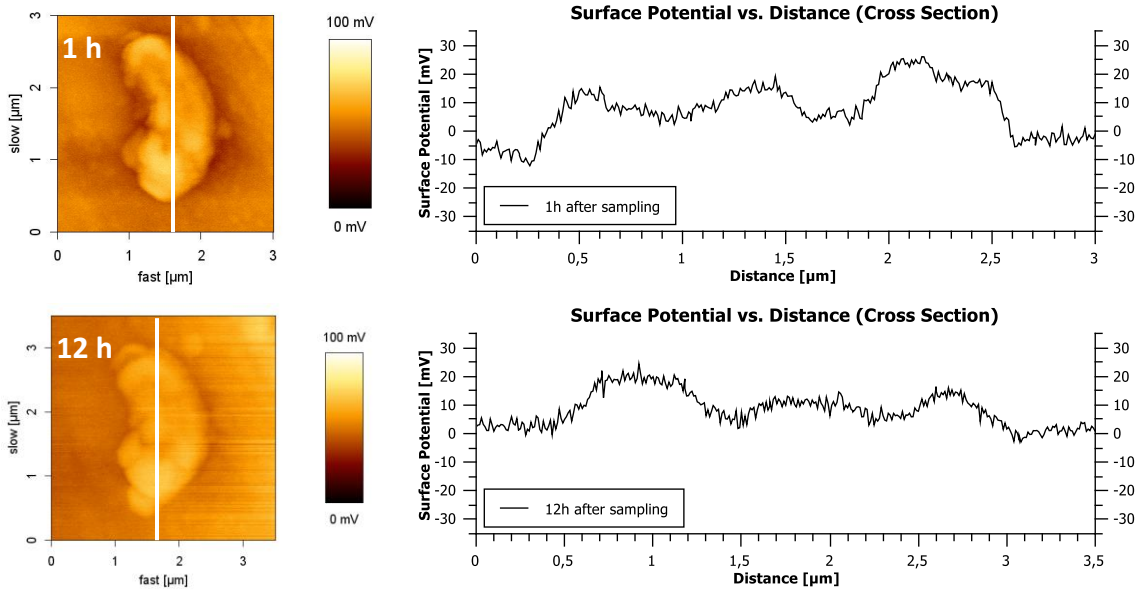

Figure 17 Time-dependent variation in CPD of cells after emersion. (Left) SKPFM potential Images show cells 1 h and 12 h after emersion (from figure 16), (right) cross-sectional surface potentials along the white lines indicated on left side. A wet ground (SiC P180) carbon steel coupon (20 x 15 x 1 mm) was rinsed with deionised water, cleaned with ethanol (70 %), de-greased with acetone and sterilised for 8h at 130 °C under N_2. The coupon was incubated with *Desulfovibrio vulgaris* (initial cell number 5 x 10^8 ml^{-1}) in yeast-free Postgate medium C under anoxic conditions (80 % N_2, 10 % H_2, 10 % CO_2) at a temperature of 30 ± 2 °C for 30 min. Afterwards, the coupon was thoroughly rinsed with N_2-flushed sterile deionised water, immediately dried under a nitrogen stream, glued to an objective slide and visualised by SKPFM. CPD mapping was done using an ElectriTap 300 cantilever in SKPFM hover mode with a 50-nm air gap at a vibration amplitude of 2.5 V and a tip velocity of 2.5 µm s^{-1}.

Figure 17 shows the development of the average CPD difference between cell and surface within 48 h after emersion.

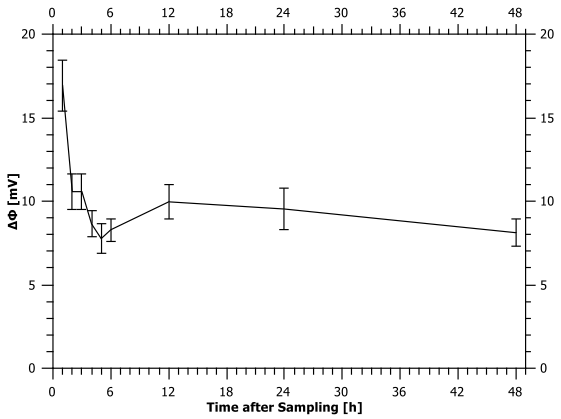

Figure 18 Reduction in CPD gap between cell and material after emersion. A wet ground (SiC P180) carbon steel coupon (20 x 15 x 1 mm) was rinsed with deionised water, cleaned with ethanol (70 %), de-greased with acetone and sterilised for 8h at 130 °C under N_2. The coupon was incubated with *Desulfovibrio vulgaris* (initial cell number 5 x 10^8 ml^{-1}) in yeast-free Postgate medium C under anoxic conditions (80 % N_2, 10 % H_2, 10 % CO_2) at a temperature of 30 ± 2 °C for 30 min. Afterwards, the coupon was thoroughly rinsed with N_2-flushed sterile deionised water, immediately dried under a nitrogen stream, glued to an objective slide and visualised by SKPFM. CPD mapping was done using an ElectriTap 300 cantilever in SKPFM hover mode with a 50-nm air gap at a vibration amplitude of 2.5 V and a tip velocity of 2.5 µm s^{-1}. The CPD gap between cells and surface was determined according to chapter 3.4.4 from cross sections of at least 3 individual cells per time point.

It clearly demonstrates a strong reduction in the cell-to-surface CPD difference within the first 6 h after emersion. Directly after sample preparation (i.e. 1 h after emersion), typical values of approximately +17 mV were estimated. The CPD difference quickly diminished and stabilised at around 8 mV after more than 6 h, meaning that time is a critical factor in the investigation of surfaces after the MIC experiments.

4.2.3 Development of CPD above and below cells of *Desulfovibrio vulgaris* on pure iron, carbon and alloyed steel

To visualise and estimate the direct electrochemical influence of microorganisms on different metal surfaces, pure iron, carbon, and alloyed steel coupons were incubated for up to 7 d with *Desulfovibrio vulgaris*.

On pure iron, a non-continuous, patchy film of *Desulfovibrio vulgaris* cells was visible after 24 h incubation (figure 19). Single cells were clearly recognisable in both the EFM as well as the topographic AFM images. Fluorescence signals of the red-coloured EPS were only visible in direct proximity to the cells. The potential mapping showed areas with both increased and decreased CPD on the surface. Cells attached to areas with increased CPD had a cell-to-surface CPD difference of approximately +25 mV. In contrast, the cells attached to areas with decreased CPD showed a more negative CPD difference to the surface of -25 to -30 mV. The removal of cells by ultrasound treatment was not possible, even under strict and careful handling strong artefacts were visible in both the topographic as well as the CPD images.

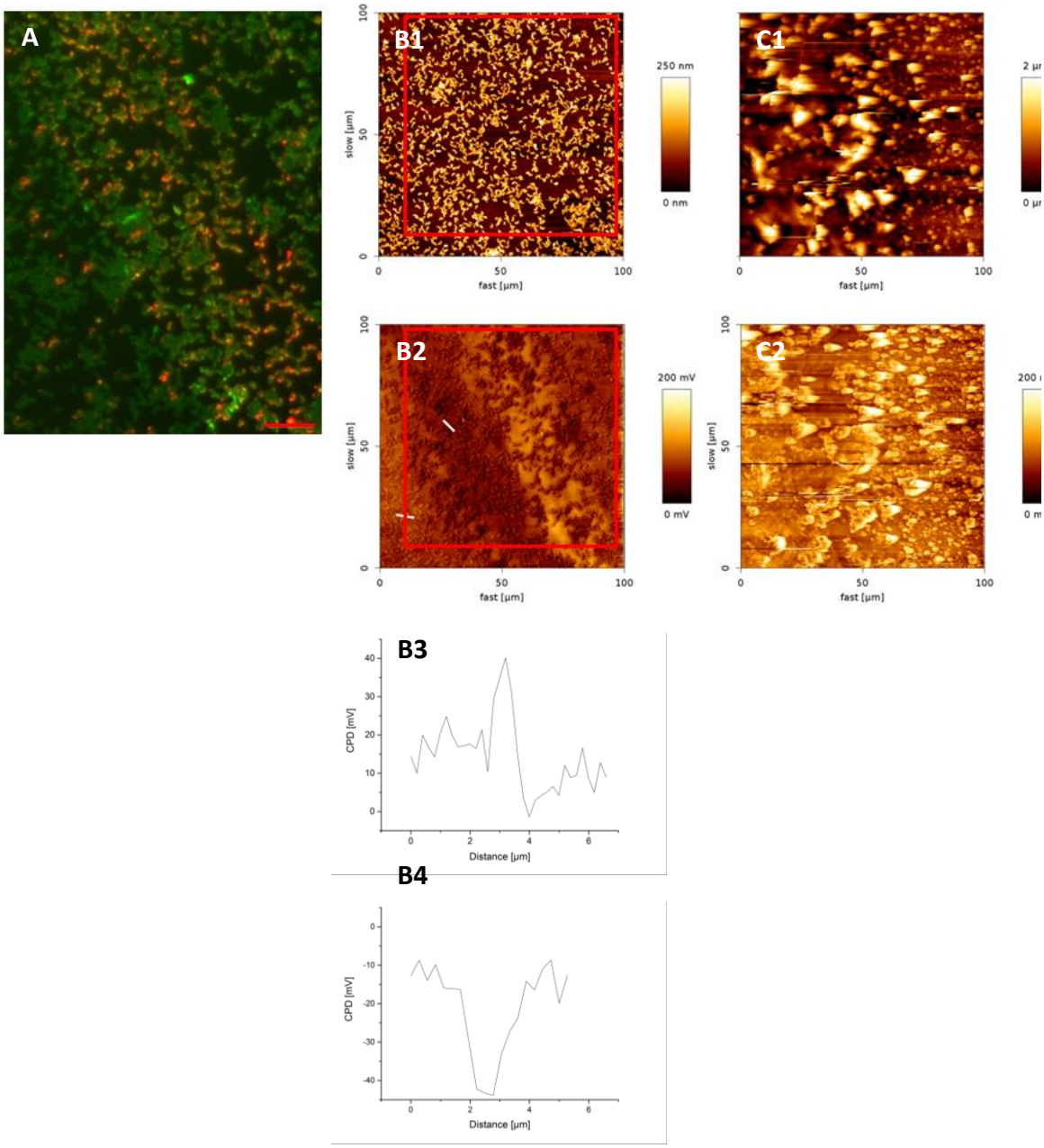

Figure 19 Combined SKPFM & EFM visualisation of pure iron after 24 h incubation with *Desulfovibrio vulgaris*. (A) EFM image showing cells (green) and EPS (red) in the red squared area indicated in images B1 and B2, (B) topography (1) and CPD mappings (2,3,4) before ultrasound treatment; (C) topography (1) and CPD mapping (2) after ultrasound treatment with SDS 0.5 %. The coupon was incubated with *Desulfovibrio vulgaris* (initial cell number 5 x 10^6 ml^{-1}) in yeast-free Postgate medium C under anaerobic conditions at a temperature of 37 ± 2 °C for 72 h. The coupon was carefully rinsed with N_2-flushed sterile dH_2O, immediately dried under a N_2 stream, glued to an objective slide and visualised by SKPFM. Afterwards, the glass slides with coupons were put into 50 mL centrifuge vessels, 35 mL 0.5 % (w/v) SDS solution were added and the samples were treated for 30 min in an ultrasonic bath in the dark. Afterwards, the coupons were thoroughly rinsed with 2 x 5 mL dH_2O, dried under a N_2 stream and the same spot was visualised again. Fluorescence image: Scale bar equals 10 µm. SKPFM: The topography was recorded at a vibration amplitude of 8 V. The CPD mapping was done in SKPFM hover mode using an ElectriTap 300 cantilever with a 50-nm air gap at a vibration amplitude of 2.5 V. Tip velocity was fixed at 60 µm s^{-1}.

After more than 24 h incubation, all coupons were wholly covered in black deposits. The EFM images still showed clear cell and EPS signals, with dense biofilms covering the surface

completely. However, in SKPFM it was not possible to differentiate between individual cells, corrosion deposits, nor the surface (data not shown). Thus, CPD measurements of the cell-to-surface CPD differences were not possible. Similar observations were made with carbon steel coupons (data not shown).

On alloyed steel, EFM images show clearly distinct single cells (green coloured) with a red-coloured EPS capsule after 24 h of incubation. The cells are also identifiable in the topographic SKPFM image (figure 20).

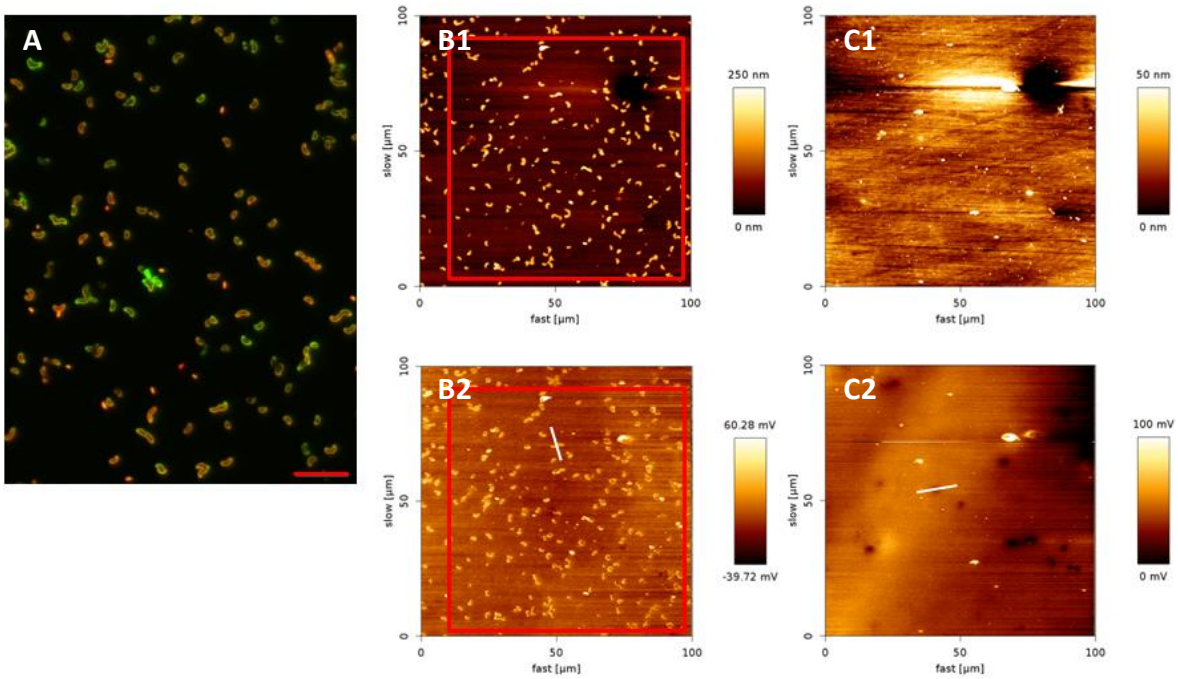

Figure 20 Combined SKPFM & EFM visualisation of alloyed steel after 24 h incubation with *Desulfovibrio vulgaris*. (A) EFM image showing cells (green) and EPS (red) in the red squared area indicated in images B1 and B2, (B) topography (1) and CPD mapping (2) before ultrasound treatment; (C) topography (1) and CPD mapping (2) after ultrasound treatment with SDS 0.5 %. The coupon was incubated with *Desulfovibrio vulgaris* (initial cell number 5 x 10^6 ml^{-1}) in yeast-free Postgate medium C under anaerobic conditions at a temperature of 37 ± 2 °C for 24 h. The coupon was carefully rinsed with N_2-flushed sterile dH_2O, immediately dried under a N_2 stream, glued to an objective slide and visualised by SKPFM. Afterwards, the glass slides with coupons were put into 50 mL centrifuge vessels, 35 mL 0.5 % (w/v) SDS solution were added and the samples were treated for 30 min in an ultrasonic bath in the dark. Afterwards, the coupons were thoroughly rinsed with 2 x 5 mL dH_2O, dried under a N_2 stream and the same spot was visualised again. Fluorescence image: Scale bar equals 10 µm. SKPFM: The topography was recorded at a vibration amplitude of 8 V. The CPD mapping was done in SKPFM hover mode using an ElectriTap 300 cantilever with a 50-nm air gap at a vibration amplitude of 2.5 V. Tip velocity was fixed at 60 µm s^{-1}.

In the CPD mapping, cells showed an increased CPD compared to the surface. The average cell-to-surface CPD difference of +22.1 ± 2.9 mV vs. the material surface was determined from cross-sectional profiles across three individual cells. After ultrasound treatment, the topographic SKPFM image shows the typical image of a polished alloyed steel surface without any indication of cell residues, but some particles (diameter approximately 2 - 3 µm) of

unknown origin are also visible. The corresponding potential mapping shows circular areas with a diameter of 5 – 10 µm and significantly lower potentials than the surrounding surface (-20.6 ± 1.6 mV.)

After 72 h incubation (figure 21), a dense but inhomogeneous biofilm is visible by EFM.

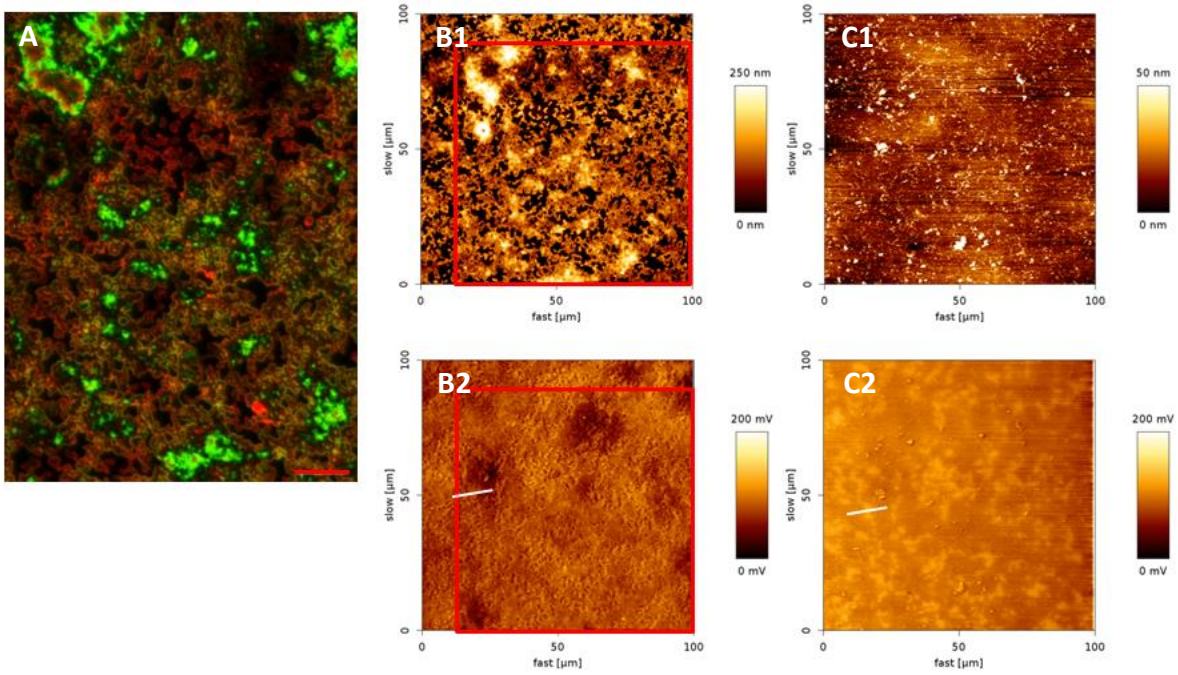

Figure 21 Combined SKPFM & EFM visualisation of alloyed steel after 72 h incubation with *Desulfovibrio vulgaris*. (A) EFM image showing cells (green) and EPS (red) in the red squared area indicated in images B1 and B2, (B) topography (1) and CPD mapping (2) before ultrasound treatment; (C) topography (1) and CPD mapping (2) after ultrasound treatment with SDS 0.5 %. The coupon was incubated with *Desulfovibrio vulgaris* (initial cell number 5 x 10^6 ml^{-1}) in yeast-free Postgate medium C under anaerobic conditions at a temperature of 37 ± 2 °C for 72 h. The coupon was carefully rinsed with N_2-flushed sterile dH_2O, immediately dried under a N_2 stream, glued to an objective slide and visualised by SKPFM. Afterwards, the glass slides with coupons were put into 50 mL centrifuge vessels, 35 mL 0.5 % (w/v) SDS solution were added and the samples were treated for 30 min in an ultrasonic bath in the dark. Afterwards, the coupons were thoroughly rinsed with 2 x 5 mL dH_2O, dried under a N_2 stream and the same spot was visualised again. Fluorescence image: Scale bar equals 10 µm. SKPFM: The topography was recorded at a vibration amplitude of 8 V. The CPD mapping was done in SKPFM hover mode using an ElectriTap 300 cantilever with a 50-nm air gap at a vibration amplitude of 2.5 V. Tip velocity was fixed at 60 µm s^{-1}.

Compared to 24 h incubation, the EPS signal appears much stronger and seems to partially fill the intercellular space. Individual cells remain clearly visible in both the topographic SKPFM as well as the potential mapping image. The cross-sectional potential profiles along individual cells show a CPD of +15.8 ± 4.0 mV vs. the surface. After removal of the biofilm by ultrasound, topographic SKPFM images show a flat surface covered by several particles with a diameter of around 2 – 3 µm. Measurements with the KPFM tip indicated a hard surface of the particles (comparable to the working material; data not shown), indicating that these particles were not microbial cell residues. The potential mapping showed that

areas which were cell-free before the ultrasound treatment, possessed a considerably increased CPD compared to the areas which were once covered by cells. From cross-sectional CPD profiles, a typical CPD increase of +24.8 ± 1.7 mV vs. the surface was estimated. Measurements of cell-to-surface CPD differences after more than 72 h were not possible anymore because the surface was completely covered in multilayer biofilms and, hence, cross-sectional profiles could not be constructed anymore (data not shown).

Considering the CPD changes over time, the cells consistently show an increased CPD compared to the bare material surfaces of at least +20.7 ± 5 mV after 24 h.

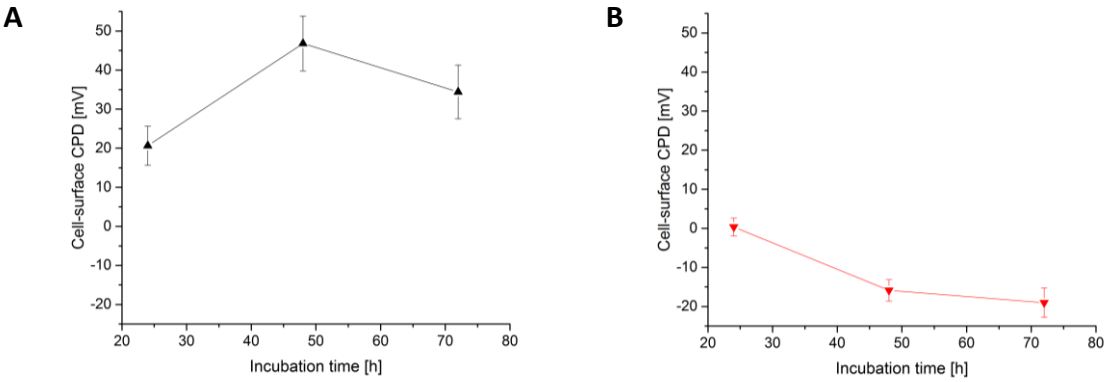

Figure 22 Development of cell-surface CPD on alloyed steel vs. incubation time. (▲) Difference in cell-surface CPD directly after incubation and (▼) after removal of the cells by ultrasound. Coupons were incubated with *Desulfovibrio vulgaris* (initial cell number 5 x 10^6 ml^{-1}) in yeast-free Postgate medium C under anaerobic conditions at a temperature of 37 ± 2 °C for 24, 48, and 72 h, respectively. The coupons were removed, carefully rinsed with N_2-flushed sterile dH_2O, immediately dried under a N_2 stream, glued to an objective slide and visualised by SKPFM. Afterwards, the glass slides with coupons were put into 50 mL centrifuge vessels, 35 mL 0.5 % (w/v) SDS solution were added and the samples were treated for 30 min in an ultrasonic bath in the dark. Afterwards, the coupons were thoroughly rinsed with 2 x 5 mL dH_2O, dried under a N_2 stream and the same spot was visualised again. The CPD mapping was done in SKPFM hover mode using an ElectriTap 300 cantilever with a 50-nm air gap at a vibration amplitude of 2.5 V and a line rate of 0.3 Hz (tip velocity 60 µm s^{-1}). The difference in CPD between cells and surface was determined according to chapter 3.4.4 from 5 individual cells for each time point.

However, after ultrasound treatment the areas previously covered by cells showed a slightly decreased CPD compared to the bare metal surface. After 24 h incubation, no difference in the CPD of cell-covered areas and bare metal could be observed. The working material showed a homogeneous surface potential without any difference exceeding the background noise of the Kelvin signal. After 72 h of incubation, the CPD difference reached a value of -19 ± 4 mV versus the bare metal. As stated before, estimating the CPD cell-to-surface difference was not possible due to the dense biofilm formation after more than 72 h.

Summarising, a significant reduction in the surface potential of alloyed steel at the direct interface (beneath the cells) was visible during the first after prolonged incubation. Assessment of the influence of SRB on the interface on pure iron, however, was not possible.

4.3 Influence of metal substrata on the biochemical composition of EPS from *Desulfovibrio vulgaris*

The influence of different working materials on the EPS composition of *Desulfovibrio vulgaris* was studied by growing *Desulfovibrio vulgaris* in presence of alloyed steel and pure iron, respectively, harvesting the cells and finally extracting both the loosely and tightly bound EPS fractions from the cells. Aliquots of the EPS extracts were then analysed for polysaccharides and proteins using colorimetric methods. The EPS yield was determined by lyophilising defined amounts of EPS extract to correlate the colorimetric results to the respective EPS amount. Furthermore, the estimation of fatty acids and sugar monomers in each extract was done by gas chromatography.

The total EPS yield from planktonic cells grown in presence of alloyed steel, pure iron, and without any metal present is summarised in table 18.

Table 18 Yield of EPS from *Desulfovibrio vulgaris* in presence and absence of different working materials

Substratum	EPS fraction	EPS yield in mg 10^{-10} cells[‡]
None (control)	Loosely bound	32.5 ± 9.9
	Tightly bound	4.3 ± 1.9
Alloyed steel	Loosely bound	43.8 ± 42.4
	Tightly bound	4.1 ± 1.6
Pure iron	Loosely bound	488.2 ± 485.6
	Tightly bound	17.7 ± 14.9

[†] *with reference to the original culture volume*
[‡] *determined from 2 independent biological replicates*

The highest yield of loosely bound EPS was acquired in the presence of pure iron and alloyed steel with approximately 490 and 44 mg EPS 10^{-10} cells, respectively, while only approximately 33 mg 10^{-10} cells were extracted from the controls without metal substrata. Generally, the amount of tightly bound EPS is considerably lower than the amount of loosely bound EPS under each condition. Furthermore, the yields in presence of alloyed

steel and control do not differ on a statistically significant scale. However, in presence of (corroding) pure iron, the amount of both loosely bound and tightly bound EPS are increased.

Qualitatively, proteins, polysaccharides and uronic acids represent the three major compounds of booth loosely and tightly bound EPS fractions under all conditions. No significant difference was observed (table 19). Generally, the total amounts of all compounds are significantly lower (approximately 5 – 10-fold) in the respective loosely bound fractions compared to tightly bound fractions. This is also reflected in the total amount of EPS dry weight that could be analytically identified (figure 23): a total of 7 – 15 % of the loosely bound EPS were identified compared to 39 – 64 % of the tightly bound EPS fractions.

In presence of both alloyed steel and pure iron, the amount of nucleic acids is about 2-fold higher compared to the control. Additionally, the amount of uronic acids is about 3.5-fold higher in the loosely bound fractions but no significant difference was observed for this substance group in the tightly bound fractions. Lipids were 2 times more abundant in the loosely bound EPS fraction in presence of alloyed steel, but no difference was found in presence of pure iron. However, in presence of pure iron the amount of Fe(III) ions in both fractions is approximately 4-fold higher than in EPS extracted from cells grown in presence of alloyed steel as well as the control.

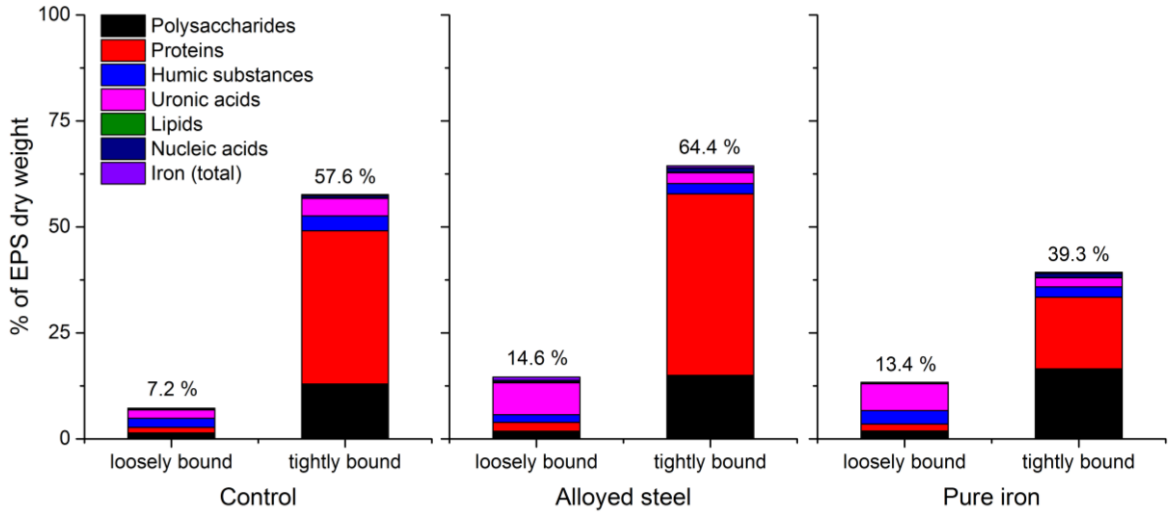

Figure 23 Relative biochemical composition of EPS fractions from *Desulfovibrio vulgaris* grown in presence of different working materials. Graphs show the relative composition of loosely vs. tightly bound EPS fraction based on EPS dry weight after extraction from cells grown without metal (left), in presence of alloyed steel (middle) and pure iron (right). The cells were grown until reaching a cell number of approximately 5×10^8 mL^{-1} in modified, yeast-free Postgate medium C under anaerobic conditions at 37 °C with constant N_2 bubbling to strip emerging H_2S. The total area of the metal substrata was 2000 cm^2. EPS was extracted as described in chapter 3.5.1.

Table 19 Biochemical composition of EPS fractions from *Desulfovibrio vulgaris* grown in presence of different working materials

		In µg mg^{-1} DW of EPS													
Substratum	**EPS fraction**	**Polysaccharides**		**Proteins**		**Uronic acids**		**Nucleic acids**		**Humic acids**		**Lipids†**		**Fe(III) ions†**	
None (control)	Loosely bound	14.2	± 2.4	12.8	± 0.7	19.4	± 2.4	0.4	± 0.2	21.8	± 3.5	1.2	± 0.3	2.0	± 0.4
	Tightly bound	92.9	± 34.5	361.4	± 180.5	41.3	± 16.3	5.8	± 1.9	35.3	± 30.3	0.7	± 0.2	0.6	± 0.2
Alloyed steel	Loosely bound	17.8	± 6.3	23.3	± 13.2	75.1	± 62.0	3.1	± 2.6	18.2	± 8.6	2.6	± 1.4	0.6	± 0.5
	Tightly bound	113.5	± 58.9	428.4	± 248.8	25.6	± 19.5	10.4	± 2.1	24.0	± 21.1	1.0	± 0.03	0.4	± 0.4
Pure iron†	Loosely bound	18.5	± 1.3	16.4	± 11.2	63.1	± 35.0	0.7	± 0.7	31.9	± 4.9	1.4	± 0.3	7.5	± 6.8
	Tightly bound	174.5	± 59.7	169.3	± 78.6	21.1	± 10.4	9.5	± 3.4	24.3	± 11.1	1.0	± 0.2	2.6	± 2.2

†*determined from 2 independent biological replicates*

To check the plausibility of the colorimetric assays, the TOC content of the extracts was calculated from the sum parameters and compared with the results of an instrumental TOC determination. Table 20 shows the amount of TOC calculated for the standards used in the colorimetric assays.

Table 20 Estimated TOC of the standards in colorimetric assays

Assay	Standard	Hill formula	TOC (g C g^{-1})
Polysaccharides	Glucose	$C_6H_{12}O_6$	0.40
Proteins	Bovine serum albumin	-	0.53[†]
Humic acids	Humic acid	$C_9H_9NO_6$	0.48
Uronic acids	Glucuronic acid	$C_6H_{10}O_7$	0.37
Lipids	Palmitic acid	$C_{16}H_{32}O_2$	0.75
DNA	Λ-DNA (44% GC)	A=T: $C_{20}H_{20}N_7P_2O_{11}$ G≡C: $C_{19}H_{19}N_8P_2O_{11}$	0.39

[†]*from Rouwenhorst,* et al. *(1991)*

Table 21 shows a comparison of instrumentally determined TOC of the EPS samples versus the calculated values from the standards used in the colorimetric determinations.

Table 21 TOC content of EPS fractions

Substratum	EPS fraction	TOC in µg mg^{-1} DW of EPS		Recovery rate
		Colorimetric[†]	Instrumental[‡]	$TOC_{col}/TOC_{instr} \times 100$
None (control)	Loosely bound	31.1 ± 4.2	17.7 ± 2.1	175 %
	Tightly bound	278.2 ± 145.0	325.7 ± 55.1	85 %
Alloyed steel	Loosely bound	57.9 ± 38.6	22.6 ± 0.0	256 %
	Tightly bound	312.7 ± 184.0	321.7 ± 40.25	97 %
Pure iron	Loosely bound	56.1 ± 22.2	14.5 ± 0.1	386 %
	Tightly bound	179.6 ± 72.4	300.0 ± 6.5	60 %

[†]*Estimated from colorimetric determinations based on the respective standard*
[‡]*Determined by instrumental TOC analysis of EPS from at least 2 biological replicates per condition*

The results indicate a 2- to 4-fold overestimation for the loosely bound EPS fractions, i.e. the actual total amount of EPS constituents identified is lower than the 7 – 14 % calculated from the colorimetric determinations (figure 23). In contrast, the constituents of the tightly bound EPS are underestimated by 3 to 40 % (table 21) indicating that up to 90 % of the EPS components have been identified.

To exclude cell lysis during the extraction procedure (and, hence, a contamination with intracellular compounds), KDO was assessed as a typical marker. However, no reproducible results were obtained (data not shown). Hence, the enzymatic activity of glucose-6-phophate dehydrogenase (G6PDH) in the EPS extracts as well as the remaining cell pellets after the EPS extraction was determined. Figure 24 shows exemplary results for alloyed steel (which are also valid for pure iron and carbon steel; data not shown).

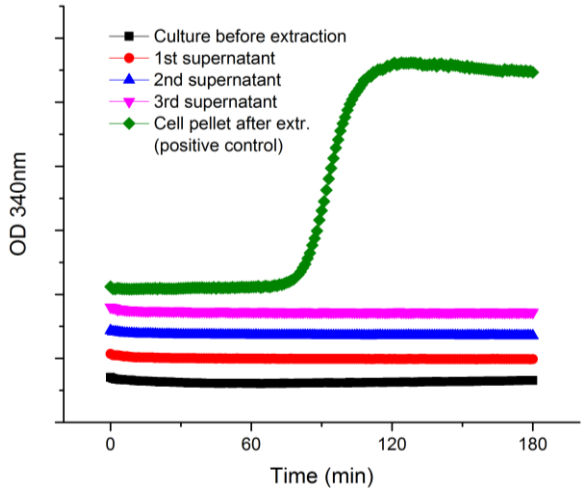

Figure 24 G6PDH activity in EPS extracts. Diagram shows results for EPS extraction in presence of alloyed steel. The remaining cell pellet after the CER extraction procedure served as positive control (◆). The other graphs show the activity of the cell-free medium from the culture before extraction (■) as well as the 1st (●),2nd (▲), and 3rd (▼) EPS-containing supernatant from the CER extraction. The cells were grown to a cell number of approximately 5 x 10^8 mL^{-1} in modified, yeast-free Postgate medium C under anaerobic conditions at 37 °C with constant N_2 bubbling to strip emerging H_2S. The total area of the metal substratum was 2000 cm^2. EPS was extracted as described in chapter 3.5.1. Graphs were stacked along the y-axis to allow discrimination between the graphs without activity.

The remaining cell pellets after the CER extraction (positive control) showed a distinct activity of G6PDH (after the cells were lysed by ultrasound). In contrast, no activity (i.e. no intracellular enzyme) was found in the respective EPS-containing supernatants (indicating that no contamination of the EPS occurred). Further pre-concentration of the EPS extracts by vacuum centrifugation (to increase the sensitivity of the assay) led to a complete loss of activity also in the positive controls (data not shown).

To gain further insight into the influence of the materials on the composition of the polysaccharides and lipids in both the loosely and tightly bound EPS aliquots, the respective (sugar or lipid) fraction was analysed by gas chromatography. Table 22 shows the monosaccharide composition of the sugar fractions extracted from the EPS of cells grown without metal (control) and in presence of alloyed steel or pure iron, respectively.

Table 22 Chemical constituents of the sugar and lipid fraction from EPS of *Desulfovibrio vulgaris*

	Substratum / EPS fraction					
	Control		Alloyed steel		Pure iron	
	LB[†]	TB[‡]	LB	TB	LB	TB
Sugars						
Rha	37.9 %	4.1 %	22.4 %	83.3 %	79.6 %	38.3 %
Fuc	32.2 %	20.2 %	52.8 %			41.3 %
Ara	5.5 %	23.5 %	5.8 %			2.4 %
Rib	9.2 %	35.5 %	5.9 %			6.3 %
Xyl						
Sor	5.0 %	9.4 %	6.4 %	7.5 %	10.2 %	2.9 %
Gal	5.9 %	6.1 %	4.5 %	5.8 %	6.8 %	5.5 %
Man	4.4 %	1.2 %	2.2 %	3.0 %	3.3 %	3.4 %
Saturated fatty acids						
C6:0		2.0 %		4.3 %		1,1%
C8:0	2.6 %	2.2 %	9.5 %	5.2 %	5.1 %	0.9 %
C9:0	2.0 %					
C10:0	2.7 %	20.0 %	3.5 %	5.7 %	9.0 %	3.2 %
C11:0						
C12:0	3.5 %					
C14:0	3.2 %					0.6 %
C16:0	16.0 %	16.8 %	41.2 %	23.4 %	31.0 %	
C18:0	5.0 %	14.7 %	7.2 %	20.8 %	20.8 %	22.1 %
C19:0			15.1 %			1.8 %
C20:0		6.0 %			7,1%	11.2 %
C21:0						
C22:0						1.7 %
C23:0						
C24:0						
(Poly)unsaturated fatty acids						
C14:1	65.0 %			16.5 %		0.3 %
C16:1		6.5 %		24.0 %	6.7 %	0.9 %
C18:1		4.5 %	7,6%			7.2 %
C18:2		4.8 %	7,7%		5,5%	7.0 %
C18:3		13.4 %	8,6%		14,9%	17.0 %
C20:1		5.1 %				5.2 %
C22:1						

[†]Loosely bound, [‡]tightly bound

Rhamnose and fucose represent the main compounds of the loosely bound EPS of the control (70 % of the sugar fraction) besides lower amounts of arabinose, ribose, galactose and mannose. In presence of alloyed steel, the sugar spectrum is comparable but the amount of fucose is approximately doubled while the amount of rhamnose is halved. In contrast, rhamnose is the dominant compound attributing to more than 80 % of the sugar fraction in presence of pure iron, while fucose, arabinose and ribose were not detected. Under all conditions, the amounts of sorbitol, galactose and mannose were comparable, with a 1.5-fold increase in the amount of sorbitol in presence of alloyed steel and a 2-fold increase in presence of pure iron (compared to the control). In the tightly bound fraction of the control, a significantly higher amount of ribose (approximately 36 %) was found than in the respective loosely bound EPS. Additionally, the amount of arabinose showed a 4-fold increase, while fucose and rhamnose were considerably less dominant (20 % and 4 %, respectively). In contrast, in presence of alloyed steel rhamnose represented the dominant constituent (more than 80 %) while fucose, arabinose and ribose were not detected. In presence of pure iron, finally, fucose and rhamnose were the major compounds with significantly lower amounts of arabinose and ribose compared to EPS from the control. Sorbitol, shows an opposite trend compared to the loosely bound EPS, with an approximately 1.5-fold decrease in presence of alloyed steel and 2-fold decrease in presence of pure iron. The amounts of galactose and mannose do not differ significantly.

The total amount of fatty acids identified by GC varied between 1.4 and 3.3 % of the EPS dry weight in loosely bound EPS (22 µg mg EPS^{-1} in the control, 14, and 33 µg mg EPS^{-1} in presence of alloyed steel and pure iron, respectively; data not shown). In the tightly bound fractions comparable amounts were found in the control as well as in presence of alloyed steel (20 and 22 µg mg EPS^{-1}, respectively). In presence of pure iron, however, a 9-fold increase in the total fatty acid amount was observed (91 µg mg EPS^{-1}).

Regarding the relative distribution of the fatty acids, a generally increased variability of the fatty acid composition was observed in the tightly bound EPS compared to loosely bound EPS. In the latter, 8 different lipids were identified in the control, with C14:1 representing the major constituent (65 %) followed by C16:0 (16 %). In presence of alloyed steel and pure iron the composition of saturated fatty acids was comparable, but C12:0 and C14:0 were not found. Under both conditions, C16:0 represented the dominant substance. In

presence of alloyed steel, C19:0 was additionally identified (15 %). The amount of C18:0 was at the same time decreased by approximately the same amount (8 % compared to 21 % in presence of pure iron). In contrast, the composition of (poly)unsaturated fatty acids differed considerably. In presence of both metals no C14:1 was identified but unsaturated and polyunsaturated C18 compounds were found.

Compared to the loosely bound EPS, the total amount of unsaturated fatty acids was 2-fold lower than in the tightly bound EPS. However, a shift to higher molecular weight fatty acids was observed with C18:3 being the predominant substance. In contrast, the total amount of unsaturated and poly-unsaturated fatty acids was approximately 1.5-fold higher in presence of metals compared to the respective loosely bound EPS. In presence of both alloyed steel and pure iron, C14:1 and C16:1 were identified. Additionally, (poly)unsaturated C18 compounds and C20:1 were found in presence of pure iron, with C18:3 being the predominant compound (17 %).

4.4 Effect of cyclodextrins on MIC of steel

4.4.1 Native (non-polymerised) cyclodextrin films

To assess the influence of cyclodextrins with different functional groups on the corrosion rate of carbon steel in presence of *Desulfovibrio vulgaris*, two initial screening experiments with a total of 25 different cyclodextrins were performed. In the first series of 15 cyclodextrins (figure 25, left) carboxylated poly(1->4)-ß-D-glycosyl-(1->4)-ß-glucose (compound B) showed the highest protective effect reducing the corrosion rate by 47 % compared to uncoated controls. All other cyclodextrins in this series showed a smaller protective or even corrosion-promoting effect, including those containing Fe(II)/Fe(III) salts.

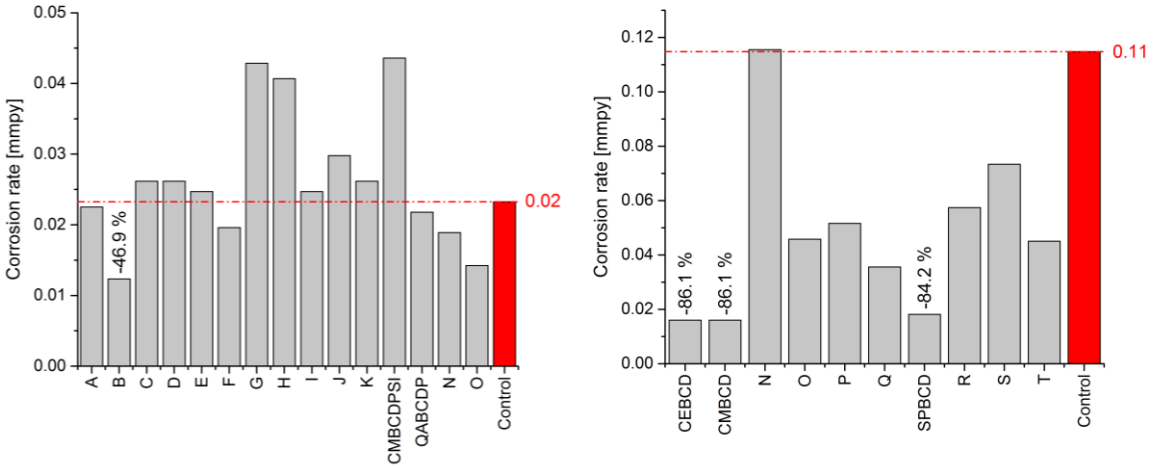

Figure 25 Influence of cyclodextrin films on MIC of carbon steel by *Desulfovibrio vulgaris* after 7 d of incubation. (Series 1, left) (A) 6-mono-O-((1-4)-a-D-glucuronyl-(1-4)-a-Dglucosyl)-ß-cyclodextrin, (B) carboxylated poly(1->4)-ß-D-glycosyl-(1->4)-ß-glucose, (C) diethylaminoethylated poly((1->4)-ß-D-glucosyl-(1->4)-ß-D-glucose, (D) highly oxidized ß-cyclodextrin, (E) highly oxidized ß-cyclodextrin Fe(III)-salt, (F) oxidized ß-cyclodextrin, (G) oxidized ß-cyclodextrin Fe(III)-salt, (H) Poly((1->4)-D-galacturonyl(1->4)-D-galacturonyl-(1->2)-L-rhamnose) Fe(II)/Fe(III) salt, (I) poly((1->4)-ß-L-guluronyl(1->4)-a-D-mannuronic acid, (J) poly(1->6)-D-glucosyl-(1->6)-a-D-glucose, (K) Poly(1->6)-D-glucosyl-(1->6)-a-D-glucose, (CMBCDPSI) soluble carboxymethyl ß-cyclodextrin polymer, (QABCDP) soluble quaternary-amino-ß-cyclodextrin polymer, (L) sulphated poly((1->3)-ß-D-(2-N-acetylamido)-galacturonyl-(1->4)-ß-D-glucoronic acid)-Na salt, (M) sulphated poly((1->6)-D-glucosyl-(1->6)-a-D-Glucose). **(Series 2, right)** (CEBCD) carboxyethylated ß-cyclodextrin, (CMBCD) carboxymethylated ß-cyclodextrin, (N) poly((1->4)-D-galacturonyl(1->4)-D-galacturonyl-(1->2)-L-rhamnose), (O) sulphated ß-cyclodextrin (DS 12), (P) sulphobutyl-ether-ß-cyclodextrin (DS 4), (Q) sulphobutyl-ether-ß-cyclodextrin (DS 6.2), (SPBCD) sulphopropylated ß-cyclodextrin, (R) amylose, (S) microcrystalline cellulose, (T) chitosan. Red bars represent uncoated controls, dashed lines indicate the corrosion rate of the respective control. Percent values represent the relative corrosion reduction by the respective coating compared to the uncoated control. Sterile carbon steel coupons (wet-ground, SiC P180) were precisely weighed, dip-coated in the respective cyclodextrin solution (10 mg mL^{-1} in dH_2O) and dH_2O (controls), respectively, for 2 h at 30 ± 2 °C and transferred into sterile 30 mL screw-cap bottles. Afterwards, 25 mL yeast-free, Postgate medium C were added and the medium was inoculated with *Desulfovibrio vulgaris* (initial cell number 5 x 10^6 mL^{-1}). The bottles were tightly sealed, placed in anaerobic jars and incubated at 37 ± 2 °C for 128 h. Afterwards, the coupons were removed, treated with EDTA solution in an ultrasonic bath for 5 min to remove corrosion products, dried and weighed again. All handling was performed under anoxic conditions (80% N_2, 10% H_2, 10% CO_2) in a glove box and all solutions were thoroughly flushed with N_2 for at least 30 min before use.

Based on the results from the first series and the general assumption that carboxyl-groups might positively influence corrosion rates of metal in presence of *Desulfovibrio vulgaris*, a second series of experiments using 10 further cyclodextrin variants was performed. Three variants significantly reduced the corrosion rates: carboxyethylated ß-cyclodextrin (figure 25, CEBCD) and carboxymethylated ß-cyclodextrin (figure 25, CMBCD) showed the highest protective effect (86 % lower corrosion rate) followed by sulphopropylated ß-cyclodextrin (figure 25, SPBCD, 84 % lower corrosion rate). However, as the synthesis of sulphopropylated β-cyclodextrin required the use of toxic educts it was decided to focus on carboxylated cyclodextrins for further experiments.

As a result, in the final 3rd series of experiments six carboxy(m)ethylated cyclodextrins with varying ring size (α-, β-, and γ-cyclodextrins, respectively) as well as a highly polymerised carboxymethylated β-cyclodextrin (CMHPBCD) were selected for 7 and 21 d MIC simulations (figure 26).

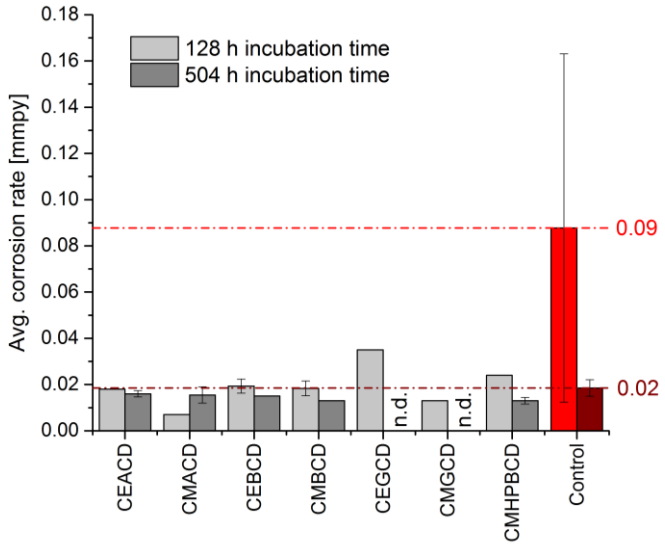

Figure 26 Influence of carboxy(m)ethylated cyclodextrin films on MIC of carbon steel by *Desulfovibrio vulgaris* after 7 d and 21 d incubation. Abbreviations: (CE...) Carboxyethylated, (CM...) carboxymethylated, (ACD) α-cyclodextrin, (BCD) β-cyclodextrin, (GCD) γ-cyclodextrin, (CMHPBCD) carboxymethyl hydroxypropyl ß-cyclodextrin Na-salt. Red bars represent uncoated controls, dashed lines indicate the corrosion rate of the respective control. Average values and error bars were calculated from at least 2 independent biological replicates. Sterile carbon steel coupons (wet-ground, SiC P180) were precisely weighed, dip-coated in the respective cyclodextrin solution (10 mg mL^{-1} in dH_2O) and dH_2O (controls), respectively, for 2 h at 30 ± 2 °C and transferred into sterile 30 mL screw-cap bottles. Afterwards, 25 mL yeast-free, Postgate medium C were added and the medium was inoculated with *Desulfovibrio vulgaris* (initial cell number 5 x 10^6 mL^{-1}). The bottles were tightly sealed, placed in anaerobic jars and incubated at 37 ± 2 °C for 128 h and 504 h, respectively. Afterwards, the coupons were removed, treated with EDTA solution in an ultrasonic bath for 5 min to remove corrosion products, dried and weighed again. All handling was performed under anoxic conditions (80% N_2, 10% H_2, 10% CO_2) in a glove box and all solutions were thoroughly flushed with N_2 for at least 30 min before use.

Films of carboxymethylated variants of all three ring sizes exhibited a slightly higher protective effect against MIC by *Desulfovibrio vulgaris* than carboxyethylated cyclodextrins after both 7 d and 21 d incubation. After 7 d, α-cyclodextrins reduced the corrosion rates by 90 % for the carboxyethylated and 96 % for the carboxymethylated variant, respectively. After 3 weeks, the protective effect was significantly lower with a MIC reduction by 11 and 16 %, respectively. β-cyclodextrins reduced the corrosion rate by each 89 % after 7 d and 18 % for the carboxyethylated vs. 28 % for the carboxymethylated variant. The protective effect of the highly polymerised hydroxypropyl-β-cyclodextrin was comparable to the carboxymethylated β-cyclodextrins. The γ-cyclodextrins reduced MIC by 93 and 81 % after

7 d, respectively. However, due to the limited amount of γ-cyclodextrins available compared to α- and β-cyclodextrins, no longer term experiments were performed.

To elucidate their influence of cyclodextrin films on biofilm formation by *Desulfovibrio vulgaris*, further experiments with these carboxy(m)ethylated cyclodextrins were performed. Figure 27 shows the relative average surface coverage by biofilms in presence of the respective films and on uncoated controls.

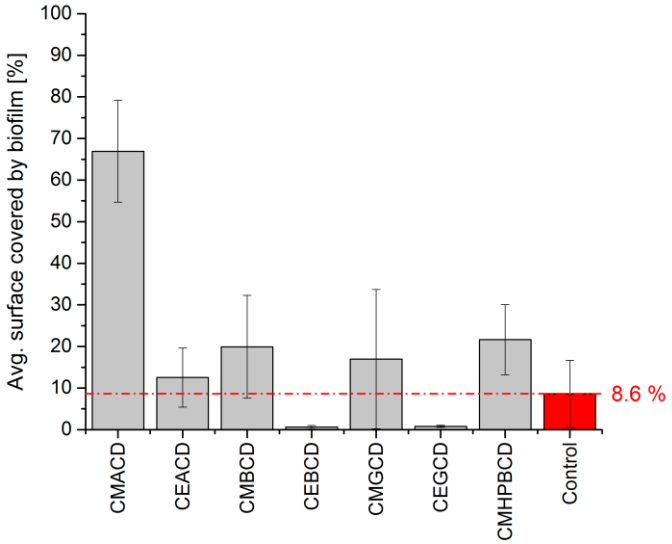

Figure 27 Influence of carboxy(m)ethylated cyclodextrin films on biofilm formation of *Desulfovibrio vulgaris* on alloyed steel. Abbreviations: (CE) Carboxyethylated, (CM) carboxymethylated, (ACD) α-cyclodextrin, (BCD) β-cyclodextrin, (CMHPBCD) carboxymethyl hydroxypropyl ß-cyclodextrin Na-salt. Sterile carbon steel coupons (wet-ground, SiC P180) were precisely weighed, dip-coated in the respective cyclodextrin solution (10 mg mL^{-1} in dH_2O) and dH_2O (controls), respectively, for 2 h at 30 ± 2 °C and transferred into sterile 30 mL screw-cap bottles. Afterwards, 25 mL yeast-free, Postgate medium C were added and the medium was inoculated with *Desulfovibrio vulgaris* (initial cell number 5 x 10^6 mL^{-1}). The bottles were tightly sealed, placed in anaerobic jars and incubated at 37 ± 2 °C for 128 h. Afterwards, the coupons were carefully rinsed with dH_2O, overlaid with DAPI solution (0.01 %) for 5 min, carefully rinsed again and visualised by EFM. 10 different visual fields from 2 parallel coupons were automatically analysed by ImageJ using a custom script.

On uncoated controls, 8 ± 8 % of the surface were covered by *Desulfovibrio vulgaris*. CEBCD and CEGCD strongly reduced biofilm formation with an average covered surface area of 0.6 ± 0.4 % and 0.8 ± 0.3 %. However, due to the large standard deviation of the positive control, the difference could not be regarded as significant ($p > 0.05$).

To illustrate the bacterial colonisation on the cyclodextrin films, figure 28 shows exemplary fluorescence images of the respective biofilms.

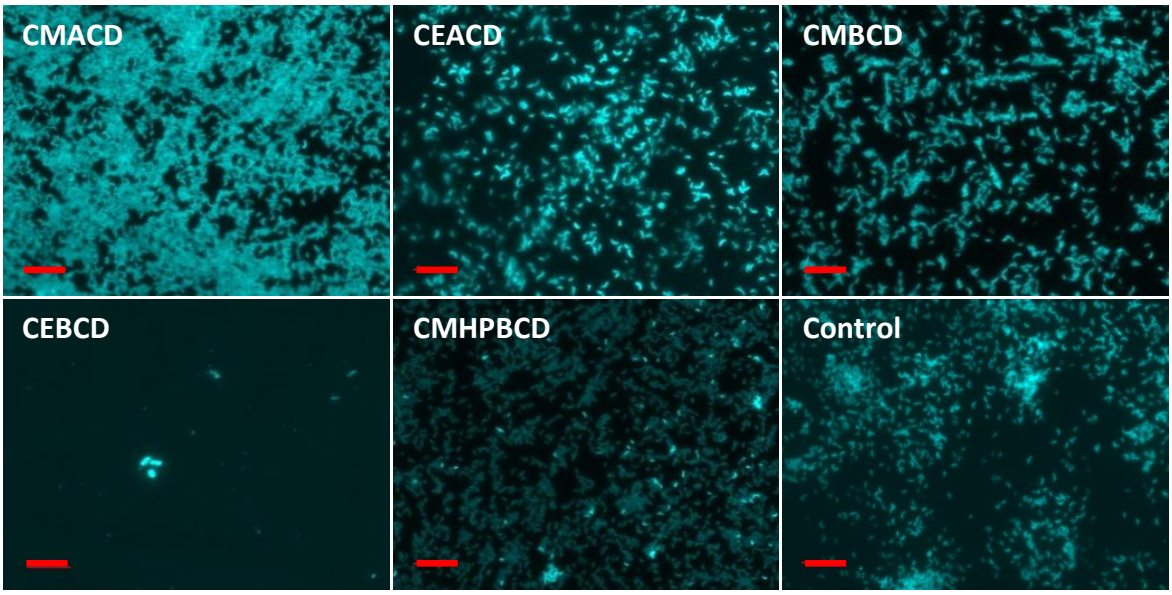

Figure 28 Biofilm formation of *Desulfovibrio vulgaris* on carboxy(m)ethylated cyclodextrin films on alloyed steel. Abbreviations: (CE) Carboxyethylated, (CM) carboxymethylated, (ACD) α-cyclodextrin, (BCD) β-cyclodextrin, (CMHPBCD) carboxymethyl hydroxypropyl ß-cyclodextrin. Sterile alloyed steel coupons (wet-ground, SiC P180) were weighed, dip-coated in the respective cyclodextrin solution (10 mg mL^{-1} in dH_2O) and dH_2O (controls), respectively, for 2 h at 30 ± 2 °C and transferred into sterile 30 mL screw-cap bottles. Afterwards, 25 mL yeast-free Postgate medium C were added and the medium was inoculated with *Desulfovibrio vulgaris* (initial cell number 5 x 10^6 mL^{-1}). The bottles were tightly sealed, placed in anaerobic jars and incubated at 37 ± 2 °C for 128 h. Afterwards, the coupons were carefully rinsed with dH_2O, overlaid with DAPI solution (0.01 %) for 5 min, carefully rinsed again and visualised by EFM. Scale bars equal 10 µm

Generally, a stronger biofilm formation was observed on carboxymethylated cyclodextrins compared to their carboxyethylated counterparts. For α-cyclodextrins, the biofilm formation on carboxyethylated cyclodextrin was approximately 5-fold lower than on the carboxymethylated variant. The largest difference was observed for the β-cyclodextrins with an approximately 33-fold lower biofilm formation on the carboxyethyl-functionalised variant.

Furthermore, the resistance of the cyclodextrins against microbial degradation was assessed. This and the general stability against dissolution represent major factors in the longer-term protection against MIC by cyclodextrin films. Hence, a simple short term experiment with cyclodextrins replacing lactate as carbon source in fully defined Postgate medium C was devised. Harvested and cleaned stationary phase cells of *Desulfovibrio vulgaris* from a freshly grown culture were added to the media to an initial cell density of 5 x 10^6 mL^{-1}. After 7 d of incubation, cell numbers of growth controls containing lactate as sole carbon source reached 7 ± 0.6 x 10^8 mL^{-1} whereas the cell numbers of the negative controls (without lactate) reached only 6 ± 0.6 x 10^7 mL^{-1} (figure 29). In terms of cell duplication, the negative controls equal approximately 1 exponential duplication and the positive controls

> 2 exponential duplications. Cell numbers in presence of all cyclodextrins were comparable to the negative controls and significantly lower than the positive controls ($p << 0.01$), i.e. no biodegradation was observed.

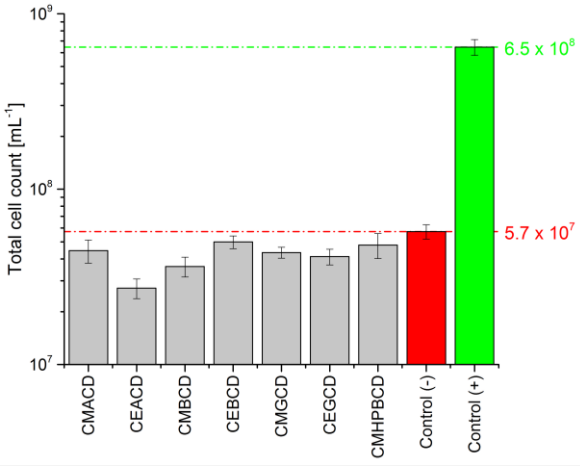

Figure 29 Growth of *Desulfovibrio vulgaris* on cyclodextrins as sole carbon source. Abbreviations: (CE...) Carboxyethylated, (CM...) carboxymethylated, (ACD) α-cyclodextrin, (BCD) β-cyclodextrin, (CMHPBCD) carboxymethyl hydroxypropyl ß-cyclodextrin Na-salt. To test the biodegradability, the carbon source in yeast-free Postgate medium C was replaced by the same amount of cyclodextrin (grey bars), not replaced (negative control, red bar) and compared to carbon-containing medium (positive control, green bar). Dashed lines indicate the cell numbers of both negative (red) and positive control (green). 20 mL of the respective medium were filled into 20 mL serum flasks, which were tightly sealed and thoroughly flushed with N_2. Afterwards, the medium was inoculated with *Desulfovibrio vulgaris* (initial cell number 5 x 10^6 mL^{-1}) and incubated for 128 h at 37 °C. Finally, the cell number was determined again.

Finally, the influence of cyclodextrins on the electrochemical properties (surface potential) of steel was assessed. An initial experiment was performed using carbon steel partially dip-coated with fluorescently labelled CMBCD (figure 30).

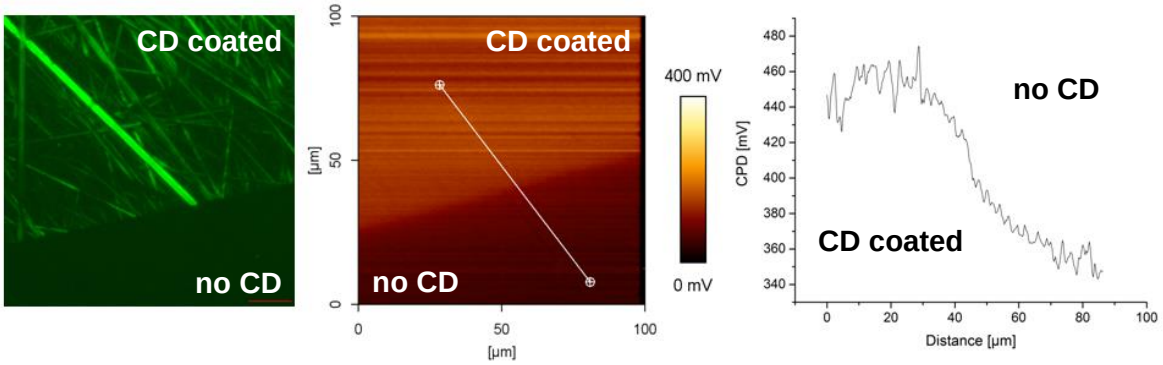

Figure 30 Influence of carboxymethylated cyclodextrin on CPD of alloyed steel. (Left) fluorescence image, (middle) SKPFM CPD mapping, (right) cross-sectional CPD profile along the white line indicated in the CPD mapping image. A sterile carbon steel coupon (wet-ground, SiC P180) was half dip-coated in a mixture of FITC-CMBCD and CMHPBCD (final concentration 0.1 and 9.9 mg mL^{-1} in dH_2O, respectively) for 1 h at 30 ± 2 °C, the coating solution was removed and the coupon was dried for 12 h at RT in the dark. Afterwards the boundary region between coated and uncoated surface was visualised by EFM and SKPFM. CPD mapping: air gap 10 nm, 1 V target amplitude at a line rate of 0.5 Hz (tip velocity 100 µm s^{-1}), cantilever ElectriTap 300

Both the labelled CMBCD film as well as the CPD were visualised using the novel SKPFM & EFM combination. In the boundary region between coated and uncoated areas, the fluorescing cyclodextrin film (green) was clearly distinguishable from the uncoated material surface (black). Areas covered by cyclodextrin film showed a strong CPD increase of about +100 mV vs. the bare steel surface indicating an ennoblement of the material. However, it should be noted that no systematic study on the CPD influence of cyclodextrins on steel surfaces was conducted in this thesis and these results are hence preliminary.

4.4.2 Polymerised cyclodextrin films

Due to the relative increase in corrosion rates after 21 d (figure 26), cyclodextrins were additionally polymerised by glutardialdehyde as polymerising agent (chapter 3.6.1) in order to improve the film stability and their effectiveness against MIC (Badruddoza, et al., 2013; Fenyvesi, 2011).

First, the effect of the polymerisation on film stability in sterile phosphate buffered saline (PBS 10x) was assessed. Both non-polymerised and polymerised fluorescently labelled CMBCD films were clearly visible under the epifluorescence microscope directly after coating (figure 31). In both cases, the strongest fluorescence signal was visible along the grooves of the ground steel. Due to the much stronger signal along the grooves in case of the polymerised film, the areas between the grooves appear less covered than in case of the non-polymerised film.

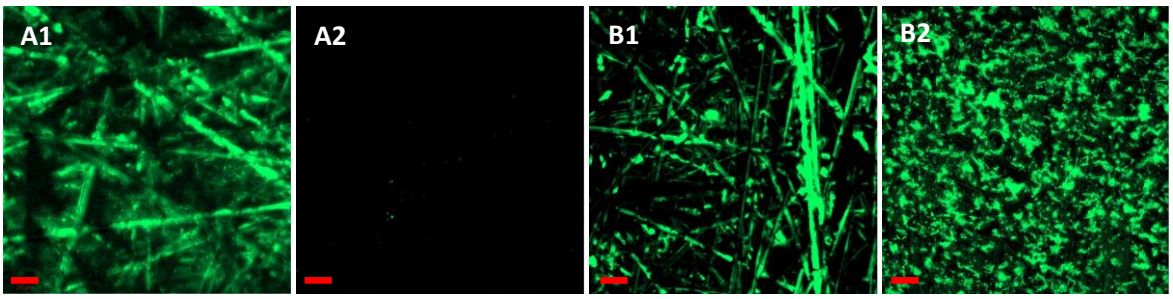

Figure 31 Influence of polymerisation on stability of cyclodextrin films an alloyed steel against dissolution in sterile buffer. (A1) Non-polymerised CMBCD film before and (A2) after immersion in sterile 10x phosphate buffered saline for 7d, (B1) polymerised CMBCD film before and (B2) after immersion. Alloyed steel coupons (wet-ground, P180, SiC) were dip-coated for 2 h in a solution of 9.9 mg mL^{-1} CMBCD solution plus 0.1 mg mL^{-1} CMBCD-FITC, dried for at least 2 d under sterile conditions and visualised by CLSM. Then, coupons were immersed in sterile PBS 10 x for 7 d at RT, removed, thoroughly rinsed with dH_2O, dried and visualised again. All images show single z-slices, scale bars equal 20 µm

After 7 d of exposure to PBS 10x, virtually no fluorescence signal was detectable for non-polymerised films (figure 31 A2). In contrast, polymerised films still showed a strong fluorescence signal (figure 31 B2), but with a different surface pattern than before exposure. As stated before, AFM images did not show any significant difference between the film surface before and after exposure.

To further elucidate the influence of the polymerisation on the cyclodextrin film structure, sectional CLSM images of both non-polymerised and polymerised fluorescently labelled CMBCD films on alloyed steel were compared. After 7 d immersion in PBS 10x, only low residual fluorescence was observed for non-polymerised films. Closer inspection showed that residual cyclodextrin was only present in the grooves of the material surface, and lateral x- and y-images clearly showed the absence of a continuous cyclodextrin film (figure 32, left). In contrast, continuous films were visible for polymerised films and the lateral images showed a dense residual film with an average thickness exceeding 20 µm.

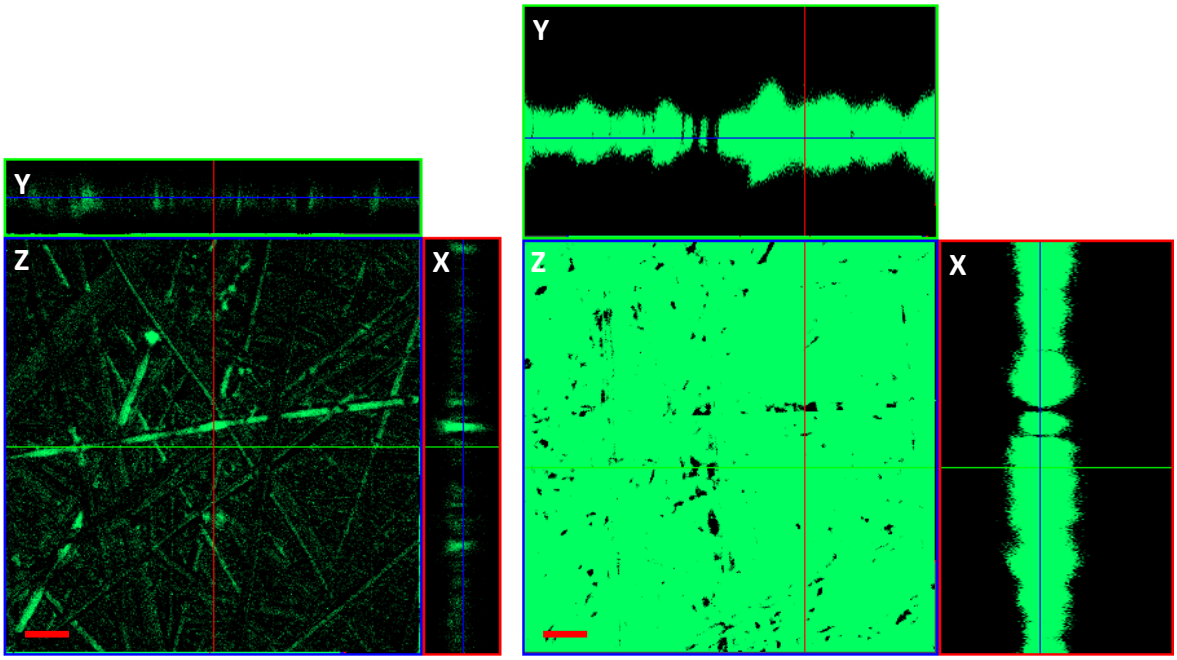

Figure 32 Influence of polymerisation on carboxymethylated β-cyclodextrin film on alloyed steel. (Left) non-polymerised film, (right) polymerised film. Alloyed steel coupons (wet-ground, P180, SiC) were dip-coated for 2 h in a solution of 9.9 mg mL^{-1} CMBCD solution plus 0.1 mg mL^{-1} CMBCD-FITC with or without additional polymerisation at 45 °C for 8 h, respectively, and dried for at least 2 d under sterile conditions. Afterwards, the cyclodextrin films were visualised by CLSM. Then, coupons were immersed in sterile 10x PBS for 7 d at RT, removed, thoroughly rinsed with dH_2O, dried and again visualised by CLSM. Orthogonal images were constructed from 200 individual images along the z-axis. Top and right images show lateral y- and x-slices along the red and green lines of the z-images (centre), respectively. Scale bars equal 20 µm

However, several pores of around 2 µm reaching the material surface through the films were visible in both the vertical as well as the lateral images (figure 32, right hand side).

The influence of polymerisation on the protective effect of cyclodextrin films against MIC was assessed by comparing the performance of non-polymerised films versus polymerised films. After incubation, non-polymerised CEBCD and CMBCD showed a corrosion reduction compared to uncoated controls by 19 and 30 %, respectively (figure 33). After 21 d of incubation coating with polymerised cyclodextrins such as CEBCD and CMBCD showed a strong protective effect with a corrosion reduction of 77 and 78 %, respectively.

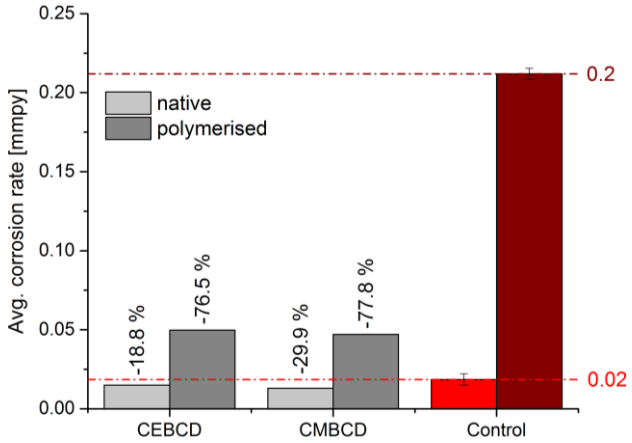

Figure 33 Influence of polymerisation on protective effect of carboxy(m)ethylated cyclodextrin films on MIC of carbon steel by *Desulfovibrio vulgaris* after 21 d of incubation. (CEBCD) Carboxyethylated β-cyclodextrin, (CMBCD) carboxymethylated β-cyclodextrin. Red bars represent uncoated controls, dashed lines indicate the corrosion rate of the respective control. Average values and error bars were calculated from at least 2 parallels. Sterile carbon steel coupons (wet-ground, SiC P180) were precisely weighed, dip-coated in the respective cyclodextrin solution (10 mg mL^{-1} in dH_2O) and dH_2O (controls), respectively, for 2 h at 30 ± 2 °C and transferred into sterile 30 mL screw-cap bottles. Afterwards, 25 mL yeast-free, Postgate medium C were added and the medium was inoculated with *Desulfovibrio vulgaris* (initial cell number 5 x 10^6 mL^{-1}). The bottles were tightly sealed, placed in anaerobic jars and incubated at 37 ± 2 °C for 504 h. Afterwards, the coupons were removed, treated with EDTA solution in an ultrasonic bath for 5 min to remove corrosion products, dried and weighed again. All handling was performed under anoxic conditions (80 % N_2, 10 % H_2, 10 % CO_2) in a glove box and all solutions were thoroughly flushed with N_2 for at least 30 min before use.

Finally, the effect of polymerised CMBCD films on microbial surface colonisation was investigated by CLSM.

Figure 34 shows DAPI-stained cells of *Desulfovibrio vulgaris* (blue) were clearly distinguishable from the FITC-labelled cyclodextrin film (green). The lateral projection along the y-axis shows a clear separation of the biofilm from the material surface by the cyclodextrin film. Orthogonal projections along a coherent biofilm segment showed no penetration of the cells through the cyclodextrin film after 7 d of incubation.

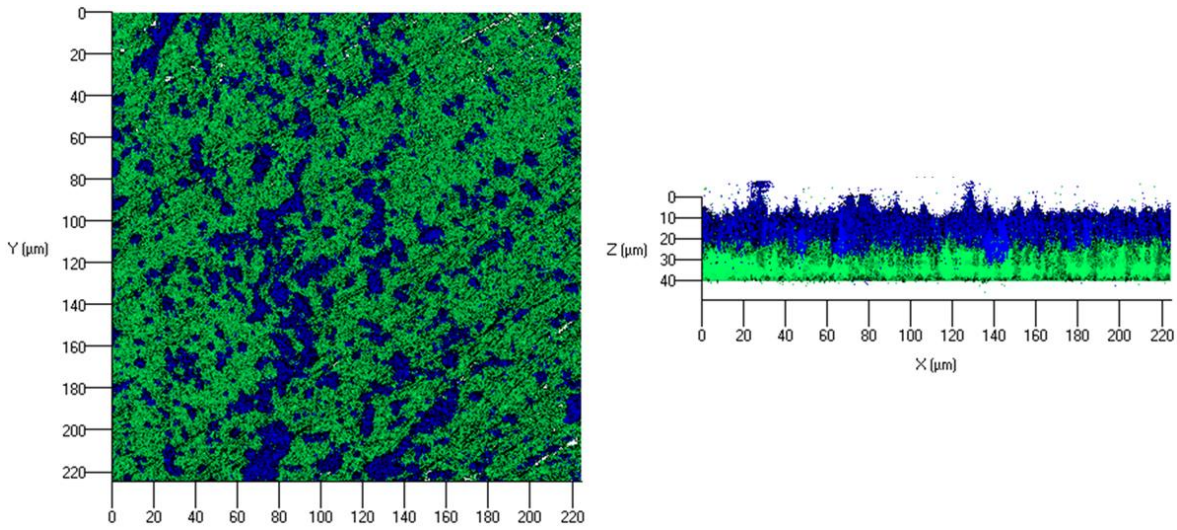

Figure 34 Influence of polymerised carboxymethylated β-cyclodextrin film on biofilm formation of *Desulfovibrio vulgaris* after 7 d of incubation. (Blue) whole cells, (green) cyclodextrin film. Alloyed steel coupons (wet-ground, SiC P180) were dip-coated in a hydrochloric solution (pH 2) with 9.9 mg mL^{-1} CMBCD plus 0.1 mg mL^{-1} CMBCD-FITC for 2 h and polymerised at 45 °C for 8 h. The coupons were transferred into sterile 30 mL screw-cap bottles, 25 mL yeast-free Postgate medium C were added and the medium was inoculated with *Desulfovibrio vulgaris* (initial cell number 5 x 10^6 mL^{-1}). The bottles were tightly sealed, placed in anaerobic jars and incubated at 37 ± 2 °C for 128 h. Afterwards, the coupons were carefully rinsed with dH_2O, overlaid with DAPI solution (0.01 %) for 5 min, carefully rinsed again and visualised by CLSM. Blue and green channels were merged and 3d images were constructed from 200 individual images along the z-axis.

Summarising, the polymerisation of cyclodextrin films significantly improves the film stability in liquid media and produces a dense, impenetrable film over a period of 7 d.

5 DISCUSSION

Biofilms play a pivotal role in both accelerating and inhibiting corrosion (Zarasvand & Rai, 2014; Videla & Herrera, 2009; Mansfeld, 2007; Sand, 1997). Despite the huge economic impact of MIC, the underlying mechanisms still are only poorly understood (Kuklinski & Sand, 2014). The very same is true for MICI, where several studies are available but only few show a systematic approach. Hence, this study aimed at (I) visualising the direct electrochemical influence of SRB on material surfaces by a novel combination of SKPFM & EFM, (II) elucidating the role of EPS in MIC and MICI by comparative biochemical analyses of the EPS composition of cells grown with or without metals, and (III) mimicking the protective effects of EPS against biocorrosion using functionalised cyclodextrins as EPS-analogue substances.

5.1 Development of a fully defined growth medium for MIC simulations with *Desulfovibrio vulgaris*

According to several studies, the choice of the growth medium has a strong influence not only on bacterial metabolism and attachment to surfaces but also on their corrosivity to metals. In a review, Little & Ray (2002) described that most corrosion studies have been performed in yeast-containing media, despite yeast has been demonstrated to strongly influence corrosion rates and electrochemical measurements (potentially including SKPFM). Other authors provided evidence for a corrosion-inducing effect of yeast extract under abiotic conditions, but a strong protective effect under biotic conditions (which has previously been attributed to Escherichia coli; Javed, et al., 2014). Additionally, it was demonstrated that proteins (the predominant component of yeast extract; Ribbons & Norris, 1970) strongly reduce the dissolution rate of CuNi 70-30 alloy as well as influence the chemical characteristics of the oxide layers (Carvalho, et al., 2014). Apart from yeast extract, the carbon source is of great importance in MIC experiments. Javed, et al., (2014) demonstrated that varying levels of lactate and glucose strongly influenced corrosion rates of *Escherichia coli* on 1010 carbon steel.

Hence, a fully defined medium was developed with yeast being replaced by trace element- and vitamin solutions. Lactate levels (approximately 5.5 g L^{-1}), however, were not altered in order to prevent (I) its accumulation on the working materials, (II) a potential influence

in cell attachment (which has been described under both highly nutrient-rich and nutrient-poor conditions; Javed, et al., 2014; Little & Ray, 2002) and (III) an impact on the corrosivity, which is directly linked to the metabolic activity of the microorganisms (Javed, et al., 2014). The use of alternative carbon sources such as pyruvate have been considered but discarded due to observations of Traore, et al., (1981). Pyruvate shows a strong influence on the sulphate metabolism and hydrogen evolution of *Desulfovibrio vulgaris*. In presence of pyruvate, significantly lower levels of hydrogen accumulated in the medium (approximately 2-fold lower than compared to lactate). To date, most corrosion studies with sulphate-reducing bacteria have been conducted using lactate-media. Due to the strong influence of H_2S-formation on the corrosion rates as demonstrated in several studies (Pérez, et al., 2007; Lee, et al., 1995; Little, et al., 2000), a critical evaluation of the results from this thesis with other studies would have been strongly impeded.

The final medium did not show any influence on the growth of *Desulfovibrio vulgaris*, its corrosivity or the quantity of EPS produced. Hence, it is regarded as a suitable alternative to yeast-containing media without strongly influencing MIC experiments allowing high-resolution investigations with Scanning Kelvin probe force microscopy (SKPFM) while minimising potential effects not related to bacterial activity.

5.2 Analysis of the CPD of biofilms and material surfaces by combined SKPFM & EFM

At the time of the practical execution of this thesis, no SKPFM-studies had been used to visualise the direct influence of bacteria on the electrochemical properties of different materials. Hence, the suitability of this technique and the experiment design had to be carefully scrutinised.

First, standard scanning parameters had to be defined to allow reproducible and reliable visualisation of the surface potentials. Two factors exert the biggest impact on the potential contrast: (I) the air gap between cantilever tip and surface and (II) the tip velocity (or line rate; Rohwerder & Turcu, 2007; Zerweck, et al., 2005). Basically, the Kelvin signal in SKPFM strongly depends on the tip-surface distance as the cantilever geometry becomes more important with increasing distances. Rohwerder & Turcu (2007) expected that at distances of 100 nm the full potential contrast would be recorded for surface features > 500 nm.

Zerweck, et al., (2005) demonstrated that full contrast was achieved at distances below 30 nm with a lateral resolution of approximately 50 nm (in ultra-high vacuum, the resolution is expected to be lower under ambient conditions). However, the controller maintaining the tip-surface distance was found to be unreliable at distances above 30 nm. In this thesis, an air gap of 50 nm was used, as no increase in potential contrast and resolution was visible (compared to distances of down to 10 nm). Similar observations were made by Zerweck, et al., (2005) and Guillaumin, et al., (2001) who did not see any significant increase in contrast at tip-sample distances below 30 and 50 nm, respectively. According to Rohwerder & Turcu (2007), a low dependency of the potential contrast to the tip-surface distance indicates a low influence of stray capacities. This suggests a proper experimental set-up and a high reliability of the obtained data.

In SKPFM, the air gap is maintained by lifting the cantilever based on the topography recorded in the first pass. As the quality of the topographic imaging is strongly dependent on the tip velocity (especially on rough surfaces such as corroding metals), it also strongly influences the quality of the potential visualisation. As already implied before, varying distances between tip and surface will strongly influence the potential contrast as well as reduce the lateral resolution (Rohwerder & Turcu, 2007; Zerweck, et al., 2005). Generally, lower tip velocities will increase the quality of the topographical image. When visualising the surface potential of *Escherichia coli* and MRSA cells, Birkenhauer & Neethirajan (2014b; 2014a) obtained best results at scanning speeds of 0.02 – 0.05 lines s^{-1} (tip velocity approximately 0.1 – 0.5 µm s^{-1}), leading to a scanning duration of 2.8 to 7.1 h per image. However, results from this thesis show a strong influence of the time after sample emersion on the surface potentials recorded (+30 mV difference between cells and surface after 1 h, stabilises at around +10 mV after 6 h and more). Hence, image quality and scanning duration had to be balanced. The quick diminishing of the surface potentials could be related to observations of Rohwerder & Turcu (2007), who demonstrated a quick return of the work function of ferric materials after emersion to initial values prior to corrosion experiments. The authors suggested that this may be related to the work function of iron oxides depending on the Fe(III)/Fe(II) ratio, which will quickly re-equilibrate after emersion (depending on humidity and partial oxygen pressure). The best compromise of image quality vs. scanning time was obtained at a line rate of 0.3 Hz (i.e. tip velocity of 1.5 to 50 µm s^{-1}, depending on x- and y-distance).

Both factors themselves, however, strongly depend on the cantilever geometry and type. In this study, Cr/Pt coated cantilevers with a typical tip diameter of < 25 nm, a spring constant of 20 – 75 N m^{-1} and a resonance frequency of 300 kHz were used. These relatively stiff cantilevers were selected based on observations of Zerweck, et al., (2005), who found the full lateral resolution to be achieved for objects smaller than the tip diameter. Spring constant and resonance frequency of the cantilever did not have any effect on the absolute CPD values measured but a resistant and undamaged coating was imperative for stable Kelvin signals. Additionally, empirical knowledge from several hundred scans of different materials with the instrument from this thesis showed that stiff cantilevers provide the best topographic image quality for rough surfaces in intermittent contact mode.

To estimate the potential differences between cells and material surface, cross-sectional profiles were used. A similar approach has, for example, been successfully used to quantify the effect of hematite nanoparticles on *Escherichia coli* cells (Zhang, et al., 2012). Since the surface potential of the cell surface averted from the working material not necessarily reflects the conditions at the interface between cell and surface, a method was devised to remove the cells and their matrix (i.e. the EPS) without influencing the visualisation by SKPFM. Ultrasound treatment with 0.5 % SDS solution removes organic matter reliably (Whittaker, et al., 1984) and does not show any negative effect (i.e. corrosion) of the working material when anaerobic conditions are strictly maintained. Additionally, SDS is well-known for its ability to solubilise proteins, a substance class of particular concern. Proteins are major part of both the conditioning layer needed for bacterial attachment (Compère, et al., 2009; Neu, 1996) as well as the EPS matrix of established biofilms (Jahn, et al., 1999) and tend to spontaneously (re-)adsorb to metal surfaces (Williams & Williams, 1988; Williams, et al., 1985).

Initial corrosion experiments with pure iron and alloyed steel as working materials showed no signs of corrosion for both materials after up to 7 d under abiotic conditions. The topographic SKPFM images correspond to observations by Wikieł, et al., (2014; made with carbon steel under marine conditions) with the grooves from the polishing process on pure iron and alloyed steel still intact. Additionally, no “anodic” or “cathodic” areas were visible in the CPD images. These results were expected, since in sterile anaerobic environments at near-neutral pH the rate of proton reduction and, thus, iron dissolution is negligible

(Enning, et al., 2012). However, these results verified the suitability of the experimental set-up to maintain both anaerobic and abiotic conditions.

In presence of *Desulfovibrio vulgaris*, SKPFM investigations were only possible after 24 h incubation as after longer incubation times dense, continuous precipitates (presumably FeS) formed on the metal surface and proper identification of cells by either EFM or SKPFM was no longer possible. However, the metal surface itself showed both more positive and negative areas (approximately 50 mV difference). The surface potential of the cells was approximately +25 mV vs. the surrounding surface. Unfortunately, no visualisation of the surface potentials at the cell-surface interface (i.e. beneath the cells) was possible due to strong formation of artefacts during the cell removal procedure. It can only be speculated that the formation of precipitates increased the vulnerability of iron to corrosion.

Comparable to pure iron, cells on alloyed steel showed a surface potential of approximately +20 to +25 mV during the whole time of the experiment (72 h). To date, measurements of the cell surface potential by SKPFM have only been used to estimate the strength of cellular adhesion to surfaces. Birkenhauer & Neethirajan (2014a) estimated the absolute surface potentials of stainless steel, *Pseudomonas aeruginosa* and MRSA cells. When attached to stainless steel, the potential difference between MRSA and the surface was approximately +10 to +20 mV. An even stronger effect was observed for *Pseudomonas aeruginosa* with surface potentials of approximately +100 mV vs. the material surface. However, using the scanning Kelvin probe (SKP) technique, Gehrke, et al., (1998) found a significant positive shift of the surface potential in biofilms of *Acidithiobacillus ferrooxidans* on pyrite in presence of EPS (approximately +200 mV vs. the surface potential of the material). They suggested that potential shift is being caused by electrochemical processes facilitated by EPS, i.e. the oxidation-reduction of Fe(II) to Fe(III) and back between the EPS matrix and material surface.

After cell removal, surface potentials at areas formerly covered by cells showed a shift to more negative potentials of about -25 mV compared to the surrounding surface. To date, no other studies are known to the author directly visualising the influence of cells onto the material surface beneath the microorganisms. However, SKPFM studies of several authors found potential differences of the same magnitude between austenitic and ferritic phases of stainless steel (Örnek & Engelberg, 2015; Pan, 2012; Sathirachinda, et al., 2009). The

ferritic phases, prone to corrosion, showed a significant negative shift vs. the austenitic phases. Explanatory models suggest that the difference in surface potential is related to a depletion of Ni and promoted the formation of local galvanic couples on a microscale. It can be assumed that SRB exhibit a direct influence on the passive oxide layer of stainless steel as demonstrated by Gonzalez, et al., (1998; cited from Angell, 1999). The authors suggested that breakdown of the passive layer is caused by metabolic sulphide production. Furthermore, Scotto & Lai (1998; cited from Angell, 1999) found a direct correlation between the susceptibility of stainless steel to pitting corrosion and the amount of extracellular carbohydrates produced by the biofilm. Additionally, it is a well-established fact that microbial biofilms can accumulate certain heavy metals (such as Ni and Pb, respectively) with high affinity (Templeton, et al., 2001; Basnakova, et al., 1998; Percival, et al., 1998; Nelson, et al., 1995). However, it should be noted that in this thesis pitting of the working material was neither observed nor expected since the chloride concentration of the medium was well below the critical concentration of about 3 mg L^{-1} at near-neutral pH.

Summarising, SKPFM results in this thesis provide strong evidence on a direct microbial influence on the passivating oxide layer of stainless steel. However, caution is required when considering quantitative SKPFM results (and especially when comparing them to SKP data). Rohwerder & Turcu (2007) observed an approximately 10-fold lower potential difference between Al inclusions of roughly the size of microbial cells (2 µm) in pure Mg surfaces (70 mV) than expected from SKP measurements of the pure materials themselves (600 mV). Additionally, Kelvin signal inversion was reported by several authors (Hochwitz, et al., 1996; Henning, et al., 1995; cited from Rohwerder & Turcu, 2007) and has frequently been observed when establishing the standard method for this thesis (data not shown).

5.3 Influence of metal substrata on the biochemical composition of EPS from *Desulfovibrio vulgaris*

To elucidate the role of EPS in biocorrosion by SRB, the composition of both loosely (easily extractable) and tightly bound (strongly associated to the cell surface) EPS fractions from cells grown in the presence of alloyed steel, pure iron, or without metallic substrata were extracted and analysed. Several reports demonstrated that the extraction procedure itself has a great influence on the biochemical composition of the EPS extracts (Michalowski, 2012; Aguilera, et al., 2008). The method used in this thesis was carefully developed and

evaluated by Wikieł (2013) for the extraction of EPS from marine *Desulfovibrio alaskensis* and was only slightly adapted. In total, only 7 – 15 % of the loosely bound fractions were accessible to the colorimetric determinations used in this thesis. In contrast, 39 – 64 % of the components of the tightly bound fractions were identified. Based on TOC results, loosely bound fractions are in fact overestimated by 1.8 up to 3.9 times. Under all conditions, the TOC content of the tightly bound fractions indicates a slight underestimation and when considering these results, approximately 65 % were identified under all conditions. The remaining compounds are probably of inorganic origin and have not been identified, yet.

In presence of pure iron, the total EPS yield was significantly higher for both loosely and tightly bound fractions (10-fold and 3.5-fold, respectively) compared to alloyed steel and control. The amount of nucleic acids in both EPS fractions was approximately 2-fold higher in presence of both alloyed steel and pure iron. Intracellular contamination can be excluded since G6PDH measurements did not show any indication of cell lysis. Nucleic acids (or eDNA) have been demonstrated to be a major structural component of EPS and have been suggested to play an important role in microbial attachment to surfaces (Vilain, et al., 2009; Boeckelmann, et al., 2006). The present results support these findings.

In all conditions, proteins and polysaccharides represent the major compounds of all EPS, regardless of the growth conditions (substratum) or fraction (loosely or tightly bound, respectively). This is well in agreement with reports on the typical EPS composition reported for several different microorganisms (Flemming & Wingender, 2010; Flemming, et al., 2007; Branda, et al., 2005; Tsuneda, et al., 2003; Jahn, et al., 1999; Beech & Cheung, 1995) and SRB in particular (Wikieł, 2013). On closer examination, however, the total amount of proteins in the tightly bound fraction are approximately 2-fold lower in presence of pure iron. Similar observations were made by Zinkevich, et al. (1996), who were analysing the EPS of the marine SRB strains *Desulfovibrio alaskensis* and *Desulfovibrio indonesiensis*. In presence of carbon steel, they found a 2 to 3-fold decrease in the total protein content while the total EPS yield remained constant. In contrast to proteins, the total amount of polysaccharides in presence of alloyed steel and pure iron was considerably higher, but only the increase in sugar content in presence of pure iron can be regarded as significant. Similar observations were reported by Beech, et al., (1991) when studying the influence of

alloyed steel and carbon steel on the EPS composition of *Desulfovibrio desulphuricans*. In contrast, Zinkevich, et al., (1996) did not observe any significant changes in polysaccharide content of the EPS from *D. alaskensis* and *D. indonesiensis* in presence of carbon steel. Other authors observed varying responses in sugar and protein content in presence of different heavy metals (Yue, et al., 2015). All the mentioned authors demonstrated a strong influence of the substratum on the qualitative composition of the polysaccharide and protein moieties. In this study, however, only the qualitative composition of the polysaccharide fraction was analysed and no significant difference was found in presence of alloyed steel or pure iron, respectively. Rhamnose, fucose and arabinose represented the major compounds under all conditions. In the EPS of *D. alaskensis* and *D. indonesiensis*, in contrast, mannose, glucose and ribose were found to be the major constituents (Zinkevich, et al., 1996). Generally, proteins are assumed to play a pivotal role in the attachment of microorganisms to surfaces, especially when these are hydrophobic (Conrad, et al., 2003; Bruinsma, et al., 2001). It may be speculated that the highly hydrophilic properties of corroding iron, together with the strong increase in surface area (due to the formation of iron oxide particles in the medium) might trigger a downregulation in protein production. In contrast, functional groups such as carboxyl or hydroxyl groups, which are responsible for heavy-metal sorptive effects of EPS (Yue, et al., 2015; Wei, et al., 2011; Guibaud, et al., 2010; Alvarado Quiroz, et al., 2006) are associated to acidic polysaccharides (Chan, et al., 2009). Hence, an increase in heavy metal ions (i.e. Fe) might cause an upregulation of these polysaccharides. However, to date this remains purely speculative, as no studies in this regard are available to the author's knowledge.

A similar effect was observable for uronic acids. In presence of alloyed steel and pure iron the total amount of uronic acids in the loosely bound EPS fraction was more than 3-fold higher than in the control (while, at the same time, the amount in the tightly bound EPS fraction was approximately 2-fold lower). When considering the amount of Fe(III) ions in the EPS which is strongly increased in presence of pure iron (3-fold higher than in presence of alloyed steel and control, respectively), a ratio of 2 moles glucuronic acids to 1 mole Fe(III) ions was observed. A similar upregulation of uronic acids with the same molar ratio was reported by Gehrke, et al., (1998) when investigating the role of EPS in metal-sulphide leaching by *Acidithiobacillus (At.) ferrooxidans*. This certain molar ratio indicates the for-

mation of a glucuronic acid-Fe(III) complex (Geesey & Lang, 1989) and in case of *Acidithiobacillus ferrooxidans* it is assumed that Fe(III) ions are retained within the EPS in direct proximity to the material surface and act as an oxidising agent against it (Gehrke, et al., 2001; Gehrke, et al., 1998). Interestingly, in presence of alloyed steel the molar ratio exceeded 30:1, as no increase in Fe(III) ions was found (and expected) in the EPS matrix (due to the lack of excess Fe ions from metal dissolution). It may be assumed that the increase in uronic acid content in the loosely bound EPS fractions is a direct response to metals. This indicates a special role of uronic acids in the corrosion-increasing effect of SRB to metals comparable to their role in bioleaching by *Acidithiobacillus ferrooxidans* and could help explain the intrinsic corrosiveness of EPS from *Desulfovibrio vulgaris* as reported by Stadler, et al., (2008).

Lipids, finally, are another substance class important for bacterial attachment to surfaces. In this study, the total lipid content of the loosely bound EPS fraction was found to be 3-fold higher compared to pure iron and control, respectively. No difference was found in the tightly bound fractions. Lipids are known to be largely responsible for hydrophobic properties of the EPS matrix (Flemming & Wingender, 2010). Gehrke, et al., (1998) demonstrated that hydrophobic surfaces lead to an increase in total lipid content. They are presumably helping to overcome repulsive effects of hydrophobic surfaces and, thus, facilitate bacterial attachment. As already mentioned, corroding pure iron can be regarded as being highly hydrophilic, while stainless steel can generally be expected to be more hydrophobic due to its passive oxide layer (experimental results show increasing contact angles, i.e. hydrophobicity, when a previously removed oxide layer re-establishes; Anonymous, 2003; Mantel & Wightman, 1994). Thus, no up-regulation in lipid content is necessary for bacterial attachment in presence of pure iron or without any metal substrata present. The qualitative analysis of the lipid fraction did not show any significant response to the metal substrates. Generally, loosely bound fractions are comprised mainly of C6 to C20 saturated fatty acids with C16 being the predominant form. In the tightly bound fractions of cells grown in presence of pure iron and the control, respectively, several (poly)unsaturated fatty acids, especially C16:1, C18:1-3, and C20:1 were identified. Interestingly, in presence of alloyed steel these unsaturated fatty acids were predominant in the loosely bound fraction and less abundant in the tightly bound fraction. Comparable fatty acid compositions were found when studying methane-oxidising SRB consortia in marine sediment (Elvert, et

al., 2003). The authors concluded that less abundant unsaturated fatty acids (such as C16:1) were suitable markers indicating the presence of SRB like *Desulfobacteracea*. Edlund, et al., (1985) used the typical fatty acid composition to identify several members of the *Desulfovibrio* family, including *Desulfovibrio vulgaris.* The typical fatty acid profiles reported are also comparable to the general profiles identified in this thesis. To date, no detailed reports are available on the influence of metal substrata on the fatty acid composition of the EPS' lipid fraction. However, several authors report a shift in the cis/trans ratio of fatty acids as a response to external stress but cis/trans forms were inseparable with the method used in this thesis.

5.4 Effect of cyclodextrins on MIC of steel

25 differently functionalised cyclodextrins have been investigated regarding their general potential as anti-corrosive agents in MIC and to identify the most effective functional groups. The strongest protective effect against MIC by *Desulfovibrio vulgaris* (more than 90 % reduction in corrosion rates) was found when the molecules were functionalised with carboxymethyl- and carboxyethyl groups, independent from the ring-size of the cyclodextrin itself. It has been speculated before that carboxylic groups inside the EPS matrix are directly responsible for protective effects of crude EPS extracts (Scheerder, et al., 2012; Finkenstadt, et al., 2011). In recent studies, the pivotal role of carboxy(m)ethyl groups on corrosion has been demonstrated by various authors. In a comprehensive review, Umoren & Eduok (2016) compiled more than 20 reports on the protective effect of carboxy(m)ethylcellulose against abiotic corrosion. For various metals and corrosive (sterile) media, the corrosion-inhibition could be directly attributed to the formation of protective films on the material surfaces as well as the complexation of corrosion products such as Zn and Fe ions, respectively. The formation of such (passive) protective barriers can also be assumed as the main mechanism in this thesis since the films did not show any effect on biofilm formation by *Desulfovibrio vulgaris* (negating hypothetical biocidal or adhesion-preventing effects), but the cells were not able to penetrate the cyclodextrin film for the duration of the corrosion experiments. However, the latter is only true for additionally polymerised films. Initially, only a short-term protective effect was achieved. After more than 1 week of incubation corrosion rates approached these of uncoated controls. CLSM studies showed the

same effect in sterile media. Additionally, no biodegradation of the cyclodextrins by *Desulfovibrio vulgaris* have been observed and, hence, purely physical desorption can be assumed (caused by insufficient adsorption of the cyclodextrin to the material surface). This contradicts (to a certain extent) the report of Liu, et al., (2015), who investigated the adsorption of β-cyclodextrin modified allylcarboxymethyl chitosan to carbon steel. They found a strong interaction between the material and the polymer and proposed that chemical adsorption of Fe(II) from the material surface to both hydroxy- and carboxymethyl-groups (of the chitosan part) as well as a physical adsorption between adsorbed hydrogen ions (on the material surface) and hydroxy groups from the cyclodextrin were responsible. However, considering the structure of the chitosan polymer compared to single cyclodextrin-molecules, much weaker interactions are expected. Hence, a sol-gel-like polymerisation of the cyclodextrins under acidic conditions using glutaraldehyde as a linker (Poon, et al., 2014; Badruddoza, et al., 2013; Singh, et al., 2012) was used to increase the film stability. Regarding short-term corrosion experiments (7 d), the polymerisation did not improve the protective effect. After 21 d incubation, however, it significantly enhanced the MIC-reducing effect (about 77 % lower corrosion rates vs. controls). CLSM images showed dense, stable films with a thickness of up to 10 µm fully overgrown by biofilms. These findings are in good agreement with several studies reporting exceptional stability of glutaraldehyde-linked polysaccharides such as lipopolysaccharides from *E. coli* (Eskenazy, 1970), chitosan (Janes, et al., 2001; Felt, et al., 1998) and, most importantly, cyclodextrins (Poon, et al., 2014; Badruddoza, et al., 2013; Singh, et al., 2012). Regarding their potential to permanently fix biomolecules to material surfaces, Charles, et al., (1975) demonstrated that lactase retained more than 80 % of its initial activity for more than 80 days in liquid media when immobilised, indicating an irreversible attachment to the material surface. Certainly, glutaraldehyde is known as a potent biocide (Laopaiboon, et al., 2006; Gorman, et al., 1980) that is also effective for biofilms (Wen, et al., 2009). It is known that glutaraldehyde is effectively polymerising cell membranes (McGucken & Woodside, 1973) and, thus, inhibiting metabolic mass transfer. However, in this study, no influence of glutaraldehyde-linked cyclodextrins and (probably self-polymerised) glutaraldehyde-films on steel surfaces on *Desulfovibrio vulgaris* biofilms was observed. This indicates that no residual non-polymerised glutaraldehyde was present in the films or leached into the medium.

Regarding the electrochemical effects of cyclodextrins on ferric materials, only SKPFM-imaging was used in this thesis. The results indicate a strong influence of the cyclodextrin films on the surface potential of steel but do not allow any prediction for the corrosion behaviour of the material. Two studies are currently explicitly investigating the electrochemical influence of the cyclodextrins from this thesis on MIC by various SRP (Holuscha, in prep) and Mn-Oxidisers (Thyssen, in prep).

5.5 Conclusions

The novel combination of SKPFM & EFM introduced in this thesis represents a valuable tool for visualising and estimating the direct electrochemical influence of microorganisms and their EPS on metallic working materials. It was successfully used to visualise the effect of *Desulfovibrio vulgaris* to alloyed steel (with a strong indication of a direct influence on the passivating oxide layer) while EFM allowed to properly identify single cells with high accuracy. The versatility of EFM and fluorescent markers for specific substances such as polysaccharides, lipids, and the possibility to identify certain species from mixed consortia will help to further the knowledge of localised processes in MIC and MICI. However, the method did show shortcomings as well. In fact, the strong formation of corrosion products (probably FeS) on carbon steel made proper mapping of surface potentials impossible. However, as SKPFM & EFM can be further expanded and combined with other techniques such as CLSM or electrochemical microelectrodes, it bears a tremendous future potential for the research of MIC and MICI.

Comparative analyses of EPS grown with or without different metals clearly demonstrated a biochemical response of *Desulfovibrio vulgaris* to the presence of different materials. Several substance groups which have been connected to attachment (such as proteins, lipids, and nucleic acids) were upregulated in presence of metals, particularly in presence of the more hydrophobic stainless steel, indicating an important role in attachment to surfaces. Interestingly, the strongest upregulation was found in the loosely bound EPS fractions, and hence, it is highly probable that these substances are pivotal to the formation of a conditioning layer. Other substance groups showing a significant increase in the presence of metals were polysaccharides and uronic acids. Polysaccharides usually possess polyanionic or –cationic features and might (I) promote strong cohesion of the EPS matrix itself, (II) irre-

versible attachment to surfaces by electrostatic and weak interactions, and (III) play an important role in MIC or MICI (e.g. carboxyl groups). Uronic acids are probably a major factor in the corrosive impact of SRB on metals. Akin to leaching bacteria such as *Acidithiobacillus ferrooxidans*, uronic acids will promote the formation of uronic acid - Fe(III) complexes, from which Fe(III) may act as an oxidising agent attacking the material surface.

Experiments with differently functionalised cyclodextrins underlined the assumption that carboxyl groups might play a significant role in the corrosion-reducing effect of several EPS (as reported in recent studies). The strongest protective effect was achieved with carboxy(m)ethyl-modified cyclodextrins with a reduction in corrosion rates caused by *Desulfovibrio vulgaris* of up to 90 %. Despite the use of glutaraldehyde as polymerising agent, no toxic substances were leached into the environment. However, considering the biocidal products directive, polymerisation by less toxic compounds seems desirable. A potential approach could be the covalently bind cyclodextrins to surfaces (as suggested already in 1990 in a patent filed in the US; Weisz, et al., 1993). Additionally, the electrochemical effects of cyclodextrins on the working material are yet to be elucidated, but two studies are currently investigating these effects (Holuscha, in prep; Thyssen, in prep). Additionally, their performance under real-life conditions (i.e. mixed microbial consortia, varying flow conditions) is yet to be assessed. Nevertheless, cyclodextrins seem to be a promising approach for greener corrosion protection, which is also reflected in several patents filed in the last years (e.g. Gabbay, 2011; The Procter & Gamble Company, 2002).

6 REFERENCES

Africa, C.-J., Harrison, S., Becker, M. & van Hille, R., 2010. In situ investigation and visualisation of microbial attachment and colonisation in a heap bioleach environment: The novel biofilm reactor. *Min Eng 23(6)*, pp. 486-491.

Aguilera, A., Souza-Egipsy, V., San Martín-Úriz, P. & Amils, R., 2008. Extraction of extracellular polymeric substances from extreme acidic microbial biofilms. *Appl Microbiol Biotechnol 78*, pp. 1079-1088.

Allison, D. G. et al., 1998. Extracellular products as mediators of the formation and detachment of Pseudomonas fluorescens biofilms. *FEMS Microbiol Lett 167*, pp. 179-184.

Alvarado Quiroz, N. G., Hung, C. & Santschi, P. H., 2006. Binding of thorium(IV) to carbxylate, phosphate and sulfate functional groups from marine exopolymeric substances (EPS). *Mar Chem 100*, pp. 337-353.

Angell, P., 1999. Understanding microbially infleunce corrosion as biofilm-mediated changes in surface chemistry. *Curr Opin Biotechnol 10*, pp. 269-272.

Anonymous, 2003. *www.firsttenangstroms.com.* [Online]
Available at: http://www.firsttenangstroms.com/pdfdocs/ContactAnglesOnSteel.pdf
[Accessed 17 May 2016].

Auerbach, I. D., Sorensen, C., Hansma, H. G. & Holden, P. A., 2000. Physical morphology and surface properties of unsaturated Pseudomonas putida biofilms. *J Bacteriol 182(13)*, pp. 3809-3815.

Badruddoza, A. et al., 2013. Fe3O4/cyclodextrin polymer nanocomposites for selective heavy metals removal from industrial wastewater. *Carbohyd Polym 91(1)*, pp. 322-332.

Barner, J., 2007. Combining optical upright microscopy and AFM. *Imaging & Microscopy 9(4)*, pp. 42-43.

Basnakova, G., Finlay, J. A. & Macaskie, L. E., 1998. Nickel accumulation by immobilized biofilm of Cirobacter sp. containing cell-bound polycrystalline hydrogen uranyl phosphate. *Biotechnol Lett 20(10)*, pp. 949-952.

Beccaria, A. M. & Mor, E. D., 1978. Inhibiting effect of some monosaccharides on the corrosion of copper in nitric acid. *Brit Corr J 13(4)*, pp. 186-190.

Becker, K., 1996. Exopolysaccharide production and attachment strength of bacteria and diatoms on substrates with different surface tensions. *Microbiol Ecol 32*, pp. 23-33.

Beech, I. B., 1996. The potential use of atomic force microscopy for studying corrosion of metals in the presence of bacterial biofilms — an overview. *Int Biodet Biodegradat 37(3-4)*, pp. 141-149.

Beech, I. B. & Cheung, C. W. S., 1995. Interactions of exopolymers produced by sulphate-reducing bacteria with metal ions. *Ann Rev Microbiol 49*, pp. 59-72.

Beech, I. B. & Gaylarde, C., 1999. Recent advances in the study of biocorrosion: an overview. *Rev Microbiol 30(3)*, pp. 117-190.

Beech, I. B. & Sunner, I. A., 2007. Sulphate-reducing bacteria and their role in corrosion of ferrous materials. In: *Sulphate-Reducing Bacteria.* Cambridge: Cambridge University Press, pp. 459-482.

Beech, I. B. & Sunner, J. W., 2004. Biocorrosion: towards understanding interactions between biofilms and metals. *Curr Opin Biotechnol 15*, pp. 181-186.

Beech, I. B., Zinkevich, V., Tapper, R. & Gubner, R., 1998. The direct involvement of extracellular compounds form a marine sulphate-reducing bacterium in deterioration of steel. *Geomicrobiol J 15*, pp. 119-132.

Beech, I., Gaylarde, C., Smith, J. & Geesey, G., 1991. Extracellular polysaccharides from Desulfovibrio desulfuricans and Pseudomonas fluorescens in the presence of mild and stainless steel. *Appl Microbiol Biotechnol 35(1)*, pp. 65-71.

Binnig, G. et al., 1987. Atomic resolution with atomic force microscope. *Surf Sci 189/190*, pp. 1-6.

Binnig, G., Quate, C. F. & Gerber, C. H., 1986. Atomic Force Microscope. *Phys Rev Lett 56(9)*, pp. 930-933.

Birkenhauer, E. & Neethirajan, S., 2014a. Characterization of electrical surface properties of mono- and co-cultures of Pseudomonas aeruginosa and methicillin-resistant Staphylococcus aureus using Kelvin probe force microscopy. *RSC Adv 4*, pp. 42432-42440.

Birkenhauer, E. & Neethirajan, S., 2014b. Surface potential measurement of bacteria using Kelvin probe force microscopy. *J Vis Exp 93*, pp. 1-8.

Blumenkrantz, N. & Asboe-Hansen, G., 1973. New method for quantitative determination of uronic acids. *Anal. Biochem. 54(2)*, pp. 484-489.

Boeckelmann, U. et al., 2006. Bacterial extracellular DNA forming a defined network-like structure. *FEMS Microbiol Lett 262(1)*, pp. 31-38.

Booth, G. H. & Tiller, A. K., 1960. Polarisation studies of mild steel in cultures of sulphate-reducing bacteria. *Trans Faraday Soc 56*, pp. 1689-1696.

Branda, S. S., Vik, Å., Friedman, L. & Kolter, R., 2005. Biofilms: the matrix revisited. *TRENDS Microbiol 13(1)*, pp. 20-26.

Bremer, P. J., Geese, C. G. & Drake, B., 1992. Atomic force microscopy examination of the topography of a hydrated bacterial biofilm on a copper surface. *Curr Microbiol 24(4)*, pp. 223-230.

Bruinsma, G., van der Mei, H. & Busscher, H., 2001. Bacterial adhesion to surface hydrophilic and hydrophobic contact lenses. *Biomat 22*, pp. 3217-3224.

Bryant, R. D. et al., 1991. Effect of hydrogenase and mixed sulphate-reducing bacterial populations on the corrosion of steel. *Appl Environ Microbiol 57(10)*, pp. 2804-2809.

Bryant, R. & Laishley, E., 1990. The role of hydrogenase in anaerobic biocorrosion. *Can J Microbiol 36*, pp. 259-264.

Butt, H. J., Downing, K. H. & Hansma, P. K., 1990a. Imaging the membrane protein bacteriorhodopsin with the atomic force microscope. *Biophys J 58(6)*, pp. 1473-1480.

Butt, H. J. et al., 1990b. Imaging cells with the atomic force microscope. *J Struc Biol 105(1-3)*, pp. 54-61.

Carvalho, M. L. et al., 2014. Effect of protein adsorption on the corrosion behavior of 70Cu–30Ni alloy in artificial seawater. *Bioelectrochemistry 97*, pp. 34-42.

Chan, C. S. et al., 2009. Iron oxyhydroxide mineralization on microbial extracellular polysaccharides. *Geochim Cosmochim Acta 73*, pp. 3807-3818.

Characklis, W. G. & Wilderer, P. A., 1989. *Structure and function of biofilms.* Chichester: John Wiley & Sons.

Charles, M. et al., 1975. Enzymes immobilized on alumina and stainless steel supports. *Biotechnol Bioeng 17(2)*, pp. 203-210.

Cheng, Y.-S., Zheng, Y. & van der Gheynst, J. S., 2011. Rapid quantitative analysis of lipids using a colorimetric method in a microplate format. *Lipids 46*, pp. 95-103.

Chen, X. & Stewart, P., 2000. Biofilm removal caused by chemical treatments. *Wat Res 34(17)*, pp. 4229-4233.

Chongdar, S., Gunasekaran, G. & Kumar, P., 2005. Corrosion inhibition of mild steel by aerobic biofilm. *Electrochim Acta 50*, pp. 4655-4665.

Coetser, S. & Cloete, T., 2005. Biofouling and biocorrosion in industrial water systems. *Crit Rev Microbiol 31*, pp. 213-232.

Coles, B. et al., 1997. A hydrodynamic AFM flow cell for the quantitative measurement ofinterfacial kinetics. *Chem Commun 6*, pp. 619-620.

Compère, C. et al., 2009. Kinetics of conditioning layer formation on stainless steel immersed in seawater. *Biofouling*, Issue 17(2), pp. 129-145.

Comte, S., Guibaud, G. & Baudu, M., 2006a. Biosorption properties of extracellular polymeric substances (EPS) resulting from activated sludge according to their type: Soluble or bound. *Proc Biochem 41*, p. 815–823.

Comte, S., Guibaud, G. & Baudu, M., 2006b. Relations between extraction protocols for activated sludge extracellular polymeric substances (EPS) and EPS complexation properties. Part I. Comparison of the efficiency of eight EPS extraction methods. *Enzym Microbiol Technol 38*, pp. 237-245.

Connors, K. A., 1997. The stability of cyclodextrin complexes in solution. *Chem Rev 97*, pp. 1325-1357.

Conrad, A. et al., 2003. Fatty acids of lipid fractions in extracellular polymeric substances of activated sludge flocs. *Lipids 38(10)*, pp. 1093-1105.

Cord-Ruwisch, R. & Widdel, F., 1986. Corroding iron as a hydrogen-source for sulphate reduction in cultures of sulphate-reducing bacteria. *Appl Microbiol Biotechnol 25*, pp. 169-174.

Costello, J. A., 1974. Cathodic depolarization by sulphate reducing bacteria. *S Afr J Sci 70*, pp. 202-204.

Costerton, J. W. & Anwar, H., 1994. Pseudomonas aeruginosa: the microbe and pathogen. In: A. Baltch & P. Smith, eds. *Pseudomonas aeruginosa Infections and Treatment.* New York: Dekker, pp. 1-18.

Costerton, J. W. et al., 1987. Bacterial biofilms in nature and disease. *Ann Rev Microbiol 41*, pp. 435-464.

Costerton, J. W. et al., 1995. Microbial biofilms. *Annu Rev Microbiol 49*, pp. 711-745.

Costerton, J. W. et al., 1994. Biofilms: the customized microniche. *J Bacteriol 176*, pp. 2137-2142.

Cowan, M. & Busscher, H. J., 1993. Flow chamber study of the adhesion of Prevotella intermedia to glass after preconditioning with mutans strepto- coccal species: kinetics and spatial arrangement. *Microbios 73*, pp. 135-144.

Crolet, J. L., Daumas, S. & Magot, M., 1993. pH regulation by sulphate reducing bacteria. *CORROSION93, paper 303*.

Cunliffe, M. & Murrell, J. C., 2009. The sea-surface microlayer is a gelatinous biofilm. *ISME J 3*, pp. 1001-1003.

Da Silva, S., Basséguy, R. & Bergel, A., 2004. Hydrogenase-catalysed deposition of vivianite on mild steel. *Electrochim Acta 49(13)*, pp. 2097-2103.

Danese, P. N., Pratt, L. A. & Kolter, R., 2000. Exopolysaccharide production is required for development of Escherichia coli K-12 biofilm architecture. *J Bacteriol 182*, pp. 3593-3596.

de Araujo, L. V. et al., 2011. Rhamnolipid and surfactin inhibit Listeria monocytogenes adhesion. *Food Res Int 44*, pp. 481-488.

de Paiva, M., 2004. *Bacterias redutoras de sulfato (BRS): estudo de substancias polimericas extracellulares (SPE) e enzimas nos processos de adesao a substratos metalicos e de biocorrosao.* Dissertation. Rio de Janeiro: Instituto Oswaldo Cruz.

Diercks, M., Sand, W. & Bock, E., 1991. Microbial corrosion of concrete. *Experientia 47(6)*, pp. 514-516.

Dinh, H. T., 2003. *Microbiological study of the anaerobic corrosion of iron.* Dissertation. Bremen: Universität Bremen.

Dinh, H. T. et al., 2004. Iron corrosion by novel anaerobic microorganisms. *Nature 427*, pp. 829-832.

Dominiak, D., Nielsen, J. & Nielsen, P., 2011. Extracellular DNA is abundant and important for microcolony strength in mixed microbial biofilms. *Env Microbiol 13(3)*, pp. 710-721.

Dong, Z. H., Liu, T. & Liu, H. F., 2011. Influence of EPS isolated from thermophilic sulphate- reducing bacteria on carbon steel corrosion. *Biofouling 27(5)*, pp. 487-495.

Donlan, R. M. & Costerton, J. W., 2002. Biofilms: survival mechanisms of clinically relevant microorganisms. *Clinical Microbiol Rev*, Issue 15(2), pp. 167-193.

Dubiel, M. et al., 2002. Microbial iron respiration can protect steel from corrosion. *Appl Env Microbiol 68*, pp. 1440-1445.

DuBois, M. C. et al., 1956. Colorimetric method for determination of sugars and related substances. *Anal Chem 28(3)*, pp. 350-356.

Eashwar, M. & Maruthamuthu, S., 1995a. Mechanism of biologically produced ennoblement: Ecological perspectives and a hypothetical model. *Biofouling 8(3)*, pp. 203-213.

Eashwar, M., Maruthamuthu, S., Sathiyanarayanan, S. & Balakrishnan, K., 1995b. The ennoblement of stainless alloys by marine biofilms: The neutral pH and passivity enhancement model. *Corr Sci 37(8)*, pp. 1169-1176.

Edlund, A., Nichols, P. D., Roffey, R. & White, D. C., 1985. Extractable and lipopolysaccharide fatty acid and hydroxy acid profiles from Desulfovibrio species. *J Lipid Res 26*, pp. 982-988.

Elvert, M., Boetius, A., Knittel, K. & Barker Jørgensen, B., 2003. Characterization of specific membrane fatty acids as chemotaxonomic markers for sulfate-reducing bacteria involved in anaerobic oxidation of methane. *Geomicrobiol J 20*, pp. 403-419.

Enning, D. et al., 2012. Marine sulfate-reducing bacteria cause serious corrosion of iron under electroconductive biogenic mineral crust. *Env Microbiol 14(7)*, pp. 1772-1787.

Eskenazy, M., 1970. Isolation of anti-polysaccharide antibodies with glutaraldehyde cross-linked lipopolysaccharides. *Nature 226*, pp. 855-856.

European Parliament and Council, 2012. Regulation (EU) No 528/2012 of the European Parliament and of the Council of 22 May 2012 concerning the making available on the market and use of biocidal products. *OJ L 167*, 27 6, pp. 1-174.

Felt, O., Buri, P. & Gurny, R., 1998. Chitosan: A unique polysaccharide for drug delivery. *Drug Dev Ind Pharm 24(11)*, pp. 979-993.

Fenyvesi, E., 2011. Personal Communication.

Fenyvesi, E. et al., 2005. Biodegradation of cyclodextrins in soil. *Chemosphere 60(8)*, pp. 1001-1008.

Finkenstadt, V. L., Cote, G. L. & Willet, J. L., 2011. Corrosion protection of low-carbon steel using exopolysaccharide coatings from Leuconostoc mesenteroides. *Biotechnol Lett 33*, pp. 1093-1100.

Flemming, H. C., 1995. Biofouling und Biokorrosion - die Folgen unerwünschter Biofilme. *Chem Ing Tech 67*, pp. 1425-1430.

Flemming, H., Neu, T. & Wozniak, D., 2007. The EPS Matrix: The “House of Biofilm Cells”. *J Bacteriol 189(22)*, pp. 7945-7947.

Flemming, H.-C. & Wingender, J., 2002. Extracellular polymeric substances: structure, ecological functions, technical relevance. In: G. Bitton, ed. *Encyclopedia of environmental microbiology.* New York, NY: John Wiley & Sons, pp. 1223-1231.

Flemming, H. & Wingender, J., 2010. The biofilm matrix. *Nature Rev Microbiol 8*, pp. 623-633.

Florian, B. et al., 2009. Attachment behavior of leaching bacteria to metal sulfides elucidated by combined atomic force and epifluorescence microscopy. *Adv Mat Res 71-73*, pp. 337-340.

Florian, B., Noel, N. & Sand, W., 2010. Visualization of initial attachment of bioleaching bacteria using combined atomic force and epifluorescence microscopy. *Minerals Eng 23(6)*, pp. 532-535.

Folch, J., Lees, M. & Sloane Stanley, G. H., 1957. A simple method for the isolation and purification of total lipides from animal tissues. *J Biol chem*, 226(1), pp. 497-509.

Frisbie, C. D. et al., 1994. Functional group imaging by chemical force microscopy. *Science 265(5181)*, pp. 2071-2074.

Frølund, B., Palmgren, R., Keiding, K. & Nielsen, P. H., 1996. Extraction of extracellular polymers from activated sludge using a cation exchange resin. *Wat Res 30(8)*, pp. 1749-1758.

Gabbay, J. S., 2011. *Biofilm resistant materials.* United States, Patent No. US20130195841 A1.

Gana, M. et al., 2011. Antagonistic activity of Bacillus sp. obtained from an Algerian oilfield and chemical biocide THPS against sulfate-reducing bacteria consortium inducing corrosion in the oil industry. *J Ind Microbiol Biotechnol 38*, pp. 391-404.

Geesey, G. G., 1982. Microbial exopolymers: ecological and economic considerations. *ASM News 48*, pp. 9-14.

Geesey, G. G. & Lang, L., 1989. Interactions between metal ions and capsular polymers. In: T. J. Beveridge & R. J. Doyle, eds. *Metal ions and bacteria.* New York: John Wiley & Sons, pp. 325-357.

Gehrke, T., Hallmann, R., Kinzler, K. & Sand, W., 2001. The EPS of Acidithiobacillus ferrooxidans - a model for structure-function relationships of attached bacteria and their physiology. *Wat Sci Technol*, 43(6), pp. 1591-1167.

Gehrke, T., Telegdi, J., Thierry, D. & Sand, W., 1998. Importance of extracellular polymeric substances from Thiobacillus ferrooxidans for bioleaching. *Appl Env Microbiol 64(7)*, pp. 2743-2747.

Glessibl, F. J., 2005. AFM's path to atomic resolution. *Mater Today 5(6)*, pp. 32-41.

Gonzalez, J. E. G., Santana, F. J. H. & Mirza-Rosca, J. C., 1998. Effect of bacterial biofilm on 316 SS corrosion in natural seawater by EIS. *Corr Sci 40*, pp. 2141-2154.

Gorman, S. P., Scott, E. M. & Russell, A. D., 1980. Antimicrobial activity, uses and mechanism of action of glutaraldehyde. *J Appl Microbiol 48(2)*, pp. 161-190.

Gould, S. et al., 1988. Molecular resolution images of amino acid crystals with the atomic force microscope. *Nature 332*, pp. 332-334.

Gubner, R. & Beech, I. B., 2000. The effect of extracellular polymeric substances on the attachment of Pseudomonas NCIMB 2021 to AISI 304 and 316 stainless steel. *Biofouling 15(1-3)*, pp. 25-36.

Guibaud, G. et al., 2010. Effect of pH on cadmium and lead binding by extracellular polymeric substances (EPS) extracted from environmental bacterial strains. *Coll Surf B 80*, pp. 161-168.

Guillaumin, V., Schmutz, P. & Frankel, G. S., 2001. Characterization of corrosion interfaces by the scanning Kelvin probe force microscopy technique. *J Electrochem Soc 148(5)*, pp. B163-B173.

Hamilton, W., 1985. Sulphate-reducing bacteria and anaerobic corrosion. *Annu Rev Microbiol 39*, pp. 195-217.

Hansen, D. C. & McCafferty, E., 1996. The effect of various naturally occurring metal-binding compounds on the electrochemical behavior of aluminum. *J Electrochem Soc 143(1)*, pp. 114-119.

Hansma, P. K., Elings, V. B., Marti, O. & Bracker, C. E., 1988. Scanning tunneling microscopy and atomic force microscopy: application to biology and technology. *Science 242(4876)*, pp. 209-216.

Harneit, K. et al., 2006. Adhesion to metal sulfide surfaces by cells of Acidithiobacillus ferrooxidans, Acidithiobacillus thiooxidans and Leptospirillum ferrooxidans. *Hydrometallurgy 83(1-4)*, pp. 245-254.

Hedges, A. R., 1998. Industrial applications of cyclodextrins. *Chem Rev 98(5)*, pp. 2035-2044.

Henderson, E. & Sakaguchi, D. S., 1993. Imagin gF-Actinin fixed glial cells with a combined optical fluorescence/atomic force microscope. *Neuroimage*, pp. 145-150.

Henning, A. K. et al., 1995. Two-dimensional surface dopant profiling in silicon using scanning Kelvin probe microscopy. *J Appl Phys 77(5)*, pp. 1888-1896.

He, X. & Shi, X., 2009. Self-repairing coating for corrosion protection of aluminum alloys. *Prog Org Coat 65(1)*, pp. 37-43.

Hirasawa, K. A. et al., 1997. In situ electrochemical atomic force microscope study on graphite electrodes. *J Electrochem Soc 144(4)*, pp. L81-L84.

Hochwitz, T. et al., 1996. Imaging integrated circuit dopant profiles with the force-based scanning Kelvin probe microscope. *J Vac Sci Technol 14(1)*, pp. 440-446.

Holuscha, D., in prep. *Title not yet defined.* Dissertation. Frankfurt am Main: DECHEMA Forschungsinstitut e.V..

Horton, M., Charras, G., Ballestrem, C. & Lehenkari, P., 2000. Integration of atomic force and confocal microscopy. *Single Mol 2*, pp. 135-137.

Houry, A. et al., 2012. Bacterial swimmers that infiltrate and take over the biofilm matrix. *PNAS 109(32)*, pp. 13088-13093.

Hwang, G., Kang, S., Gamal El-Din, M. & Liu, Y., 2012. Impact of an extracellular polymeric substance (EPS) precoating on the initial adhesion of Burkholderia cepacia and Pseudomonas aeruginosa. *Biofouling 28(6)*, pp. 525-538.

Ishiwata, S. & Kamiya, M., 1999. Cyclodextrin inclusion: catalytic effects on the degradation of organophosphorus pesticides in neutral aqueous solution. *Chemosphere 39(10)*, pp. 1595-1600.

Ismail, K. et al., 2002. Corrosion Control of Mild Steel by Aerobic Bacteria under Continuous Flow Conditions. *Corrosion 58(5)*, pp. 417-423.

Iverson, W. P., 1983. Anaerobic corrosion mechanisms. *CORROSION83, paper 243*.

Ivnitskya, H. et al., 2007. Bacterial community composition and structure of biofilms developing on nanofiltration membranes applied to wastewater treatment. *Wat Res 41(17)*, pp. 3924-3935.

Jahn, A., Griebe, T. & Nielsen, P. H., 1999. Composition of Pseudomonas putida biofilms: Accumulation of protein in the biofilm matrix. *Biofouling 14(1)*, pp. 49-57.

Janes, K. A., Calvo, P. & Alonso, M. J., 2001. Polysaccharide colloidal particles as delivery systems for macromolecules. *Adv Drug Deliver Rev 47(1)*, pp. 83-97.

Javed, M. A. et al., 2014. Inhibition or acceleration: Bacterial test media can determine the course of microbiologically influenced corrosion. *Corr Sci 86*, pp. 149-158.

Jayaraman, A., Cheng, E., Earthman, J. & Wood, T., 1997a. Axenic aerobic biofilms inhibit corrosion of SAE 1018 steel through oxygen depletion. *Appl Microbiol Biotechnol 48*, pp. 11-17.

Jayaraman, A., Earthman, J. & Wood, T., 1997b. Corrosion inhibition by aerobic biofilms on SAE 1018 steel. *Appl Microbiol Biotechnol 47*, pp. 62-68.

Jayaraman, A. et al., 1999a. Inhibiting sulfate-reducing bacteria in biofilms on steel with antimicrobial peptides generated in situ. *Appl Microbiol Biotechnol 52*, pp. 267-275.

Jayaraman, A., Mansfeld, F. & Wood, T., 1999b. Inhibiting sulfate- reducing bacteria in biofilms by expressing the antimicrobial peptides indolicidin and bactenecin. *J Ind Microbiol Biotechnol 22*, pp. 167-175.

Julin, L., Sunila, P. & Enqvist, J., 1983. New precision method for automatic quality control of raw materials in the soap industry. *Chromatographia*, 17(10), pp. 549-552.

Juzeliunas, E. et al., 2007. Influence of wild strain Bacillus mycoides on metals: From corrosion acceleration to environmentally friendly protection. *Appl Microbiol Biotechnol 76*, pp. 1245-1253.

Karkhanis, Y., Zeltner, J., Jackson, J. & Carlo, D., 1978. A new and improved microassay to determine 2-keto-3-deoxyoctonate in lipopolysaccharide of gram-negative bacteria. *Anal Biochem 85(2)*, pp. 595-601.

Kelvin, W. T. L., 1898. Contact electricity of metals. *Phil Mag 46*, pp. 82-120.

Khan, A. R., Forgo, P., Stine, K. J. & D'Souza, V. T., 1998. Methods for selective modifications of cyclodextrins. *Chem Rev 98*, pp. 1977-1996.

Khoury, A. E., Lam, K., Ellis, B. D. & Costerton, J. W., 1992. Prevention and control of bacterial infections associated with medical devices. *ASAIO J 38*, pp. M174-M178.

Khramov, A., Voevodin, N., Balbyshev, V. & Donley, M., 2004. Hybrid organo-ceramic corrosion protection coatings with encapsulated organic corrosion inhibitors. *Thin Solid Films 447-448*, pp. 549-557.

Khramov, A., Voevodin, N., Balbyshev, V. & Mantz, R., 2005. Sol–gel-derived corrosion-protective coatings with controllable release of incorporated organic corrosion inhibitors. *Thin Solid Films*, pp. 191-196.

King, R. A., Miller, J. D. A. & Wakerley, D. S., 1973. Corrosion of mild steel in cultures of sulphate reducing bacteria: effect of changing the soluble iron concentration during growth. *Br Corros J 8*, pp. 89-93.

Kinzler, K., Gehrke, T., Telegdi, J. & W, S., 2003. Bioleaching—a result of interfacial processes caused by extracellular polymeric substances (EPS). *Hydrometallurgy 71(1-2)*, pp. 83-88.

Klause, M., Gjemanse, M., Kreft, J. U. & Tolker-Nielsen, T., 2006. Dynamics of development and dispersal in sessile microbial communities: examples from Pseudomonas aeruginosa and Pseudomonas putida model biofilms. *FEMS Microbiol Lett 261(1)*, pp. 1-11.

Kolodny, L. A. et al., 2001. Spatially correlated fluorescence/AFM of individual nanosized particles and biomolecules. *Anal Chem 73*, pp. 1959-1966.

Kratochvílová, I. et al., 2009. Surface potential of functionalised nanodiamond layers. In: *MRS Proceedings 1203.* Cambridge: Cambridge University Press, pp. 1203-J17.

Kreikenbohm, R., Eisenbeis, M., Gümpel, P. & Linhardt, P., 2003. Advanced studies on the influence of manganese on the potential increase of stainless steels. *Mat Corr*, Issue 54, pp. 510-514.

Kuklinski, A. & Sand, W., 2014. Microbiologically influenced corrosion. In: G. Kreysa, K. Ota & R. F. Savinell, eds. *Encyclopedia of Applied Electrochemistry.* New York: Springer.

Kuklinski, A. & Sand, W., 2014. Microbiologically influenced corrosion inhibition. In: G. Kreysa, K. Ota & R. F. Savinell, eds. *Encyclopedia of Applied Electrochemistry.* New York: Springer.

Kumar, A. S., Mody, K. & Jha, B., 2007. Bacterial exopolysaccharides – a perception. *J Basic Microbiol 47*, pp. 103-117.

Laishley, E. J. & Bryant, R. D., 2003. Electron flow in ferrous biocorrosion. In: *Biochemistry and physiology of anaerobic bacteria.* New York: Springer, pp. 252-260.

Laopaiboon, L., Phukoetphim, N. & Laopaiboon, P., 2006. Effect of glutaraldehyde biocide on laboratory-scale rotating contactors and biocide efficacy. *Electron J Biotechnol 9(4)*.

Lappin-Scott, H. M. & Costerton, J. W. eds., 1995. *Microbial biofilms.* Cambridge: Cambridge University Press.

Laspidou, C. S. & Rittman, B. E., 2002. A unified theory for extracellular polymeric substances, soluble microbial products, and active and inert biomass. *Wat Res 36*, pp. 2711-2720.

Lear, G., Dong, Y. & Lewis, G., 2010. Comparison of methods for the extraction of DNA from stream epilithic biofilms. *Anton Leeuw Int J G 98(4)*, pp. 567-571.

Lee, W., Lewandowski, Z., Nielsen, P. H. & Hamilton, W. A., 1995. Role of sulfate-reducing bacteria in corrosion of mild-steel – a review. *Biofouling 8*, pp. 165-194.

Leriche, V. & Carpentier, B., 2000. Limitation of adhesion and growth of Listeria monocytogenes on stainless steel surfaces by Staphylococcus sciuri biofilms. *J Appl Microbiol 88*, pp. 594-605.

Lieberman, K. N., Ben-Ami, N. & Lewis, A., 1996. A fully integrated near-field, far-field optical, and normal-force scanned probe microscope. *Rev Sci Instrum 67*, pp. 3567-3572.

Linhardt, P., 2006. MIC of stainless steel in freshwater and the cathodic behaviour of biomineralized Mn-oxides. *Electrochim Acta*, Issue 51, pp. 6081-6084.

Little, B. J., Lee, J. S. & Ray, R. I., 2008. The influence of marine biofilms on corrosion: A concise review. *Electrochim Acta 54*, pp. 2-7.

Little, B. J. & Ray, R. I., 2002. A perspective on corrosion inhibition by biofilms. *Corrosion 58*, pp. 424-428.

Little, B. J., Ray, R. I. & Pope, K., 2000. Relationship between corrosion and the biological sulfur cycle: A review. *Corrosion 56(4)*, pp. 433-443.

Little, B. J., Wagner, P. & Mansfeld, F., 1992. An overview of microbiologically influenced corrosion. *Electrochim Acta*, Issue 37(12), pp. 2185-2194.

Liu, Y. et al., 2015. β-cyclodextrin modified natural chitosan as a green inhibitor for carbon steel in acid solutions. *Ind Eng Chem Res 54*, pp. 5664-5672.

Loftsson, T. & Duchene, D., 2007. Cyclodextrins and their pharmaceutical applications. *Int J Pharma 329*, pp. 1-11.

Loto, C., 2005. Inhibition of cashew juice on the corrosion of mild steel in sulphuric acid. *Corros Prevent Contr*, pp. 13-21.

Loto, C., Loto, R. & Popoola, A., 2011. Corrosion and plants extracts inhibition of mild steel in HCl. *Int J Phys Sci 6(15)*, pp. 3616-3623.

Lovley, D. R. & Phillips, E. J. P., 1987. Competitive mechanisms for inhibition of sulfate reduction and methane production in the zone of ferric iron reduction in sediments. *Appl Environ Microbiol 53*, pp. 2636-2641.

Magonov, S. N. & Elings, V. W. M.-H., 1997. Phase imaging and stiffness in tapping-mode atomic force microscopy. *Surf Sci 375(2-3)*, pp. L385-L391.

Mangold, S. et al., 2008a. Novel combination of atomic force microscopy and epifluorescence microscopy for visualization of leaching bacteria on Pyrite. *Appl Env Microbiol 74(2)*, pp. 410-415.

Mangold, S. et al., 2008b. Visualization of Acidithiobacillus ferrooxidans biofilms on pyrite by atomic force and epifluorescence microscopy under various experimental conditions. *Hydrometallurgy 94(1-4)*, pp. 127-132.

Mansfeld, F., 2007. The interaction of bacteria and metal surfaces. *Electrochim Acta 52(27)*, pp. 7670-7680.

Mantel, M. & Wightman, J. P., 1994. Influence of the surface chemistry on the wettability of stainless steel. *Surf Int Anal 21(9)*, pp. 595-605.

Marshall, K. C., 1980. Microorganisms and interfaces. *Bio Sci 30(4)*, pp. 246-249.

Marsili, E. et al., 2008. Shewanella secretes flavins that mediate extracellular electron transfer. *PNAS 105(10)*, pp. 3968-3973.

Marti, O., Drake, B., Gould, S. & Hansma, P. K., 1988. Atomic resolution atomic force microscopy of graphite and the ‘‘native oxide’’ on silicon. *J Vac Sci Technol A 6*, pp. 287-290.

Marti, O. et al., 1988. Atomic force microscopy of an organic monolayer. *Science 239(4835)*, pp. 50-52.

Mate, C. M., Lorenz, M. R. & Novotny, V. J., 1989. Atomic force microscopy of polymeric liquid films. *J Chem Phys 90*, pp. 7550-7555.

McGucken, P. V. & Woodside, W., 1973. Studies on the mode of action of glutaraldehyde on Escherichia coli. *J Appl Microbiol 36(3)*, pp. 419-426.

McSwain, B. S., Irvine, R. L., Hausner, M. & Wilderer, P. A., 2005. Composition and distribution of extracellular polymeric substances in aerobic flocs and granular sludge. *Appl Env Microbiol 71(2)*, pp. 1051-1057.

Meyer, G. & Amer, N. M., 1988. Novel optical approach to atomic force microscopy. *Appl Phys Lett 53*, pp. 1045-1047.

Meyer, G. & Amer, N. M., 1990. Optical-beam-deflection atomic force microscopy: The NaCl (001) surface. *Appl Phys Lett 56*, pp. 2100-2101.

Meylheuc, T. et al., 2006. Adsorption on stainless steel surfaces of biosurfactants produced by gram-negative and gram-positive bacteria: Consequence on the bioadhesive behavior of Listeria monocytogenes. *Coll Surf B: Biointerfaces 52*, pp. 128-137.

Michalowski, W., 2012. *Composition, dynamics and function of extracellular polymeric substances in drinking-water biofilms.* Dissertation. Essen: Universität Duisburg-Essen.

Molnar, M. et al., 2002. Effects of RAMEB on bioremediation of different soils contaminated with hydrocarbons. *J Inclusion Phenom 44(1-4)*, pp. 447-452.

Molnar, M. et al., 2005. Enhanced biodegradation of transformer oil in soils with cyclodextrin – from the laboratory to the field. *Biodegradat 16(2)*, pp. 159-168.

Mori, K., Tsurumaru, H. & Harayama, S., 2010. Iron corrosion activity of anaerobic hydrogen-consuming microorganisms isolated from oil facilities. *J Biosci Bioeng 110(4)*, pp. 426-430.

Müller, B., 2002. Corrosion inhibition of aluminium and zinc pigments by saccharides. *Corr Sci 44(7)*, pp. 1583-1591.

Nagiub, A. & Mansfeld, F., 2001. Microbiologically influenced corrosion inhibition (MICI) due to bacterial contamination. *Mat Corr 52(11)*, pp. 817-826.

Nelson, Y. M. et al., 1995. Lead distribution in a simulated aquatic environment: Effects of bacterial biofilms and iron oxide. *Wat Res 29(8)*, pp. 1934-1944.

Neu, T., 1992. Microbial "footprints" and the general ability of microorganisms to label interfaces. *Can J Microbiol 38(10)*, pp. 1005-1008.

Neu, T., 1996. Significance of bacterial surface-active compounds in interaction of bacteria with interfaces. *Microbiol Rev*, Issue 60(1), pp. 151-166.

Ng, F. & Dawes, E., 1973. Chemostat studies on the regulation of glucose metabolism in Pseudomonas aeruginosa by citrate. *Biochem J 132*, pp. 129-140.

Noel, N., Florian, B. & Sand, W., 2010. AFM & EFM study on attachment of acidophilic leaching organisms. *Hydrometallurgy 104(3-4)*, pp. 370-375.

Nonnenmacher, M., O'Boyle, M. P. & Wickramasinghe, H. K., 1991a. Kelvin probe force microscopy. *Appl Phys Lett 58*, p. 2921.

Nonnenmacher, M., O'Boyle, M. & Wickramasinghe, H., 1991b. Surface investigations with a Kelvin Probe Force microscope. *Appl Phys Lett 58*, pp. 2921-.

Nunez, M. E., Martion, M. O., Chan, P. H. & Spain, E. M., 2005. Predation, death, and survival in a biofilm: Bdellovibrio investigated by atomic force microscopy. *Coll Surf B 43(3-4)*, pp. 263-271.

Oguzie, E., 2007. Corrosion inhibition of aluminium in acidic and alkaline media by Sansevieria trifasciata extract. *Corr Sci 49(3)*, pp. 1527-1539.

Oguzie, E., 2008. Evaluation of the inhibitive effect of some plant extracts on the acid corrosion of mild steel. *Corr Sci 50(11)*, pp. 2993-2998.

Oguzie, E. et al., 2010. Adsorption and corrosion-inhibiting effect of Dacryodis edulis extract on low-carbon-steel corrosion in acidic media. *J Coll Int Sci 349(1)*, pp. 283-292.

Oguzie, E., Li, Y. & Wang, F., 2007. Corrosion inhibition and adsorption behavior of methionine on mild steel in sulfuric acid and synergistic effect of iodide ion. *J Coll Int Sci 310(1)*, pp. 90-98.

Omoike, A., J., C., Kwon, K. & Kubicki, J., 2004. Adhesion of bacterial expolymers to α-FeOOH: Inner-sphere complexation of phosphodiester groups. *Langmuir 20*, pp. 11108-11114.

Örnek, C. & Engelberg, D. L., 2015. SKPFM measured Volta potential correlated with strain localisation in microstructure to understand corrosion susceptibility of cold-rolled grade 2205 duplex stainless steel. *Corr Sci 99*, pp. 164-171.

Örnek, D. et al., 2001. Pitting corrosion control using regenerative biofilms on aluminium 2024 in artificial seawater. *Corr Sci 43*, pp. 2121-2133.

Örnek, D., Wood, T., Hsu, C. & Mansfeld, F., 2002. Corrosion control using regenerative biofilms (CCURB) on brass in different media. *Corr Sci 44*, pp. 2291-2302.

O'Toole, G., Kaplan, H. & Kolter, R., 2000. Biofilm formation as microbial development. *Ann Rev Microbiol*, Issue 54, pp. 49-79.

Ozturk, S. & Aslim, B., 2010. Modification of exopolysaccharide composition and production by three cyanobacterial isolates under salt stress. *Environ Sci Pollut Res 17*, pp. 595-602.

Pannekens, M., 2012. *Biofilmbildung Sulfat-reduzierender Bakterien auf Cyclodextrin-beschichteten Stahloberflächen.* Bachelor thesis. Essen: Universität Duisburg-Essen.

Pan, T., 2012. Corrosion behavior of a duplex stainless steel under cyclic loading: a scanning Kelvin probe force microscopy (SKPFM) based microscopic study. *J Appl Electrochem 42(12)*, pp. 1049-1056.

Parkar, S., Flint, S. & Brooks, J., 2003. Evaluation of the effect of cleaning regimes on biofilms of thermophilic bacilli on stainless steel. *J Appl Microbiol 96(1)*, pp. 110-116.

Pedersen, A. & Hermansson, M., 2009. The effects on metal corrosion by Serratia marcescens and a Pseudomonas SP.. *Biofouling 1(4)*, pp. 313-322.

Percival, S. L., Knapp, J. S., Edyvean, R. & Wales, D. S., 1998. Biofilm development on stainless steel in mains water. *Wat Res 32(1)*, pp. 243-253.

Pérez, E. J., Cabrera-Sierra, R., González, I. & Ramírez-Vives, F., 2007. Influence of Desulfovibrio sp. biofilm on SAE 1018 carbon steel corrosion in synthetic marine medium. *Corr Sci 49(9)*, p. 3580–3597.

Peterson, T. & Neilands, J., 1979. Revised structure of a catecholamide spermidine siderophore. *Tetrahedron Lett 50*, pp. 4805-4808.

Poon, L., Wilson, L. D. & Headley, J. V., 2014. Chitosan-glutaraldehyde copolymers and their sorption properties. *Carb Polym 109*, pp. 92-101.

Potekhina, J. et al., 1999. Role of microorganisms in corrosion inhibition of metals in aquatic habitats. *Appl Microbiol Biotechnol 52(5)*, pp. 639-646.

Pratt-Terpstra, I., Weerkamp, A. & Busscher, H., 1989. Microbial factors in a thermodynamic approach of oral streptococcal adhesion to solid substrata. *J Coll Int Sci 129*, pp. 568-574.

Rajendran, S., Thangavelu, C., Angamuthu, A. & Jayakumar, S., 2013. Inhibition of corrosion of aluminium in alkaline medium by glutaric acid in conjunction with zinc sulphate and diethylene triamine penta (Methylene phosphonic acid). *Archives of Applied Science Research 5(1)*, pp. 202-212.

Ribbons, D. W. & Norris, J. R., 1970. *Methods in Microbiology.* London: Academic Press.

Richter, H. et al., 2009. Cyclic voltammetry of biofilms of wild type and mutant Geobacter sulfurreducens on fuel cell anodes indicates possible roles of OmcB, OmcZ, type IV pili, and protons in extracellular electron transfer. *Energy Environ Sci 8*, pp. 506-516.

Rohwerder, M. & Turcu, F., 2007. High-resolution Kelvin probe microscopy in corrosion science: Scanning Kelvin probe force microscopy (SKPFM) versus classical scanning Kelvin probe (SKP). *Electrochim Acta 53(2)*, pp. 290-299.

Rohwerder, T., Gehrke, T., Kinzler, K. & Sand, W., 2003. Bioleaching review part A. *Appl Microbiol Biotechnol 63(3)*, pp. 239-248.

Ron, E. & Rosenberg, E., 2001. Natural roles of biosurfactants. *Env Microbiol 3(4)*, pp. 229-236.

Rouwenhorst, R. J., Jzn, J. F., Scheffers, W. A. & van Dijken, J. P., 1991. Determination of protein concentration by total organic carbon analysis. *J. Biochem. Biophys. Methods 22*, pp. 119-128.

Roux, S. et al., 2010. Influence of a biopolymer admixture on corroson behaviour of steel rebars in concrete. *Mat Corr 61(12)*, pp. 1026-1033.

Rust, M. J., Bates, M. & Zhuang, X., 2006. Sub-diffraction-limit imaging by stochastic optical reconstruction microscopy (STORM). *Nature Methods 3*, pp. 793-796.

Ryder, C., Byrd, M. & Wozniak, D. J., 2007. Role of exopolysaccharides in Pseudomonas aeruginosa biofilm development. *Curr Opin Microbiol 10*, pp. 644-648.

Saenger, W., 1980. Cyclodextrin inclusion complexes in research and industry. *Angew Chemie Int Edit 19*, pp. 344-362.

Sand, W., 1987. Importance of hydrogen sulfide, thiosulfate, and methylmercaptan for growth of Thiobacilli during simulation of concrete corrosion. *Appl Env Microbiol 53(7)*, pp. 1645-1648.

Sand, W., 1997. Microbial mechanisms of deterioration of inorganic substrates - a general mechanistic overview. *Int Biodet Biodegradat 2(4)*, pp. 183-190.

Sand, W. & Bock, E., 1984. Concrete corrosion in the Hamburg sewer system. *Env Technol Lett 5(12)*, pp. 517-528.

Sand, W., Florian, B. & Noel, N., 2009. Mechanisms of bioleaching and the visualization of these by combined AFM & EFM. *Adv Mat Res 71-73*, pp. 297-302.

Sand, W. & Gehrke, T., 2003. Microbially influenced corrosion of steel in aqueous environments. *Rev Environ Sci Biotechnol 2*, pp. 169-176.

Sand, W. & Gehrke, T., 2006. Extracellular polymeric substances mediate bioleaching/biocorrosion via interfacial processes involving iron(III) ions and acidophilic bacteria. *Res Microbiol 157(1)*, pp. 49-56.

Sand, W., Gehrke, T., Hallmann, R. & Schippers, A., 1995. Sulfur chemistry, biofilm, and the (in)direct attack mechanisms - a critical evaluation of bacterial leaching. *Appl. Microbiol. Biotechnol. 43*, pp. 961-966.

San, N. O., Nazir, H. & Dönmez, G., 2012. Evaluation of microbiologically influenced corrosion inhibition on Ni-Co alloy coatings by Aeromonas salmonicida and Clavibacter michiganensis. *Corr Sci 65*, pp. 113-118.

San, N. O., Nazir, H. & Dönmez, G., 2014. Microbiologically influenced corrosion and inhibition of nickel-zinc and nickel-copper coatings by Pseudomonas aeruginosa. *Corr Sci 79*, pp. 177-183.

Sathirachinda, N., Pettersson, R. & Pan, J., 2009. Depletion effects at phase boundaries in 2205 duplex stainless steel characterized with SKPFM and TEM/EDS. *Corr Sci 51*, pp. 1850-1860.

Sauer, K., 2003. The genomics and proteomics of biofilm formation. *Genome Biol*, Issue 4(6), pp. 219.1-219.5.

Schaschl, E., 1980. Elemental sulphur as a corrodent in deaerated, neutral aqueous solutions. *Water Performance 7*, pp. 9-12.

Scheerder, J. et al., 2012. Exopolysaccharides (EPS) as anti-corrosive additives for coatings. *Prog Org Coat 25*, pp. 224-230.

Schooling, S. R. & Beveridge, T. J., 2006. Membrane vesicles: an overlooked component of the matrices of biofilms. *J Bacteriol 188*, pp. 5945-5947.

Scotto, V. & Lai, M. E., 1998. The ennoblement of stainless steel in seawater: a likely explanation coming from the field. *Corr Sci 40*, pp. 1007-1018.

Singh, K., Ingole, P. G., Bajaj, H. C. & Gupta, H., 2012. Preparation, characterization and application of β-cyclodextrin-glutaraldehyde crosslinked membrane for the enantiomeric separation of amino acids. *Desalination 298*, pp. 13-21.

Spruit, C. J. P. & Wanklyn, J. N., 1951. Iron/sulphide ratios in corrosion by sulphate-reducing bacteria. *Nature 168*, pp. 951-952.

Stadler, R. et al., 2008. First evaluation of the applicability of microbial extracellular polymeric substances for corrosion protection of metal substrates. *Electrochim Acta 54(1)*, pp. 91-99.

Stadler, R. et al., 2010. Influence of bacterial exopolymers in cell adhesion of Desulfovibrio vulgaris on high alloyed steel: Corrosion inhibition by extracellular polymeric substances. *Mat Corr 61(12)*, pp. 1008-1016.

Steele, A., Goddard, D. T. & Beech, I. B., 1994. An atomic force microscopy study of the biodeterioration of stainless steel in the presence of bacterial biofilms. *Int Biodet Biodegradat 34(1)*, pp. 35-46.

Stelzer, E. H. K., 2002. Light microscopy: Beyond the diffraction limit?. *Nature 417*, pp. 806-807.

Stoodley, P., Boyle, J. D., DeBeer, D. & Lappin-Scott, H. M., 1999. Evolving perspectives of biofilm structure. *Biofouling 14(1)*, pp. 75-90.

Stoodley, P., Sauer, K., Davies, D. G. & Costerton, J. W., 2002. Biofilms as complex differentiated communities. *Ann Rev Microbiol*, Issue 56, pp. 187-209.

Surman, S. B. et al., 1996. Comparison of microscope techniques for the examination of biofilms. *J Microbiol Met 25(1)*, pp. 57-70.

Sutherland, I. W., 2001. The biofilm matrix – an immobilized but dynamic microbial environment. *TRENDS Microbiol 9(5)*, pp. 222-227.

Szejtli, J., 1988. *Cyclodextrin Technology.* Dordrecht, The Netherlands: Kluwer Academic Publishers.

Tadros, A. B., 2005. Application of natural materials in marine paint formulations. *Pig Res Technol 34(6)*, pp. 340-346.

Telegdi, J. et al., 1998. Microbially influenced corrosion visualized by atomic force microscopy. *Appl Phys A 66(1)*, pp. S639-S642.

Templeton, A. S. et al., 2001. Pb(II) distributions at biofilm-metal oxide interfaces. *PNAS 98(21)*, pp. 11897-11902.

The Procter & Gamble Company, 2002. *Compounds, compositions, and methods for controlling biofilms.* United States, Patent No. US 7018642 B2.

Thierry, D. & Sand, W., 2011. Microbiologically influenced corrosion. In: *Corrosion Mechanisms in Theory and Practice.* 3 ed. Boca Raton: CRC Press, pp. 737-776.

Thyssen, C., in prep. *Title not yet determined.* Dissertation. Essen: Universität Duisburg-Essen.

Traore, A. S., Hatchikian, C. E., Belaich, J.-P.-. & Le Gall, J., 1981. Microcalorimetric Studies of the Growth of Sulfate-Reducing Bacteria: Energetics of Desulfovibrio vulgaris Growth. *J Bacteriol 145(1)*, pp. 191-199.

Tsuneda, S. et al., 2003. Extracellular polymeric substances responsible for bacterial adhesion onto solid surface. *FEMS Microbiol Lett 223*, pp. 287-292.

Umoren, S. A. & Eduok, U. M., 2016. Application of carbohydrate polymers as corrosion inhibitors for metal substrates in different media: A review. *Carbohyd Polym 140*, pp. 314-341.

van Kranenburg, R., Marugg, J., van Swam, I. W. N. & de Vos, W., 1997. Molecular characterization of the plasmid encoded eps gene cluster essential for exopolysaccharide synthesis in Lactococcus lactis. *Mol Microbiol 24*, pp. 387-397.

van Leeuwen, S. S. et al., 2008. Structural analysis of the a-D-glucan (EPS180) produced by the Lactobacillus reuteri strain 180 glucansucrase GTF180 enzyme. *Carb Res 343*, pp. 1237-1250.

Velraeds, M., van der Mei, H., Reid, G. & Busscher, H., 1996. Inhibition of initial adhesion of uropathogenic Enterococcus faecalis by biosurfactants from Lactobacillus isolates. *Appl Environ Microbiol 62(6)*, pp. 1958-1963.

Venzlaff, H. et al., 2013. Accelerated cathodic reaction in microbial corrosion of iron due to direct electron uptake by sulfate-reducing bacteria. *Corr Sci 66*, pp. 88-96.

Vera, M. et al., 2013. Shotgun proteomics study of early biofilm formation process of Acidithiobacillus ferrooxidans ATCC 23270 on pyrite. *Proteomics 13(7)*, pp. 1133-1144.

Verstichel, S., De Wilde, B., Fenyvesi, E. & Szejtli, J., 2004. Investigation of the aerobic biodegradability of several types of cyclodextrins in a laboratory-controlled composting test. *J Polym Env 12(2)*, pp. 47-55.

Videla, H. & Herrera, L., 2009. Understanding microbial inhibition of corrosion. A comprehensive overview. *Int Biodeter Biodegr 36*, pp. 896-900.

Vilain, S., Pretorius, J. M. & Theron, J. B. V. S., 2009. DNA as an adhesin: Bacillus cereus requires extracellular DNA to form biofilms. *Appl Env Microbiol 75(9)*, pp. 2861-2868.

Villiers, A., 1891. Sur la fermentation de la fécule par l'action du ferment butyrique. *Compt Rend Acad Sci 112*, p. 536.

Volkland, H. et al., 2001a. Repair of damaged vivianite coatings on mild steel using bacteria. *Corr Sci 43*, pp. 2135-2146.

Volkland, H. et al., 2000a. Corrosion inhibition of mild steel by bacteria. *Biofouling 15*, pp. 287-297.

Volkland, H. et al., 2000b. Bacterial phosphating of mild (unalloyed) steel. *Appl Env Microbiol 66(10)*, pp. 4389-4395.

Volkland, H., Harms, H., Wanner, O. & Zehnder, A., 2001b. Corrosion protection by anaerobiosis. *Wat Sci Technol 44(8)*, pp. 103-106.

von Canstein, H., Ogawa, J., Shimizu, S. & Lloyd, J. R., 2008. Secretion of flavins by Shewanella species and their role in extracellular electron transfer. *Appl Environ Microbiol 74(3)*, pp. 615-623.

von Rège, H., 1999. *Bedeutung von Mikroorganismen des Schwefelkreislaufes für die Korrosion von Metallen.* Herzogenrath: Shaker.

von Wolzogen-Kühr, C. H. A., 1961. Unity of anaerobic and aerobic iron corrosion process in the soil. *Corrosion 17*, pp. 119-125.

von Wolzogen-Kühr, C. H. A. & van der Vlugt, L. S., 1934. De graphiteering can gietijzer als electrobiochemisch process in anaerobe gronden. *Water 18*, pp. 147-165.

Watnik, P. I. & Kolter, R., 1999. Steps in the development of a Vibrio cholerae El Tor biofilm. *Mol Microbiol 34*, pp. 586-595.

Weisenhorn, A. L. et al., 1990a. Immobilized proteins in buffer imaged at molecular resolution by atomic force microscopy. *Biophys J 58(5)*, pp. 1251-1258.

Weisenhorn, A. L. et al., 1990b. Imaging single-stranded DNA, antigen-antibody reaction and polymerized Langmuir-Blodgett films with an atomic force microscope. *Scanning Microscopy 4(3)*, pp. 511-516.

Weisz, P. B., Shing, Y. W. & Folkman, J., 1993. *Cyclodextrin polymers and cyclodextrins immobilized on a solid surface.* United States, Patent No. US5183809 A.

Wei, X. et al., 2011. Influence of extracellular polymeric substances (EPS) on Cd absorption by bacteria. *Env Poll 159*, pp. 1369-1374.

Wen, J., Zhao, K., Gu, T. & Raad, I. I., 2009. A green biocide enhancer for the treatment of sulfate-reducing bacteria (SRB) biofilms on carbon steel surfaces using glutaraldehyde. *Int Biodet Biodegradat 63(8)*, pp. 1102-1106.

Werner, S. E. et al., 1998. Pitting of Type 304 stainless steee in the presence of a biofilm containing sulphate reducing bacteria. *Corr Sci 40(2-3)*, pp. 465-480.

Whittaker, C., Ridgway, H. & Olson, B. H., 1984. Evaluation of cleaning strategies for removal of biofilms from reverse-osmosis membranes. *Appl Environ Microbiol 48(2)*, pp. 395-403.

Wikieł, A. J., 2013. *Role of extracellular polymeric substances on biocorrosion initiation or inhibition.* Dissertation. Essen: Universität Duisburg-Essen.

Wikieł, A. J., Datsenko, I., Vera, M. & Sand, W., 2014. Impact of Desulfovibrio alaskensis biofilms on corrosion behaviour of carbon steel in marine environment. *Bioelectrochemistry 97*, pp. 52-60.

Williams, D. F., Askill, I. N. & Smith, R., 1985. Protein adsorption and desorption phenomena on clean metal surfaces. *J Biomed Mat Res 19(3)*, pp. 313-320.

Williams, R. L. & Williams, D. F., 1988. Albumin adsorption on metal surfaces. *Biomat 9(3)*, pp. 206-212.

Wimpenny, J., 2000. An overview of biofilms as functional communities. In: *SGM symposium 59: Community structure and co-operation in biofilms.* Cambridge: Cambridge University Press, pp. 1-24.

Wingender, J., Neu, T. & Flemming, H.-C., 1999. What are bacterial extracellular polymeric substances?. In: J. Wingender, T. Neu & H. Flemming, eds. *Microbial extracellular polymeric substances.* Heidelberg, Berlin: Springer, pp. 1-19.

Wingender, J. et al., 2001. Isolation and biochemical characterization of extracellular polymeric substances from Pseudomonas aeruginosa. *Meth Enzymol 336*, pp. 302-314.

Wright, C. J., Shah, M. K., Powell, L. C. & Armstrong, I., 2010. Application of AFM from microbial cell to biofilm. *Scanning 32(3)*, pp. 134-149.

Xu, L.-C., Chan, K.-Y. & Fang, H. H. P., 2002. Application of atomic force microscopy in the study of microbiologically influenced corrosion. *Mater Character 48(2-3)*, pp. 195-203.

Yee, S., Oriani, R. A. & Stratmann, M., 1991. Application of a Kelvin microprobe to the corrosion of metals in humid atmospheres. *J Electrochem Soc 138(1)*, pp. 55-61.

Yue, Z.-B.et al., 2015. Component analysis and heavy metal adsorption ability of extracellular polymeric substances (EPS) from sulfate reducing bacteria. *Biores Technol 194*, pp. 399-402.

Zarasvand, K. & Rai, V., 2014. Microorganisms: Induction and inhibition of corrosion in metals. *Int Biodet Biodegradat*, pp. 66-74.

Zeraik, A. E. & Nitschke, M., 2010. Biosurfactants as agents to reduce adhesion of pathogenic bacteria to polystyrene surfaces: Effect of temperature and hydrophobicity. *Curr Microbiol 61*, pp. 554-559.

Zerweck, U. et al., 2005. Accuracy and resolution limits of Kelvin probe force microscopy. *Phys Rev B 71*, pp. 12524-1-12524-9.

Zevenhuizen, L., 1986. Selective synthesis of polysaccharides by Rhizobium trifolii, strain TA-1. *FEMS Microbiol Lett 35(1)*, pp. 43-47.

Zhang, W., Hughes, J. & Chen, Y., 2012. Impacts of hematite nanoparticle exposure on biomechanical, adhesive, and surface electrical properties of Escherichia coli cells. *Appl Env Microbiol 78(11)*, pp. 3905-3915.

Zhang, X. & Liu, Z., 2008. Superlenses to overcome the diffraction limit. *Nature Materials 7*, pp. 435-441.

Zheludkevich, M. L., Salvando, I. M. & Ferreira, M. G. S., 2005. Sol–gel coatings for corrosion protection of metals. *J Mater Chem 15*, pp. 5099-5111.

Zheludkevich, M. L. et al., 2007. Anticorrosion coatings with self-healing effect based on nanocontainers impregnated with corrosion inhibitor. *Chem Mater 19(3)*, pp. 402-411.

Zheng, S. & Li, J., 2010. Inorganic–organic sol gel hybrid coatings for corrosion protection of metals. *J Sol-Gel Sci Technol 54(2)*, pp. 174-187.

Zinkevich, V. et al., 1996. Characterisation of exopolymers produced by different isolates of marine sulphate-reducing bacteria. *Int Biodet Biodegradat 37(3)*, pp. 163-172.

Zisman, W. A., 1932. A new method of measuring contact potential differences in metals. *Rev Sci Instr 3*, p. 369.

Zuo, R., 2007. Biofilms: strategies for metal corrosion inhibition employing microorganisms. *Appl Microbiol Biotechnol*, Issue 76, pp. 1245-1253.

Zuo, R. et al., 2004. Inhibiting mild steel corrosion from sulfate-reducing bacteria using antimicrobial-producing biofilms in Three-Mile-Island process water. *Appl Microbiol Biotechnol 64*, pp. 275-283.

Zuo, R. & Wood, T., 2004. Inhibiting mild steel corrosion from sulfate-reducing and iron-oxidizing bacteria using gramicidin-S-producing biofilms. *Appl Microbiol Biotechnol 65(6)*, pp. 747-753.

7 APPENDIX

7.1 ImageJ macros

Code 1 Automated calculation of particle (cell) number and relative surface coverage

```
macro "ak-CellCount" {
 requires("1.43s");

 dirseparator = File.separator;
 outputfolder = "_selections";

 if ( getArgument() != "" ) {
  sourcefile  = getArgument();
  outputdir   = File.getParent( sourcefile ) + dirseparator +
                outputfolder;
  outputfile  = outputdir + dirseparator + substring( File.getName(
                sourcefile ), 0, ( lengthOf( File.getName( sourcefile
                ) ) - 4 ) ) + outputfolder;
  open( sourcefile );
  saveResults   = 0;
 }

 else {
  run( "Clear Results" );
  run( "Options...", "iterations=20 count=1 edm=8-bit" );
  sourcefile  = File.name;
  outputdir   = File.directory + dirseparator + outputfolder;
  outputfile  = outputdir + dirseparator + File.nameWithoutExtension +
                outputfolder;
  saveResults = 1;
 }

 if ( File.exists( outputdir ) == 0 ) {
  File.makeDirectory( outputdir );
 }

 //process image and calculate area covered by cells
 run( "8-bit" );
 run( "Maximum...", "radius=1" );
 run( "Find Maxima...", "noise=15 output=[Point Selection]" );
 saveAs( "Tiff", outputfile+".tif" );
 maskname     = substring( File.getName( sourcefile ), 0,
                ( lengthOf( File.getName( sourcefile ) ) -4 ) );
 run( "Create Mask" );
 rename( maskname );
 run( "Analyze Particles...", "size=0-Infinity circularity=0.00-1.00
      show=Nothing summarize" );
 if ( saveResults == 1 ) {
  selectWindow( "Summary" );
  saveAs( "text", outputfile+".xls" );
 }
 close();
}
```

Code 2 Automated calculation of the relative fluorescing area

```
macro "ak-ParticleArea" {
 requires("1.43s");

 dirseparator   = File.separator;
 outputfolder   = "_particle area";

 if ( getArgument() != "" ) {
  sourcefile  = getArgument();
  outputdir   = File.getParent( sourcefile ) + dirseparator +
                outputfolder;
  outputfile  = outputdir + dirseparator +
                substring( File.getName( sourcefile ), 0,
                ( lengthOf( File.getName( sourcefile ) ) - 4 ) ) +
                outputfolder;
  open( sourcefile );
  saveResults = 0;
 }

 else {
  run( "Clear Results" );
  run( "Options...", "iterations=20 count=1 edm=8-bit");
  sourcefile  = File.name;
  outputdir   = File.directory + dirseparator + outputfolder;
  outputfile  = outputdir + dirseparator + File.nameWithoutExtension +
                outputfolder;
  saveResults = 1;
 }

 if ( File.exists( outputdir ) == 0 ) {
  File.makeDirectory( outputdir );
 }

 //process image and calculate area covered by cells
 run( "8-bit" );
 setThreshold( 50, 255 );
 run( "Convert to Mask" );
 saveAs( "jpeg", outputfile+".jpg" );
 run( "Measure" );
 if ( saveResults == 1 ) {
  saveAs( "Measurements", outputfile+".xls" );
 }
 close();
}
```

Code 3 Automated batch processing for both cell count and relative fluorescing area

```
1    //this macro is designed to allow batch processing of images using
2    //separate macros. Used macros can be set within the array
3    //"macros". at this moment, only images in jpeg- or Zeiss
4    //Axiovision-format (.jpg or .jpeg and .zvi, respectively; case
5    //insensitive) are batch-processed. remark for .zvi: only Ch0 is
6    //processed; multichannel-images can not be opened at the moment.
7    //this macro is based on a macro written by Felipe Leon.
8    //andrzej kuklinski; no copyright. feel free to use and to modify.
9
10   //global variables for sourcefiles and -folders as well as
11   //respective counters
12
13   var sourcefile = newArray(1000);
14   var sourcefolder = newArray(250);
15   var sourcefileindex = 0;
16   var sourcefolderindex = 0;
17
18   macro "ak-BatchAnalysis" {
19     requires("1.43s");
20
21     macrodir  = getDirectory("macros");
22     macroname = newArray("ak-ParticleArea.txt", "ak-CellCount.txt",
23                 "ak-VoronoiArea.txt");
24     macrosavailable = newArray("Calculate Particle Area", "Count
25                       Cells", "Voronoi Area", "Full Analysis");
26
27     workingdir = newArray("_particle area", "_selections",
28                  "_voronoi");
29     acceptedfileformats = newArray(".zvi", ".jpg", ".jpeg");
30
31     function setOptions() {
32       run("Clear Results");
33       run("Options...", "iterations=20 count=1 edm=8-bit");
34       run("Set Measurements...", "area area_fraction display
35       redirect=None decimal=3");
36       if (isOpen("Summary")) {
37         selectWindow("Summary");
38         run("Close");
39       }
40       if (isOpen("Results")) {
41         selectWindow("Results");
42         run("Close");
43       }
44     }
45
46     function checkMacro(macrofile) {
47       if (!File.exists(macrofile)) {
48         exit("File not found: "+macrofile);
49       }
50     }
51
52     function showWarningDialog() {
53       txt1 = "This macro is designed to batch process complete images
54       folders.";
55       txt2 = "Only jpeg-images will be processed (.jpg or .jpeg); A
56       other file types will be omitted.";
57       txt3 = "Please close all images before running this macro!";
58       Dialog.create("Warning!");
59
```

Code 3 Continued

```
60      function chooseMacro(choices) {
61        Dialog.create("Choose Processing Mode");
62        Dialog.addChoice("Select processing mode for images:",
63        choices,choices[0]);
64        Dialog.show();
65        chosen = Dialog.getChoice();
66        return chosen;
67      }
68
69      function chooseDirectory() {
70        dir = getDirectory("Choose a Directory ");
71        listFiles(dir);
72        if (sourcefileindex==0) {
73          exit("No images found!");
74        }
75      }
76
77      function listFiles(dir) {
78        list = getFileList(dir);
79        for (i=0; i<list.length; i++) {
80          if (sourcefolderindex==0) {
81            sourcefolder[sourcefolderindex] = substring(dir, 0,
82            (lengthOf(dir)-1));
83            sourcefolderindex++;
84          }
85          if (endsWith(list[i], "/") && list[i]!="_particle area/" &&
86          list[i]!="_selections/" && list[i]!="_voronoi/") {
87            sourcefolder[sourcefolderindex] = dir+substring(list[i],
88            0, (lengthOf(list[i])-1));
89            sourcefolderindex++;
90            listFiles(""+dir+list[i]);
91          }
92          else {
93            for (j=0; j<acceptedfileformats.length; j++) {
94              if (endsWith(toLowerCase(list[i]),
95          acceptedfileformats[j])) {
96            sourcefile[sourcefileindex] = dir+list[i];
97            sourcefileindex++;
98          }
99        }
100         }
101       }
102     }
103     function saveResults(resultdir, resultname) {
104       if (!File.exists(resultdir)) {
105         File.makeDirectory(resultdir);
106       }
107       if (isOpen("Summary")) {
108         selectWindow("Summary");
109         resultfile = resultdir+File.separator+resultname+".txt";
110         saveAs("Text", resultfile);
111         selectWindow("Summary");
112
113         run("Close");
114         run("Clear Results");
115         if (isOpen("Results")) {
116           selectWindow("Results");
117           run("Close");
118         }
119       }
```

Code 3 Continued

```
120       else if (isOpen("Results")) {
121         selectWindow("Results");
122         resultfile = resultdir+File.separator+resultname+".txt";
123         saveAs("Measurements", resultfile);
124         run("Clear Results");
125         selectWindow("Results");
126         run("Close");
127       }
128     }
129     for (i=0; i<macroname.length; i++) {
130       macrofile = macrodir+macroname[i];
131       checkMacro(macrofile);
132     }
133     setOptions();
134     showWarningDialog();
135     chosen=chooseMacro(macrosavailable);
136     chooseDirectory();
137     setBatchMode(true);
138     startingtime = getTime();
139     for (i=0; i<macrosavailable.length; i++) {
140       if (chosen==macrosavailable[i] && i<3) {
141         macroactive = macrodir+macroname[i];
142         for (j=0; j<sourcefolderindex; j++) {
143         resultdir = sourcefolder[j]+File.separator+workingdir[i];
144           resultname = workingdir[i];
145           for (k=0; k<sourcefileindex; k++) {
146             if (isOpen("Exception")) {
147               exit("JAVA error detected.");
148             }
149             else if (sourcefolder[j]==File.getParent(sourcefile[k]
150             {
151               runMacro(macroactive, sourcefile[k]);
152             }
153           }
154           saveResults(resultdir, resultname);
155         }
156         }
157       else if (chosen==macrosavailable[i] && i==3) {
158         for (m=0; m<3; m++) {
159           macroactive = macrodir+macroname[m];
160           for (j=0; j<=sourcefolderindex; j++) {
161             resultdir = sourcefolder[j] + File.separator +
162             workingdir[m];
163             resultname = workingdir[m];
164             for (k=0; k<sourcefileindex; k++) {
165               if (isOpen("Exception")) {
166                 exit("JAVA error detected.");
167               }
168               else if (sourcefolder[j]==
169               File.getParent(sourcefile[k])) {
170                 runMacro(macroactive, sourcefile[k]);
171               }
172             }
173             saveResults(resultdir, resultname);
174           }
175         }
176       }
177     }
178
```

Code 3 Continued

```
179    endtime = getTime;
180    workingtime = endtime - startingtime;
181    Dialog.create("Success!");
182    Dialog.addMessage(sourcefileindex+ " images from
183    "+sourcefolderindex+" folders have been processed.");
184    Dialog.addMessage("Working time: "+d2s((workingtime/60000),2)+"
185    minutes.");
186    beep();
187    Dialog.show();
188
189  }
```

7.2 Publications

Referred Publications

Kuklinski, A., Stadler, R., Grooters, M., Fürbeth, W., & Sand, W. (2011). Microbial EPS and analogues for protection against microbiologically influenced corrosion. *Oral presentation and paper, proceedings of the 18th International Corrosion Conference, Perth, Australia (CD-ROM)*.

Kuklinski, A., Stadler, R., Grooters, M., Fürbeth, W., & Sand, W. (2011). Studies on corrosion protection for metals by extracellular polymeric substances. *Oral presentation and paper, proceedings of the Eurocorr 2011, Stockholm, Sweden (CD-ROM)*.

Stadler, R., Kuklinski, A., Fürbeth, W., & Sand, W. (2011). Korrosionsschutz durch Bakterien? *BioSpektrum 17(3)*: pp. 287-290

Stadler, R., Wei, L., Fürbeth, W., Grooters, M., & Kuklinski, A. (2010). Influence of bacterial exopolymers on cell adhesion of *Desulfovibrio vulgaris* on high alloyed steel: Corrosion inhibition by extracellular polymeric substances EPS). *Materials and Corrosion 61(12):* pp. 1008-1016

Book Chapters

Kuklinski, A. & Sand, W. (2014). Microbiologically Influenced Corrosion. In: G. Kreysa, et al., (eds.), *Encyclopedia of Applied Electrochemistry*. New York: Springer Science+Business.

Kuklinski, A. & Sand, W. (2014). Microbiologically Influenced Corrosion Inhibition. In: G. Kreysa, et al., (eds.), *Encyclopedia of Applied Electrochemistry*. New York: Springer Science+Business.

Oral Presentations

Holuscha, D., Thyssen, C., Kuklinski, A., Fürbeth, W., & Sand, W. (2013). Effect of EPS-analogues on the corrosion behaviour of steel. Abstract in: *Proceedings of the Eurocorr 2013, Estoril, Portugal CD-ROM)*

Thyssen, C., Kuklinski, A., Holuscha, D., Fürbeth, W., & Sand, W. (2013). Influence of steel on the EPS composition and complementary corrosion analysis of *Leptothrix discophora.* Abstract in: *Proceedings of the Eurocorr 2013, Estoril, Portugal (CD-ROM)*

Kuklinski, A., Thyssen, C., Pannekens, M., Holuscha, D., Fürbeth, W., & Sand, W. (2012). Corrosion protection for metals by analogues of extracellular polymeric substances. Abstract in: *Proceedings of the Eurocorr 2012, Istanbul, Turkey (CD-ROM)*

Thyssen, C., Kuklinski, A., Holuscha, D., Fürbeth, W., & Sand, W. (2012). Manganese-oxidizing bacteria: attachment pattern, EPS composition and influence on steel corrosion. Abstract in: *Proceedings of the Eurocorr 2012, Istanbul, Turkey (CD-ROM)*

Kuklinski, A. & Sand, W. (2009). Anwendung kombinierter Rasterkraft- und Epifluoreszenzmikroskopie auf lichtundurchlässigen Oberflächen. *Oral presentation, New year's colloquium of the GDCh, Essen*

Kuklinski, A., Grooters, M., Heyer, A., & Sand, W. (2008). Corrosion protection by extracellular polymeric substances. Oral presentation, Biofilms III, Munich, Germany

Kuklinski, A. & Sand, W. (2008). Recent progress in applying combined AFM&EFM on opaque substrata. Oral presentation, COST-Meeting RO/IT.

Posters

Kuklinski, A., Thyssen, C., Holuscha, D., Fürbeth, W., & Sand, W. (2013). Studying Biocorrosion of Steel by AFM: Combining Epifluorescence- with Scanning Kelvin probe force Microscopy and the In Situ Electrochemical Cell. Abstract in: Proceedings of the Eurocorr 2013, Estoril, Portugal

Holuscha, D., Thyssen, C., Kuklinski, A., Sand, W., & Fürbeth, W. (2012). Effect of cyclodextrins on the corrosion behaviour of steel. 63rd Annual Meeting of the International Society of Electrochemistry, Prague, Czech Republic.

Kuklinski, A. & Sand, W. (2010). Combined epifluorescence- and Scanning Kelvin probe force microscopy EFM-SKPFM) for the study of microbial attachment to steel. Biofilms IV, Winchester, United Kingdom

Kuklinski, A. & Sand, W. (2010). Combined epifluorescence- and Scanning Kelvin probe force microscopy for the investigation of microbially influenced corrosion. JPK NanoBioViews, Berlin, Germany

Stadler, R., Fürbeth, W., Grooters, M., Janosch, C., Kuklinski, A., & Sand, W. (2010). Studies on the Application of Microbially Produced Polymeric Substances as Protecting Layers Against Microbially Influenced Corrosion of Iron and Steel. Paper no. 10209, Proceedings of CORROSION 2010, San Antonio, Texas

Kuklinski, A., Grooters, M., Stadler, R., Fürbeth, W., & Sand, W. (2009). Prevention of microbially influenced corrosion by extracellular polymeric substances. Poster PZ 25, Abstract in: BioSpektrum Special Issue: Proceedings of the Annual Meeting of the VAAM, Bochum, Germany

Kuklinski, A., Stadler, R., Fürbeth, W., & Sand, W. (2009). Evaluation of EPS for mitigating microbially influenced corrosion by combined atomic force-, epifluorescence and scanning Kelvin-probe microscopy. Abstract in: Proceedings of the 5th ASM Biofilm Conference, Cancun, Mexico.

Kuklinski, A., Stadler, R., Fürbeth, W., & Sand, W. (2009). Extrazelluläre polymere Substanzen zur Vermeidung mikrobiell beeinflusster Korrosion. Poster 11.03, Abstract in: Proceedings of the Annual ProcessNet and 27th Annual Biotechnology Meeting, Chemie Ingenieur Technik 818): 1274

7.3 Statement of original authorship

I declare that this document entitled

"Development of extracellular polymeric substance-derived protective films against microbiologically influenced corrosion by *Desulfovibrio vulgaris*"

has been composed by myself, and describes my own work, unless otherwise acknowledged in the text. It has not been accepted in any previous application for a degree. Material from the published or unpublished work of others, which is referred to in the dissertation, is credited to the author in the text.

Krefeld, in December 2016

(Andrzej Kuklinski)

7.4 Curriculum Vitae

The curriculum vitae has been removed from this electronic version for reasons of data protection.